

# **INTERIM REPORT**

to

California Air Resources Board

## **“Near-Source Measurement of Crystalline Silica Concentrations in California: Pilot Study”**

Contract Number 98-348

Britt A. Holmén, Principal Investigator  
Crocker Nuclear Laboratory

Ryoji Shiraki, Postdoctoral Scholar  
Crocker Nuclear Laboratory

University of California Davis

Submitted March 31, 2001  
Draft Revision April 29, 2001  
Second Draft Revision May 23, 2001  
Third Draft Revision August 5, 2001  
Final Revision August 22, 2001

The statements and conclusions in this report are those of the University and not necessarily those of the California Air Resources Board. The mention of commercial products, their source, or their use in connection with material reported herein is not to be construed as actual or implied endorsement of such products.

# Table of Contents

<b>TABLE OF CONTENTS .....</b>	<b>2</b>
<b>LIST OF FIGURES .....</b>	<b>4</b>
<b>ABSTRACT.....</b>	<b>5</b>
<b>SUMMARY.....</b>	<b>5</b>
<b>RESEARCH REPORT .....</b>	<b>8</b>
<b>1.0 INTRODUCTION .....</b>	<b>8</b>
1.1 THE PROBLEM.....	9
1.2 PREVIOUS STUDIES .....	11
1.3 PILOT STUDY OBJECTIVES .....	14
<b>2.0 EXPERIMENTAL METHODS .....</b>	<b>16</b>
2.1 PILOT SITE SELECTION.....	16
2.2 AIR SAMPLING FOR CHEMICAL ANALYSIS AND GRAVIMETRIC MASS.....	17
2.3 DRUM, PM <sub>10</sub> AND PM <sub>2.5</sub> AIR SAMPLING LOCATIONS.....	19
2.4 ANCILLARY DATA TECHNIQUES .....	20
2.5 QUANTITATIVE METHODS BY X-RAY DIFFRACTION (XRD).....	24
2.6 OTHER LABORATORY ANALYTICAL TECHNIQUES .....	32
2.7 QUALITY ASSURANCE/QUALITY CONTROL .....	33
<b>3.0 RESULTS &amp; DISCUSSION .....</b>	<b>36</b>
3.1 SITE PLAN AND SAMPLING TESTS.....	36
3.2 METEOROLOGICAL CONDITIONS .....	37
3.3 LIDAR PROFILES OF PLUMES DOWNWIND OF PLANT .....	38
3.4 PM <sub>10</sub> AND PM <sub>2.5</sub> MASS CONCENTRATIONS .....	40
3.5 MINERALOGY OF PM <sub>10</sub> AND DRUM SAMPLES.....	43
3.6 MORPHOLOGY AND GRAIN SIZE OF DRUM SAMPLES.....	44
3.7 QUARTZ RELATIVE INTENSITY IN DRUM SAMPLES.....	45
3.8 TEFLON FILTER QUARTZ AND ELEMENTAL COMPOSITION.....	47
3.9 DISTINGUISHING BACKGROUND AND SOURCE CRYSTALLINE SILICA.....	50
<b>4.0 CONCLUSIONS – Sampling Limitations &amp; Future Work .....</b>	<b>50</b>
<b>5.0 ACKNOWLEDGMENTS.....</b>	<b>52</b>
<b>6.0 REFERENCES CITED.....</b>	<b>52</b>
<b>RECOMMENDATIONS.....</b>	<b>57</b>
<b>APPENDICES.....</b>	<b>87-100</b>
<b>ATTACHMENTS</b>	
A. Standard Operating Procedures: Davis Rotating Drum Unit for Monitoring (DRUM) Impactor (34 pp)	
B. Description of the IMPROVE Network in 1999 (6 pp)	

## List of Tables

Table 1. PM Field Studies of Quarry Sites* .....	12
Table 2. Literature values for airborne quartz concentrations* .....	15
Table 3. Davis Rotating drum Universal Monitor (DRUM) Stages* .....	18
Table 4. Plant Activity Data for Pilot Study Period.....	22
Table 5. X-Ray Diffractometer Operating Conditions .....	29
Table 6. $2\theta$ values [ $^{\circ}$ ] and absorption coefficients [ $\text{cm}^2 \text{g}^{-1}$ ] for minerals of interest .....	29
Table 7. X-Y coordinates of all sampling locations [meters].....	36
Table 8. Pilot Study Sample Test Periods and Elapsed Sampling Times .....	37
Table 9. Test Period Meteorological Data Averages and Standard Deviations* .....	38
Table 10. Mass and elemental Si data for Teflon filter samples. Units are $\mu\text{g m}^{-3}$ for mass and $\text{ng m}^{-3}$ for Si. ....	41
Table 11. Mass and elemental Si concentration statistics for Teflon filter samples according to sampling location. Units are $\mu\text{g m}^{-3}$ for mass and $\text{ng m}^{-3}$ for Si.....	42
Table 12. Average quartz mass detected by XRD, quartz concentration and quartz mass fraction in $\text{PM}_{10}$ collected on Teflon filters.....	47

## List of Figures

- Figure 1. Relative locations of the sampling sites during Pilot Study.
- Figure 2. Intensity ratio  $I(Q)/I(\text{TiO}_2)$  vs.  $\text{PM}_{10}/\text{TiO}_2$  mass-ratio plot in internal reference XRD analysis.
- Figure 3. Calibration curve for quartz quantification by XRD.
- Figure 4. Meteorological data for Pilot Study.
- Figure 5. Lidar horizontal scan data: (a) horizontal scans (b) fugitive dust plume vectors (c) plume relative intensities and orientations of plume centerlines originating from Main Plant.
- Figure 6. Lidar vertical scan data: (a) June 14 morning, (b) June 14 afternoon, (c) average daily plume heights.
- Figure 7. Lidar vertical scans at different azimuth locations.
- Figure 8. Mass concentrations from Teflon filters.
- Figure 9. X-ray diffraction patterns for  $\text{PM}_{10}$  from soils at upwind U1 and downwind D1 sites.
- Figure 10. Scanning electron microphotographs of DRUM samples.
- Figure 11. DRUM X-ray diffraction results. (a) patterns for downwind D1 site DRUM stages 1 to 5, (b) quartz primary peak intensity on different DRUM stages collected at downwind D1 site on three sampling days., (c) quartz concentrations based on XRD results and DRUM sampling flow rates and test durations.
- Figure 12. Quartz Stage-1 mass concentrations for all sampling sites on (a) June 13, 2000, (b) June 16, 2000, (c) June 20, 2000.
- Figure 13. Quartz mass and  $\text{PM}_{10}$  mass concentrations for Teflon filter samples on (a) 6/16/00, (b) 6/20/00.
- Figure 14. Teflon filter quartz mass concentration relationships to  $\text{PM}_{10}$  mass and Si concentration.
- Figure 15. Average elemental ratios for Teflon filter samples. (a)  $\text{PM}_{10}$  filters, (b)  $\text{PM}_{2.5}$  filters.

### APPENDIX MATERIALS

- A. Lidar Data Analysis
- B. Raw XRD Data
- C. Site Photographs

## ABSTRACT

Quantitative determination of crystalline silica (CS) concentrations in air samples downwind of industrial sources is required to determine the general population's exposure to this potentially toxic air contaminant. A Pilot Study was carried out to develop methods to characterize near-source CS concentrations in air samples collected at multiple distances downwind of a stationary source. The sampling and analysis involved the following: (1) collection of PM<sub>2.5</sub>, PM<sub>10</sub>, and size-resolved PM samples downwind of a representative CS stationary source in California, (2) collection of bulk source material and determination of the composition of PM<sub>10</sub> derived from the source material, (3) analysis of the CS in the near-source air samples and the bulk source material. Analytical techniques included X-ray diffraction (XRD) techniques that are specific for CS, proton-induced X-ray emission (PIXE) of PM<sub>10</sub> and PM<sub>2.5</sub> filter samples to identify a trace element 'fingerprint' of the source material, and scanning electron microscopy (SEM). Light detection and ranging (lidar) was also used to monitor the dust plume characteristics downwind of the source.

**Note: quartz was the only crystalline silica mineral detected in the Pilot Study samples. Therefore, throughout this report, all references to "quartz" should be considered equivalent to "crystalline silica" (CS).**

## SUMMARY

a. A sand and gravel plant was selected as a representative CS stationary source. The site was selected because the site layout enabled positioning of multiple PM samplers downwind of the Main Plant operation to a downwind distance of approximately 500m and had a suitable location for an upwind sampler.

b. Sampling was conducted over six days in June 2000 at one upwind and four locations downwind of the plant. Meteorological conditions were similar for all tests with wind directions from the NW and average test wind speeds at 2m height that ranged from 2.6 to 4.2 m s<sup>-1</sup>. Sample test durations ranged from 2.7 to 12.5 hours and for all sampling periods, the following data was collected: lidar scans (except 6/20 and 6/21), meteorological data, PM<sub>2.5</sub>, PM<sub>10</sub>, size-

resolved PM using DRUM collecting 5 size cuts, soil samples, and rangefinder positions of all sites.

c. The PM<sub>2.5</sub> and PM<sub>10</sub> samples were analyzed for gravimetric mass and elemental composition (PIXE, XRF). Selected PM<sub>2.5</sub> and PM<sub>10</sub> and DRUM samples were analyzed for crystalline silica by X-ray diffraction (XRD) and the grain size and morphology of DRUM size fractions was determined by Scanning Electron Microscopy (SEM). Grains having a pure silica composition were not detected by SEM and therefore use of the SEM for quantifying silicate mineral abundances was not a reliable technique for the sand and gravel source PM samples. The SEM did indicate a wide size range in Stage 1 (>8.54 μm) DRUM samples that reflects the fact that near-source fugitive dust from these facilities is generally coarse.

d. Crystalline silica (quartz) was detected in downwind DRUM samples (all sizes) at concentrations up to approximately 120 μg m<sup>-3</sup> above the levels detected at the upwind site. For the Teflon filters, quartz concentrations in PM<sub>10</sub> averaged 6 μg m<sup>-3</sup> at the upwind site and 33.7 μg m<sup>-3</sup> at the four downwind sites. PM<sub>10</sub> and PM<sub>2.5</sub> mass concentrations at all sites ranged from 26 to 1026 and 0 to 62 μg m<sup>-3</sup>, respectively. Mean PM<sub>10</sub> and PM<sub>2.5</sub> mass concentrations were higher at the downwind sites [191 (± 181) and 16.9 (± 20.6) μg m<sup>-3</sup>, respectively] than the upwind site [35.2 (± 7.6) and 1.6 (± 4.5) μg m<sup>-3</sup>, respectively]. On average, approximately 15% of PM<sub>10</sub> was attributed to quartz at both the upwind and downwind sites. Quartz was very difficult to detect in the PM<sub>2.5</sub> Teflon filter samples, chiefly because most PM<sub>2.5</sub> filters had small mass loadings. In the two samples measured, concentrations were < 0.64 μg m<sup>-3</sup> at the upwind U1 site and estimated to be between 3.8 – 5.3 μg m<sup>-3</sup> at the downwind D1 site.

e. The methods used here demonstrate that as few as 2.7 hours of sampling using a flow rate of ~ 1 Lpm allowed XRD determination of the mass of quartz in size-resolved DRUM samples. Quartz was, however, below the X-ray diffraction detection limit in size cuts smaller than ~ 2 μm aerodynamic diameter in all samples analyzed. Also, the DRUM sampler Stage 1 (>8.54 μm) XRD results must be interpreted with caution because the large grain sizes observed by SEM may affect the applicability of the quartz standard curve used for XRD quantitation. A more detailed investigation would be required to examine this issue.

f. Both silicon and PM<sub>10</sub> mass concentrations showed linear correlations with XRD quartz concentrations measured in PM<sub>10</sub> Teflon filter samples for the 15 samples analyzed by XRD. This suggests the possibility of developing empirical relationships between easily-determined Si concentrations and sample mineralogy for PM compositions similar to that at the Pilot Study site.

g. The Pilot Study upwind quartz concentrations were significantly lower than the concentrations measured downwind of the plant. Therefore, most of the quartz detected downwind could be attributed to the source operation. X-ray diffraction analysis of resuspended bulk source material (=D1 site soil) showed identical mineralogy to the downwind D1 site PM<sub>10</sub> sample, therefore elemental analysis of the Teflon PM<sub>10</sub> samples collected at D1 were assumed to be representative of the source elemental profile. Elemental signatures of the upwind and downwind PM<sub>10</sub> and PM<sub>2.5</sub> samples were examined to identify a unique marker that could be used to distinguish background PM from source PM. These comparisons identified S/Fe, K/H and S/H ratios as significantly different between upwind and downwind PM samples with the differences being greater for PM<sub>2.5</sub> than PM<sub>10</sub>. The elemental data also revealed that the farthest downwind site, D4, had an elemental signature more similar to the upwind site, U1, than the other downwind sites.

h. Horizontal lidar scans indicated that plumes from the Pilot Study sand and gravel operation extended over 400 m, on average, from the edge of the main plant operation at an “optical intensity” that generally decreased by a factor up to ~ 2. The lidar vertical scan data showed that fugitive dust plumes generated by the plant routinely exceed heights of 100 meters and therefore the ground-level point samplers are only sampling a small portion of the entire dust plume. Therefore, the crystalline silica concentrations reported here for locations downwind of the plant should be considered representative of only the ground-level concentrations at those locations and should not be used to estimate the total emissions from the plant.

i. While both the impactor and Teflon filter sampling methods had specific limitations (see Section 4), downwind quartz concentrations consistently exceeded those measured in upwind samples. Future near-source studies should be conducted at other types of CS sources and should compare the Teflon filter method used here to NIOSH Method 7500.

# RESEARCH REPORT

## 1.0 INTRODUCTION

Crystalline silica ( $\text{SiO}_2$ , 'CS') occurs as five polymorphs that form under different temperature and pressure conditions and occur in different proportions in nature. The polymorphs are quartz, cristobalite, tridymite, coesite, and stishovite (Drees et al., 1989). Quartz is present in many rocks and is often an abundant mineral in soils, where it occurs mostly in the silt and sand fractions (2 to 2,000  $\mu\text{m}$ ). Cristobalite is much less common, and tridymite, coesite, and stishovite are extremely rare (Drees et al., 1989). The occurrence of these four minerals is restricted to some volcanic rocks, to some sedimentary rocks formed in depositional environments near volcanoes, and to soils formed from these rocks. In these rocks and soils, these minerals also generally occur in the sand and silt fractions, and at most constitute only a few weight percent of the total mass.

Crystalline silica (CS) was classified as a 'probable carcinogen to humans' by the International Agency for Research on Cancer (IARC) in 1987 (IARC, 1987). In California, this listing resulted in crystalline silica being added to the state's list of carcinogens under Proposition 65 in 1988, and to required warning labels on products containing respirable CS. In 1997, two crystalline silica polymorphs, quartz and cristobalite, were reclassified as 'carcinogens to humans' (IARC, 1997). In California, prior to designating a specific air pollutant as a Toxic Air Contaminant (TAC), the California Air Resources Board (CARB) must quantify the public's exposure to the pollutant and determine possible human health risks due to this exposure. Crystalline silica (CS) is currently under scrutiny as a TAC due to its potential human carcinogenic (lung cancer) and non-carcinogenic (bronchitis, silicosis) health effects. The present study was conducted to help CARB address exposure issues by measuring airborne crystalline silica concentrations downwind of a single CS source.

In 1999, California stationary sources were estimated to emit over 2.5 million pounds of crystalline silica. Of the more than 500 source facilities reporting emissions, 21 emitted more than 20,000 lb/yr and 4 emitted more than 100,000 lb/yr (CEIDARS, 1999). These sources include cotton gins, rock quarries, construction companies, mines, sand and gravel operations, and fiberglass, asphalt and paint manufacturers. These sources are located statewide, often in close

proximity to sensitive receptors and yet little is known about the transport and fate of the fine particulate fraction of CS emitted from these sources.

Federal regulations recently added ambient air quality standards for PM<sub>2.5</sub> (particulate matter with aerodynamic diameter less than or equal to 2.5 microns) to those for PM<sub>10</sub> and the other U.S. E.P.A. criteria pollutants (carbon monoxide, ozone, sulfur dioxide, lead, nitrogen dioxide). While PM<sub>2.5</sub> is a subset of PM<sub>10</sub>, the finer particulate matter is thought to be responsible for greater human health risks because the smaller particles can penetrate more deeply into the lungs than larger particles and are more difficult to remove once inhaled (Schwartz et al., 1996). The CS emissions from stationary sources in California are of utmost human health concern if they comprise significant portions of the ambient PM<sub>2.5</sub> and PM<sub>10</sub> concentrations. Currently, there is no quantitative data available on the size distribution and concentration of CS in inhalable particulate matter, despite the reported high mass emission rates from California stationary sources and the acknowledged adverse health effects of crystalline silica documented in occupational health studies.

The preliminary concentration data required to begin assessing the human health risks of airborne CS at locations near stationary sources in California are described in this report. Of special interest is the development of sampling and analysis techniques that can distinguish airborne crystalline silica generated by anthropogenic activities from the CS due to natural sources.

## **1.1 THE PROBLEM**

### **1.1.1 Generation and transport of crystalline silica in California air.**

Little is known about the transport of aerosol particles from sources to receptors and identifying a specific source aerosol in a receptor sample requires identification of a unique marker signature of the source aerosol. Such markers can be specific chemical compounds, trace elements, isotopes, or unique ratios of these markers.

Unfortunately, quantification of crystalline silica minerals alone does not uniquely identify a specific air pollution source because crystalline silica minerals are natural geologic products found in windblown dust. After oxygen, silicon is the most abundant crustal element,

and quartz is one of the most abundant minerals found in most rocks and soils. Cristobalite and tridymite, while much less common than quartz, are produced by high temperature igneous and metamorphic processes. Silicic volcanic terrains may contain cristobalite and tridymite as accessory minerals (Drees et al., 1989). In other words, crystalline silica is quite common in the natural environment and background concentrations complicate identification of CS particulate matter derived from human activities.

Anthropogenic activities such as sand and gravel quarry industries are primary sources of quartz in fugitive dust (the other silica minerals, too, if they are present in the rock). Quarrying and demolition activities tend to decrease the size of naturally-produced crystalline silica mineral grains, thereby forming potentially toxic airborne particles of aerodynamic size that are easily inhaled by humans and may become lodged in the respiratory tract. Fine particles of crystalline silica become airborne by resuspension at construction sites, mining operations, and some industrial processes such as ceramic processing. These man-made operations, while not changing the chemical composition or crystalline nature of the silica, do change the size, the particle morphology, and therefore the potential toxicity of the crystalline silica minerals. Particle size and morphology (i.e., shape, roughness, fracture pattern) are potentially useful ‘markers’ for distinguishing crystalline silica background (due to natural sources) from anthropogenic sources. In order to ensure identification of a CS source at a downwind receptor, bulk source materials of crystalline silica must be analyzed for the ‘markers’ with the same technique used for the downwind air filter samples. Ideally, the marker is little affected by atmospheric processing (both chemical and physical) during transport between source and receptor.

### 1.1.2 Quantifying crystalline silica in air samples

Quantifying crystalline silica minerals in ambient air samples is difficult due to the generally small mass of material collected on air filters. Quantitative analysis by X-ray diffraction (XRD) is suitable for bulk analysis, but the method requires relatively large sample mass (tens to hundreds of milligrams). These CS minerals tend to occur as relatively large particles, so they often constitute a very small percentage of  $PM_{10}$  and an even smaller proportion of  $PM_{2.5}$ . Work in progress (R. Southard, unpublished data) has shown that  $PM_{10}$  from almond harvest operations in the San Joaquin Valley consists mostly of the layer

aluminosilicate minerals smectite, vermiculite and biotite, whereas, quartz constituted <10% of the dust. These interpretations are based on quantitative X-ray diffraction and allocation of PIXE elemental analyses to soil minerals. Quantitative analyses for crystalline silica derived from human activities are further complicated by: (1) other than quartz, the very low abundance of pure CS minerals in natural materials; (2) the wide range of SiO<sub>2</sub> mineral crystallinity (especially in the cases of cristobalite and tridymite) and particle size; and (3) the dominance of aluminosilicate minerals (clays) in many fine particulate matter samples and the presence of amorphous silica (opal). These aluminosilicates and opal make bulk elemental Si analysis, the technique most suitable for analyzing the small masses collected on air filters, an ineffective technique for quantifying crystalline silica.

The Pilot Study was designed to overcome some of the analytical difficulties for crystalline silica by: (1) thoroughly characterizing the bulk material emitted at the crystalline silica source in order to evaluate both the dust-generating potential and a dust ‘fingerprint’ for each source, (2) fractionating the particulate matter in the air samples by aerodynamic size during sample collection in order to increase analytical sensitivity for individual size cuts, and (3) simultaneous collection of multiple samples downwind of the source plant over multiple days and different sampling durations.

## **1.2 PREVIOUS STUDIES**

### **1.2.1 PM<sub>2.5</sub> and Crystalline Silica Downwind of Quarries & Agriculture**

The National Stone Association sponsored a series of field studies conducted in 1997 by Air Control Techniques, P.C. at three quarries across the United States (Table 1). Of primary interest was determining the 24 hour average concentrations of PM<sub>2.5</sub> and PM<sub>10</sub> downwind of the stone crushing operations in order to assess the impact of EPA’s newly promulgated PM<sub>2.5</sub> National Ambient Air Quality Standard (EPA, July 18, 1997).

Table 1. PM Field Studies of Quarry Sites\*

Plant	Location	PM <sub>2.5</sub>	PM <sub>10</sub>	Crystalline Silica (CS)	Reference
Martin Marietta	Benson, North Carolina	UP = 7.6 (0–25) DN = 8.2 (0–28)	UP = 27.3 (12–48) DN = 28.7 (NR)	PM <sub>10</sub> (DN)= 33.5; CS= 8.4% (or 2.8 µg m <sup>-3</sup> )	(Air Control Techniques, 1997; Perkins et al., 1998)
Luck Stone Corporation	Leesburg, Virginia	UP = 10.2 (3.7–21.7) DN = 11.7 (4.8–23.7)	Not Measured	Insufficient PM <sub>2.5</sub> for XRD analysis	(Richards et al., 1998)
CAMAS Colorado, Inc.	Morrison, Colorado	UP = 8.2 (4.5–17.4) DN = 24.9 (7.3–49.5)	Not Measured	Insufficient PM <sub>2.5</sub> for XRD analysis	(Air Control Techniques, 1998)

\* PM concentrations are 24-hr averages in µg m<sup>-3</sup> with observed range in parentheses. NR = Not Reported.

These three studies all concluded that there was no significant difference in upwind and downwind PM<sub>2.5</sub> mass concentrations due to the stone crushing operations. Note that the reported average PM mass concentration values were based on 30-day measurements, but wind direction varied daily, and in the Leesburg, VA case was only “good” up to 50% of the sampling time. PM<sub>2.5</sub> samplers were > 1000 ft. from plant structures (Leesburg) and in the one case where downwind concentrations differed from upwind (Colorado site), the upwind-downwind mass difference was attributed to diesel exhaust PM, not mineral particulate matter. The one filter submitted for XRD analysis in the Benson Quarry study showed that quartz was easily detectable

in a 24-hour hi-vol (sampling flow rate was 39.91 ft<sup>3</sup>/min, or 1130 Lpm) PM<sub>10</sub> filter sample. In other cases, there was insufficient PM<sub>2.5</sub> mass collected for XRD analysis.

Personal exposure to crystalline silica varied greatly among different types of California agricultural operations and ranged between 4.8 and 23 % of the respirable dust mass (PM<sub>4</sub>; 30 to 447 µg/m<sup>3</sup>) (Nieuwenhuijsen et al., 1999). From these values, an upper limit on the respirable CS concentration near agricultural operations is estimated to be ~ 100 µg/m<sup>3</sup>.

### 1.2.2 X-ray Diffraction of Aerosol Filter Samples

Many studies have demonstrated quantitative measurement of quartz using SEM and X-ray diffraction (Crosby and Hamer, 1971; Davis, 1978; Davis, 1981a; Davis, 1981b; Davis and Johnson, 1982a; Davis and Johnson, 1982b; Davis et al., 1984; Esteve et al., 1997; Fukasawa et al., 1983; Lorberau and Abell, 1995; Morgan and DiCarlo, 1994; Sturges et al., 1989). Of particular interest are the studies led by Briant Davis (South Dakota School of Mines) on techniques for determining airborne quartz concentrations using X-ray diffraction (XRD). Davis and coworkers examined and developed quantitative XRD techniques for analyzing aerosols collected on filters (Davis, 1981b; Davis and Johnson, 1982a; Davis and Johnson, 1982b). Examination of sampling and analysis techniques led to the observation that XRD results were sensitive to: (a) the preferred orientation of grains and (b) filter loading density (Davis, 1981b). Therefore, standards should be prepared from aerosol rather than liquid suspensions (Crosby and Hamer, 1971; Davis and Johnson, 1982b; Lorberau and Abell, 1995). Studies of filter composition effects on XRD results led to the conclusion that Teflon filters were superior at low mass loadings, but 'quartz' (glass fiber filter) filters were best at loadings greater than 700 µg/cm<sup>2</sup> (Davis and Johnson, 1982a).

Reported results of airborne quartz concentrations measured in several studies are summarized in Table 2. Of note is the consistency with which quartz was detected in the larger size fractions in studies where size-fractionated impactor samples were collected. Quartz concentrations dropped dramatically for size cuts below approximately 2 µm (D<sub>50</sub> aerodynamic diameter). The majority of studies sampled ambient air for periods of at least 24 hr.

### **1.3 PILOT STUDY OBJECTIVES**

The Pilot Study was designed to test the sampling and analysis methods proposed to quantify the ‘inhalable’ concentrations of crystalline silica (CS) downwind of typical California stationary sources. ‘Inhalable’ particles are defined as having an aerodynamic diameter  $\leq 10 \mu\text{m}$  (PM<sub>10</sub>). In particular, the Pilot Study immediate objectives were to:

- ✓ **Identify the best sampling and analytical techniques for quantifying CS in PM samples that can distinguish stationary source CS from background sources of fugitive dust.**
  
- ✓ **Determine the crystalline silica concentrations as a function of distance downwind of a stationary source in California.**

This report describes the results of a Pilot Study where PM emissions from a single large CS source were examined using multiple sample collection and sample analysis techniques. The experimental methods used are described in Section 2 (Methods) and Section 3 discusses the meteorological, lidar and PM mass and composition data (Results & Discussion).

Table 2. Literature values for airborne quartz concentrations\*

Location	Sampler	Size Cuts ( $\mu\text{m}$ )	XRD method	Quartz Concentration ( $\mu\text{g m}^{-3}$ )	Reference		
Spain, Mediterranean Coast	Cascade impactor	9	standardless; MENGE quant.	7.94	Esteve et al. (1997)		
		5		6.32			
		3.5		1.5			
		2		0.7			
22 U.S. Cities (EPA 'inhalable' network) Five Points, CA	Hi-vol and dicotomous		direct; Teflon filters		Davis et al. (1984)		
		2.5-15		6.6 (3.2)			
		< 2.5		1.0 (1.2)			
		22 Cities		2.5-15		0.9 to 8.0	
	< 2.5	0 to 1.9					
average	2.5-15	4.9 (2.3)					
	< 2.5	0.4 (0.7)					
Surburban Toronto	Hi-vol, 3 day duration		Corundum internal standard		Sturges et al. (1989)		
		winter		2 - 15		0.33 (0.24)	
				0.65		0.06 (0.05)	
				0.37		0.01 (0.02)	
				<0.37		0.12 (0.09)	
		summer		2 - 15		0.87 (0.53)	
				0.65		0.3 (0.18)	
				0.37		0.04 (0.04)	
				<0.37		0.17 (0.11)	
		Yamanashi University, Japan		Andersen Impactor, 8 stages; Nucleopore polycarbonate filter substrate			DCM film mount
dry season	>11		X				
	7 - 11		X				
	4.7 - 7		X*				
	3.3 - 4.7		X				
	2.1 - 3.3		X				
	1.1 - 2.1		not detected				
	0.65 - 1.1		not detected				
	0.43 - 0.65		not detected				
<0.43	not detected						
wet season	>11		X*				
	7 - 11		X*				
	4.7 - 7		X*				
	3.3 - 4.7		X				
	2.1 - 3.3		X				
	1.1 - 2.1		X				
	0.65 - 1.1		not detected				
Rome, Italy	PM <sub>10</sub> ; cellulose membrane		Ag filter mount		Puledda et al. (1999)		
		Feb-94		daily averages and s.d.		0.64 (0.11)	
		May-94				1.12 (0.60)	
		Jul-94				0.95 (0.42)	
		Oct-94				1.50 (0.87)	

*note: mean diameter for silica particles was 4.3  $\mu\text{m}$  in separate Andersen impactor sample.*

\* = highest peak intensity

## **2.0 EXPERIMENTAL METHODS**

### **2.1 PILOT SITE SELECTION**

A suitable crystalline silica stationary source was selected for the Pilot Study measurements on the basis of the following criteria:

1. overall size of operation (i.e., length and width). A site that was typical of California plants was preferred. The physical layout of the site had to allow placement of four air-sampling stations downwind of the operation without interfering with the operation.
2. reliable wind conditions to ensure that samplers, once positioned, maintain their upwind versus downwind status throughout the sampling period.
3. lack of surrounding infrastructure (wires, poles, buildings) was important for collecting lidar scans. Unobstructed views of at least 500 meters were required to make meaningful lidar measurements, therefore detailed information about travel patterns on the site; locations of wires and poles, etc. were considered.
4. having a personal contact at the site to allow: (a) collection of bulk samples of the source material, (b) access to electrical power, and (c) repeated access to locations on the site property to operate the air monitoring equipment.
5. safe accessibility for field personnel. The sampling stations had to be accessible multiple times throughout the day for quality assurance checks and filter changes without compromising the safety of the field crew.
6. no other conflicting CS sources located around the study site.

With these criteria in mind, more than 20 stationary sources were visited and examined as potential study sites. Finally, a sand and gravel processing plant in Tracy, CA was selected for the Pilot Study because it met all of the above criteria. A schematic plan view of the Pilot Study site identifies the locations of the Main Plant, the 5 particulate matter (PM) sampling locations (upwind U1 and downwind D1 to D4), the meteorological tower and the lidar (Figure 1).

## **2.2 AIR SAMPLING FOR CHEMICAL ANALYSIS AND GRAVIMETRIC MASS.**

Conventional filter-based air sampling techniques are not ideal for sampling crystalline silica which must be analyzed by electron microscopy and X-ray diffraction techniques to assure identification and quantification. The problem with filter collection is that the Teflon filter typically used is an inadequate and unstable substrate for scanning electron microscopy imaging, because it is non-conductive and vaporizes under the electron beam. These drawbacks led us to propose sampling with an impactor using a new conductive impactor surface. While the impactor sampling cannot give quantitative PM mass measurements, it has the advantage of improved analytical response for the CS analytes of interest in this study because size-fractionated samples are collected for chemical analysis. In other words, the size-fractionated samples collected for CS analysis allow identification of whether or not a narrow aerodynamic size range of the particles of potential toxicity exists, and what this range is.

The Davis Rotating drum Universal Monitor (DRUM) was designed to collect time-resolved size-fractionated particulate matter samples. The samplers employ eight cylindrical drums with removable substrates mounted on their outer edges. These substrates are the impactor surfaces in the DRUM, and particles can be collected at different locations on the substrate surface over time as the drums are rotated by an electric motor. The Eight DRUM sampler (Raabe et al., 1988) has 8 critical orifices with cutpoints at: 0.07, 0.24, 0.34, 0.56, 1.15, 2.12, 4.26 and 8.54  $\mu\text{m}$  for a flow rate of 1.1 Lpm (Cahill, personal communication). During the Pilot Study, the upper 4 stages of the 8-DRUM were collected individually and a fifth composite sample that represented stages 5-8 was collected by removing orifices 5-7. The DRUM substrate material was 12mm wide double-sided copper tape (Ted Pella, Inc.; Redding, CA).

Table 3. *Davis Rotating drum Universal Monitor (DRUM) Stages\**

Stage	Size Range ( $\mu\text{m}$ )
1	> 8.54
2	4.26 – 8.54
3	2.12 – 4.26
4	1.15 – 2.12
5	0.56 – 1.15
6	0.34 – 0.56
7	0.24 – 0.34
8	0.07 – 0.24
After-filter	<0.07

\* in the Pilot Study, Stages 5 – 8 were combined into a single sample.

The DRUM samples cannot be used to quantify PM mass. Therefore, side-by-side samples of PM<sub>10</sub> and PM<sub>2.5</sub> were collected on 25mm Teflon filters (3  $\mu\text{m}$  Teflo®, Gelman R2P1025) using the Crocker Nuclear Laboratory Air Quality Group’s Interagency Monitoring of Protected Visual Environments (IMPROVE) aerosol samplers (Eldred et al., 1988; Eldred et al., 1990). EPA approved Sierra Anderson inlets (Model 246b) produced the 10  $\mu\text{m}$  size-cut, a cyclone was used for the PM<sub>2.5</sub> size-cut (John and Reischl, 1980) and flow rates were 21.7 L/min for PM<sub>2.5</sub> and 18.9 L/min for PM<sub>10</sub>. Each sampler was outfitted with a critical orifice for flow rate calibration before and after sample collection. The IMPROVE samplers (Eldred et al., 1988) are used for PM sampling at over 70 sites in a monitoring network across the U.S. maintained by the Air Quality Group at Crocker Nuclear Laboratory (CNL). Filters from the network samplers are routinely analyzed for mass and composition by CNL personnel and all relevant sampling protocols used in the IMPROVE network were used for the current study to ensure quality control. Portable gasoline-powered generators placed downwind of the samplers provided power for all sites except downwind D1 where the Plant provided power. The Tracy Airport also provided power at upwind U1 on 6/20 and 6/21.

More detail regarding the Pilot Study samplers can be found in Attachments A and B.

### **2.3 DRUM, PM<sub>10</sub> AND PM<sub>2.5</sub> AIR SAMPLING LOCATIONS.**

Field PM measurements were made upwind and downwind of the crystalline silica source. Side-by-side IMPROVE filter and DRUM impactor samplers were positioned to reflect the spatial layout of the plume based on: (a) the availability of suitable safe locations and (b) locations that were at similar elevations downwind of the Main Plant operation. Sampler siting was complicated by the presence of unpaved roads and the manmade topography (continual earth moving as well as presence of a large abandoned pit) of the active site.

The point samplers were located in five locations (see Figure 1):

1. The upwind (U1) site was on the north edge of the tarmac at the City of Tracy municipal airport;
2. The near-source downwind (D1) was located next to the diesel fuel tank adjacent to the road base product piles on the east side of the main plant;
3. The second closest downwind (D2) was across the creek bed from the downwind D1 site, but upwind of the unpaved road;
4. The third closest downwind (D3) was south of the unpaved road that follows the south side of the creek bed. D3 was also downwind of a staging area south of the unpaved road where earth moving equipment was operated intermittently; and
5. The farthest downwind location (D4) was located on the edge of the abandoned mine pit on the east side of the property.

Other monitoring equipment placed on the site property included the UC Davis miniature elastic lidar and a 10-meter meteorological tower. The lidar trailer was located on the west edge of the abandoned pit approximately 450 m south of the Main Plant. This position allowed collection of lidar scans along multiple directions downwind of the Main Plant. The meteorological tower was placed east of the Main Plant and north of the unpaved road that connected the Main Plant to the East entrance gate. The base of the meteorological tower was at a ~ 1.5 m higher elevation than the unpaved East entrance road.

## 2.4 ANCILLARY DATA TECHNIQUES

### 2.4.1 Meteorological Measurements

A 10-meter tower was erected upwind of most of the plant activity in order to collect meteorological data for the Pilot Study. The tower was equipped with Met One 014A anemometers at 0.5m, 1m, 2m, 4m, and 8m to measure wind speed. It also had Campbell Scientific 107 Air Temperature probes at 0.5m, 1m, 4m, and 8m, and a Vaisala HMP35C temperature and relative humidity probe at 2m. Wind direction was measured at 4m height using a Met One 024A Wind Vane. Solar radiation was measured at 4m height using a Campbell Scientific LI200X Pyranometer. The instruments were polled every second by a Campbell Scientific CR-10 data logger, and 1 minute averages were stored for later analysis.

### 2.4.2 Lidar

The UC Davis miniature elastic lidar instrument, described previously (Holmén et al., 1998), records range-resolved elastic backscatter signals from airborne PM with high temporal (sec) and spatial (5 m) resolution. The lidar scans are qualitative measures of relative PM backscatter, but provide useful information on PM plume variability over time in terms of spatial homogeneity, size, and shape. The lidar was employed to collect 2 dimensional (2D) vertical and horizontal scans to document the distribution of PM downwind of the Pilot Study facility between June 13 and June 16, 2000. The lidar was positioned on the SW side of the abandoned mine pit, about 430 m south of the Main Plant (see Figure 1). Note that all lidar data are presented in terms of lidar coordinates and no correction was made for true vertical distances above the ground at each location due to the variation in topography across the site. The laser pump energy was kept constant at 6.23 J during all data collection. The main objectives of the lidar measurements were to:

- ✓ locate fugitive dust plumes related to specific activities at the plant
- ✓ describe the physical dimensions of these plumes
- ✓ document the propagation of the plumes away from the plant.

2D Horizontal Scans. To obtain an overall picture of the dust distribution and propagation of the dust plumes away from the Main Plant, 2D horizontal scans were collected between 24 and 158° azimuth (see Figure 1b). The majority of the horizontal scans were collected at 3° elevation

angle (just above the horizon) to capture most of the plumes. Each horizontal scan was analyzed by recording the coordinates and intensity of the beginning and end of individual plumes. The plumes originating from the location of the Main Plant (~ 450 m from the lidar) and the plumes corresponding to the location of the plant's east entrance ("E gate", located ~600 m from the lidar) and traffic on the unpaved E-W road were then described as vectors. The vectors (X, Y, Z coordinates) of dust plumes originating from the Main Plant location (Appendix Table A.1) and those corresponding to the traffic on the E-W road (Appendix Table A.2) were adjusted based on the measured compass direction of the lidar such that all reported vector coordinates are relative to True North.

2D Vertical Scans. Vertical scans were collected sequentially at up to five azimuth locations that corresponded to lines of sight (LOS) directed from the lidar to locations: (1) downwind of the Main Plant and along the line-of-sight between the lidar and just upwind of sampler D3 (24.3° azimuth); (2) upwind of the meteorological tower (52.8°); (3) downwind of the East Gate entrance to the site (80°); (4) downwind of the D4 sampler location (102°); and (5) the southeast corner of the mine pit (158°). Increasing degrees of lidar azimuth corresponded to increasing distance downwind from the Main Plant. Note that the 158° azimuth scans were collected as background scans. Upwind scans would have been preferred for background measurements but could not be obtained due to the restrictions of siting the lidar at the site. For the 158° LOS, the lidar was pointed toward the southeast corner of the abandoned mine pit; plumes did generally not impact this line-of-sight during the sampling campaign. Vertical scans were performed at elevation angles from 2.5 to 23° (or 15.5°) in vertical steps of 0.25°.

Plume Centerline Vertical Profiles. After the range from the lidar to the centerline of the plume was determined from the 2D horizontal scans, average vertical profiles along the plume centerline were calculated as a function of the lidar azimuth position. Vertical profiles of lidar data were obtained by averaging the lidar signal at 2 m height intervals over a specified range interval centered around the plume centerline. Background vertical profiles were similarly obtained from the lidar scans collected along the line of sight directed away from the source operations (158°).

Plume Height. The physical dimensions of the plumes (maximum height, width, etc.) were described for plumes originating at the Main Plant and those corresponding to the traffic on the E-W unpaved road that connected the Main Plant to the East gate. For example, if a 2D vertical scan had multiple plumes, but the scan was collected at 24° azimuth (corresponding to the location of D3), the plume located about 500 m from the lidar was measured. This plume was considered most likely related to the activities at the Main Plant (~430 m N from lidar) based on its range location within the vertical scan. Maximum plume heights were recorded for all 2D vertical scans collected. Possible sources of error in measuring the maximum extent of the plume from the lidar vertical scans include the fact that some plumes extended higher than the programmed vertical limits of the lidar scan; when plumes were very close to the lidar this problem was most severe. Another source of measurement error resulted from near field-of-view geometric optics considerations: because of the lidar’s periscope arrangement, plumes within ~250 meters of the lidar were not fully quantified by the lidar receiver. This limitation applies to measuring the dimensions of plumes near location D3 (~190 m from lidar). Both of these factors could result in underestimation of the maximum plume height when the plume was close to the lidar instrument.

### 2.4.3 Site Activity

The plant operators provided the following activity data for the Pilot Study Plant during the days the sampling occurred. Daily truck and product shipped values were divided into activity at the aggregate plant and the asphalt plant. The aggregate plant (“Main Plant”) was the focus of the crystalline silica Pilot Study sampling, but trucks traveling to/from the asphalt plant on the site’s unpaved roads may have generated road dust containing CS.

*Table 4. Plant Activity Data for Pilot Study Period*

Date	Trucks in Plant			Active Operations	Product Shipped*	
	Aggregate	Asphalt	Total		Aggregate	Asphalt
6-13-00	483	60	543	Entire Plant	13,976	1,399
6-14-00	358	41	399	Entire Plant	10,646	915
6-15-00	282	113	395	Power Outage	6,895	2,846

6-16-00	382	54	436	Entire Plant	11,827	1,285
6-20-00	154	33	187	Entire Plant	4,601	708
6-21-00	250	81	331	Entire Plant	7,174	1,964

\*Tons

#### 2.4.4 Resuspension to Generate PM<sub>10</sub>

Source material was collected at numerous locations on the site over the course of the field sampling. Locations included the road base product material near site downwind D1 and the unpaved E-W road material. Approximately 100g samples of bulk material were collected and stored in plastic bags until mechanically mixed in the laboratory. A mineralogical XRD analysis was performed on PM<sub>10</sub> generated in the laboratory from bulk material collected at the upwind (U1) and near-source downwind (D1) sites. The PM<sub>10</sub> generated from these soil samples should be representative of the PM<sub>10</sub> composition of the background soil material and the CS source, respectively. The bulk soil collected from the upwind U1 site was dark brown in color, whereas that from the downwind D1 site was light brown.

Two PM<sub>10</sub> samples were prepared by resuspending sieved bulk soil samples (< 75 µm particles) collected at the upwind U1 and downwind D1 sites. Prior to 75 µm dry sieving, the soil fraction smaller than 2 mm was dried at 110°C over night to exclude moisture. About 0.7 to 1 g of bulk soil was repeatedly resuspended in the resuspension chamber at the Crocker Nuclear Laboratory (Carvacho et al., 1996) and PM<sub>10</sub> was collected on Teflon (3 µm Teflo®, Gelman R2P1025) filters. The resuspension chamber uses pressurized air to suspend the soil in a fluidized bed that is then sub-sampled by a PM<sub>10</sub> sampler in a collection chamber (Carvacho et al., 1996). A total of 81.1 mg PM<sub>10</sub> was obtained from 9.6 g of bulk soil (< 75 µm) from downwind D1 site, whereas 4.0 mg PM<sub>10</sub> was obtained from 5.1 g soil from upwind U1 site (< 75 µm), suggesting that the relative content of PM<sub>10</sub> in the bulk soils (< 75 µm particles) from downwind D1 and upwind U1 sites was roughly 0.84 and 0.078 wt%, respectively. After collecting the PM<sub>10</sub>, it was removed from the Teflon filters using a razor blade and stored in weighing paper until use for XRD sample preparation (see Section 2.5.2).

## 2.5 QUANTITATIVE METHODS BY X-RAY DIFFRACTION (XRD)

### 2.5.1 Internal Reference Method

Unambiguous identification of quartz in a sample containing other silicate minerals is possible using powder X-ray diffraction (XRD) on the basis of a characteristic X-ray diffraction pattern for each mineral. To quantify the quartz concentration in such a mixture, the quartz diffraction peak intensity must be quantified in the presence of the superimposed X-ray patterns from other minerals in the mixture that contribute to X-ray absorption effects. These absorption effects must be accounted for to ensure accurate quantitation. In other words, measured peak intensities are not directly proportional to the amount of mineral present in a sample until the peak intensities have been corrected for mass absorption effects. Further, the total mass absorption correction depends on the mineral assemblage present. The theory underlying XRD quantitation is discussed briefly here; further details can be found in Klug and Alexander (1974).

The total intensity of x-rays diffracted by a selected plane of component-J in a multi-component mixture,  $I_J$  [counts  $s^{-1}$ ], is given by:

$$I_J = \frac{K_J f_J}{\bar{\mu}} \quad (1)$$

Where  $K_J$  is a constant [counts  $g \text{ cm}^{-2} s^{-1}$ ] that depends upon the crystallographic nature of component-J and the geometry of the apparatus, and  $f_J$  and  $\bar{\mu}$  are the specific volume fraction [ $\text{cm}^3 \text{ cm}^{-3}$ ] occupied by component-J and the total mass absorption coefficient of the mixture [ $\text{cm}^2 \text{ g}^{-1}$ ], respectively. Substituting for  $f_J$ , Equation (1) becomes:

$$I_J = \frac{K_J X_J}{\bar{\mu} \rho_J} \quad (2)$$

Where  $\mu_J$  and  $X_J$  are the mass absorption coefficient [ $\text{cm}^2 \text{ g}^{-1}$ ] and weight fraction of component-J [ $\text{g}_J \text{ g}_{\text{mix}}^{-1}$ ] and  $\rho_J$  is the density ( $\text{g cm}^{-3}$ ) of component-J. Equations (1) and (2) imply that in quantification by the standard calibration method, it is essential to adopt a calibration standard whose total mass absorption coefficient is equal to that of the samples. The total mass absorption coefficient is given by:

$$\bar{\mu} = \frac{\sum_{J=1}^n X_J (\mu_J / \rho_J)}{\sum_{J=1}^n (\mu_J / \rho_J)} \quad (3)$$

However, the difficulty of determining the total absorption coefficient in an unknown sample matrix can be overcome by using the internal reference method described below.

In the internal reference method, a known amount of a standard component that does not exist in the sample (e.g., corundum) is added to the sample matrix. With this addition, the effect of mass absorption by the sample matrix can be cancelled out as follows. Suppose **n** grams of an internal-standard S is added to **m** grams of sample that contains the component of interest, J. The resulting specific peak intensities of components J and S in the (sample + standard) mixture,  $I_J$  and  $I_S$ , respectively, are given by:

$$I_J = \frac{K_J}{\bar{\mu} \rho_J} \left( \frac{m X_J}{m+n} \right) \quad \text{and} \quad I_S = \frac{K_S}{\bar{\mu} \rho_S} \left( \frac{n}{m+n} \right) \quad (4a, b)$$

Taking the ratio of the peak intensity of the component of interest, J, to that of the standard component, S, in the (sample + standard) mixture gives:

$$\frac{I_J}{I_S} = \left( \frac{K_J}{K_S} \cdot \frac{\rho_S}{\rho_J} \cdot X_J \right) \frac{m}{n} \quad (5)$$

Because all terms in the bracket of this equation are constant, the ratio of the peak intensity of component J to that of the internal-reference material is a linear function of the mass ratio,  $m/n$  (Note that  $X_J$  is the weight fraction of component J in the original sample). Thus, preparation of a series of (standard + sample) mixtures of different mass ratios allows one to quantify  $X_J$  from the slope of the  $I_J/I_S$  versus  $m/n$  plot assuming that the individual component K and density values are known or can be estimated. Alexander and Klug (1948) applied this method by adding fluorite as an internal-reference with a constant mass ratio (20%) to synthetic mixtures of quartz and calcium carbonate. They observed a good linear relationship between the intensity ratio of the quartz and fluorite primary peaks and the weight fraction of quartz (In their experiment,  $X_J$  was a variable at constant  $m/n$  ratio).

To determine the ratio of K's and ρ's in Equation (5), a binary mixture composed solely of J and S with one-to-one mass ratio is prepared and the following expression derived from Equation (2) applies:

$$\left(\frac{I_J}{I_S}\right)_{50:50\text{Binary}} = \frac{K_J}{K_S} \cdot \frac{\rho_S}{\rho_J} \quad (6)$$

because the weight fraction ratio of component J to that of component S is exactly unity ( $m/n=1$  and  $X'_J = X'_S=0.5$ ). The unknown variables in the slope term of the linear plot for Equation (5) can therefore be quantified from the peak intensity ratio for a 50:50 binary mixture of quartz and a reference material to quantify the weight fraction of J (quartz) in the sample. This relation was presented as the matrix-flushing theory or adiabatic principle (Chung, 1974a; Chung, 1974b). Chung also presented a technique to determine the reference intensity ratio by adopting a sample component as an internal reference. This allows one to determine the weight fraction of all components in the sample without addition of an external standard material (Chung, 1975). This technique, as well as optical microscopy for determination of amorphous constituents, has been applied to quantitative analysis of quartz in aerosol samples (Davis and Jixiang, 2000; Davis et al., 1984).

One difficulty in applying the internal reference method to the Pilot Study DRUM samples was that reference material could not be added to the DRUM substrates in a quantitative manner that would ensure reliable mixing of sample and standard. This problem was overcome by preparing a set of calibration standards from PM<sub>10</sub> samples prepared by resuspension of Pilot Study source material. The correspondence in mineralogy of the resuspended PM<sub>10</sub> and DRUM samples suggests that the total X-ray absorption coefficient of both materials was similar and, most importantly, indicates that the resuspended PM<sub>10</sub> material could be used as a calibration standard for the field aerosol samples. Therefore, the internal reference calibration method was used to determine the content of quartz in the resuspended PM<sub>10</sub> and this value was then used to quantify the quartz content of the DRUM samples.

### 2.5.2 X-ray Diffraction Sample Preparation

XRD Standards. In addition to the resuspended PM<sub>10</sub> (see Section 2.4.4), two XRD standard materials, quartz and titanium dioxide, were used. The Q-1 quartz standard was prepared by

NIOSH and the titanium oxide (anatase) NBS 154a standard was prepared by the National Bureau of Standards (now NIST). The Q-1 standard material is alpha quartz ground in a Trost Jet Mill and acid washed to produce respirable-sized particles. The cumulative percent size distribution by microscopy was as follows: <math><1\mu\text{m}</math> 40.4%; <math>1-3\mu\text{m}</math> 71.1%, <math>3-5\mu\text{m}</math> 87.7%, <math>5-7\mu\text{m}</math> 95.9%; <math>7-10\mu\text{m}</math> 99.1%, and <math>10-16\mu\text{m}</math> 100% (NIOSH Publication 79-139). Information about preparation procedures and size distribution for the  $\text{TiO}_2$  standard were not available. The  $\text{TiO}_2$  standard was considerably fine in size but was additionally ground in an agate mortar for ~10 min until a smooth texture that indicated grain sizes smaller than  $10\mu\text{m}$  was achieved.

Standard materials for XRD calibration were placed on the Cu-tape substrate by dropping aliquots of prepared aqueous suspensions of those materials using a micropipet. To prepare the standard suspensions, approximately 10 mg of the standard was weighed with the accuracy of 0.001 mg and then suspended ultrasonically in double-distilled water ( $\geq 10\text{ mL}$ ) in a glass vial. For standard mixtures, suspensions of a single standard were subsampled using a micropipet and the individual standards were mixed in separate vial. After suspension preparation, the suspension was sonicated for 5 min. and then shaken by hand before aliquots of the suspension were removed using a micropipet and placed on Cu-tape. To transfer the suspension to the Cu-tape or glass slide substrates for XRD analysis, the drops of suspension were distributed as widely as possible within the beam area of X-ray diffractometer. Prior to deposition of standard suspension on a new piece of Cu-tape, using tweezers the Cu-tape was transferred from a temporary glass slide, on which the tape was initially pasted tightly, to another glass slide in order to mimic the Cu-tape substrate mounting history of field DRUM samples. This transfer between glass slides crinkled the surface of the Cu-tape and made the surface condition of the substrate closer to that of the DRUM samples.

Field Samples. DRUM sample copper tape substrates were transferred from the rotating-drums to glass slides by cutting the Cu-tape between the test deposits using a razor blade and then removing the Cu-tape with tweezers. Once mounted on the slide glass, the perimeter of the tape was rubbed with a spatula to make the surface of the Cu-tape as smooth as possible.

PM ( $\text{PM}_{10}$  and  $\text{PM}_{2.5}$ ) collected on stretched Teflon filters was transferred to silver membrane filters for XRD analysis. The Teflon filter was placed in a clean beaker, 2-3 mL of 2-propanol was added and the solution was sonicated for 10 minutes. After sonication, the Teflon

filter was removed and the PM propanol suspension was transferred dropwise within a marked area of  $1 \text{ cm}^2$  (the size of X-ray beam) on a tared silver membrane filter (Osmonics, 0.45 micron, cut to  $\sim 1.5 \text{ cm} \times \sim 1.5 \text{ cm}$  in size) in a vacuum filtration apparatus. Only a portion of the original sample mass was transferred to each silver filter to ensure that the total PM sample mass was within that for the XRD calibration curve (i.e., less than  $479 \mu\text{g}$  total PM mass). After vacuum filtration to near dryness, the silver filter was placed in a petri dish and air dried overnight. Finally, the silver filter was re-weighed to determine the dry mass of PM transferred for XRD analysis.

### 2.5.3 X-Ray Diffractometer Conditions

Two X-ray diffractometers were used to analyze the Pilot Study samples and standards: (1) a DIANO model XRD8000 and (2) a Rigaku Miniflex (Table 5). The size of the X-ray beam area of the Rigaku Miniflex ( $10 \text{ mm} \times 10 \text{ mm}$ ) was larger than that of the DIANO XRD8000 ( $5 \text{ mm} \times 7 \text{ mm}$ ). Because the area of some field sample deposits were too large to be placed within the beam area of the DIANO instrument, the Rigaku Miniflex was used for measurements in which determination of the absolute value of peak intensity was essential, despite the fact that a monochromator was not installed on the Rigaku diffractometer. The Rigaku instrument had higher background counts than the DIANO due to the lack of monochromator, but the whole sample powder could be carefully placed in the X-ray beam area and the quartz primary diffraction peak was measured by scanning from  $2\theta = 26.0^\circ$  to  $27.5^\circ$ . Under these measurements conditions (Table 5), each reported DRUM sample quartz XRD measurement is an average of scans collected at four different sample orientations that were perpendicular to each other. (For the analysis of samples on silver membrane filters, only 2 orientations were averaged because initial tests showed much less sensitivity to sample orientation.) The peak intensity was counted as the area above a baseline drawn by the JADE software (baseline was trimmed manually when necessary). The measurement conditions for the DIANO instrument varied depending on sample type, although the X-rays were generated under constant conditions of 40kV and 20 mA. For all measurements, the  $\text{CuK}\alpha$  radiation was used and mineral identifications were based on the  $2\theta [^\circ]$  values in Table 6.

Table 5. X-Ray Diffractometer Operating Conditions

Parameter	DIANO XRD8000	RIGAKU Miniflex
X-Ray Source	Cu K $\alpha$	Cu K $\alpha$
Beam Area	5mm x 7mm	10mm x 10mm
Special Conditions	none	No monochrometer
Operating Voltage, Current	40kV, 20mA	30kV, 10mA
Scan interval	2 $\theta$ = 2 to 40 $^\circ$	2 $\theta$ = 26.0 $^\circ$ to 27.5 $^\circ$
Step size	0.02 $^\circ$ or 0.04 $^\circ$	0.01 $^\circ$
Scan Rate	1 – 25 sec/ step	30 sec/ step
Samples Analyzed	DRUM & Teflon full scans, PM <sub>10</sub> -TiO <sub>2</sub> mixtures, SiO <sub>2</sub> -TiO <sub>2</sub> mixtures (samples where peak ratios or full mineralogy were determined)	DRUMs, PM filter samples, PM <sub>10</sub> standards (for quartz peak intensity only – <u>quantitative</u> analyses)
Slit (mm)	DS 1 $^\circ$	DS 1 $^\circ$ RS 1 $^\circ$
Filter	Ni	Ni

Table 6. 2 $\theta$  values [ $^\circ$ ] and absorption coefficients [ $cm^2 g^{-1}$ ] for minerals of interest

mineral	2 $\theta$ and (I <sub>1</sub> /I)	$\mu$ <sup>1)</sup>
quartz	26.7 (100), 20.8 (35), 50.1 (17)	34.9
smectite (15A)	5.9 (100), 19.7 (80), 17.7 (60), 29.6 (60)	32.0
biotite	8.8 (100), 26.4 (100), 33.7 (80), 36.7 (80), 41.4 (80)	103.2
kaolinite	27.8 (100), 24.9 (80), 20.3 (60)	36.0
feldspar (albite)	22.0 (100), 27.7 (65), 24.3 (60)	33.3

<sup>1)</sup> from Davis (1978); 2 $\theta$  values from Joint Committee on Powder Diffraction Standards cards.

#### 2.5.4 Determination of Quartz Content in PM<sub>10</sub> from Downwind D1 Soil

The internal reference method (see Section 2.5.1) was adopted for the determination of quartz content in PM<sub>10</sub> from the downwind D1 site “soil” (= road base product), the PM<sub>10</sub> sample was then used as the calibration standard for X-ray intensity in the field samples. Titanium oxide (NBS-154a) was used as the internal reference material. Five mixtures of PM<sub>10</sub> and TiO<sub>2</sub> with different mass ratios (5.93, 3.96, 1.98, 0.976, and 0.484, respectively) were prepared and intensities of the primary and secondary peaks of quartz ( $2\theta = 26.7^\circ$  and  $20.8^\circ$ , respectively) and the primary peak of TiO<sub>2</sub> ( $2\theta = 25.3^\circ$ ) were measured. Each mixture was measured at two orientations in the diffractometer that were  $180^\circ$  opposite each other. Figure 2 shows the relationship between the intensity ratios of the primary or secondary peak of quartz to the primary peak of TiO<sub>2</sub>. Regression of these data to a straight line yielded:

For quartz primary–TiO<sub>2</sub> primary peak ratio:

$$\frac{I_J}{I_S} = 0.205(\pm 0.011) \left( \frac{m}{n} \right) \quad (r^2 = 0.964) \quad (7)$$

For quartz secondary–TiO<sub>2</sub> primary peak ratio:

$$\frac{I_J}{I_S} = 0.0340(\pm 0.0020) \left( \frac{m}{n} \right) \quad (r^2 = 0.954) \quad (8)$$

A PM<sub>10</sub>-TiO<sub>2</sub> mixture with one-to-one mass ratio was also prepared in triplicate and the average intensity ratio was determined to be 1.25 ( $\pm 0.12$ ) for the quartz primary–TiO<sub>2</sub> primary peak ratio and 0.211 ( $\pm 0.028$ ) for the quartz secondary–TiO<sub>2</sub> primary peak ratio. With those values, the content of quartz was determined to be 16.4 ( $\pm 1.8$ ) % from quartz primary–TiO<sub>2</sub> primary ratio and 16.1 ( $\pm 2.3$ ) % from quartz secondary–TiO<sub>2</sub> primary ratio using Equations (4) – (6). Results obtained from the two different peak ratios are identical within error, suggesting that the effect of an overlapping diffraction peak of the biotite (003) plane on that of the quartz (101) plane at  $2\theta = 26.7^\circ$  was not significant. The averaged value, 16.3 ( $\pm 2.1$ ) %, was adopted as the weight fraction of quartz in PM<sub>10</sub> collected by resuspending the downwind D1 site soil material.

### 2.5.5 Quartz Calibration Curve

In Figure 3, intensities of the quartz primary peak for five different mass concentrations of PM<sub>10</sub> were plotted against the mass of quartz, which was calculated by multiplying the mass of PM<sub>10</sub> by 0.163 (weight fraction of quartz in PM<sub>10</sub>). Each concentration was prepared and analyzed in duplicate or triplicate. Measurements were carried out under identical conditions as those for DRUM samples (Section 2.5.3). At each concentration, the intensity dependence on sample orientation was smaller than that found for the DRUM samples (less than  $\pm 15.5\%$  ( $\sigma$ ), error bars in Figure 3 were obtained from 8 or 12 measurements for a concentration). The five PM<sub>10</sub> data points showed good linearity (Figure 3), suggesting that the intensity of the quartz primary peak was directly proportional to the mass of quartz over the mass ranges examined ( $\leq 78.0 \mu\text{g}$  quartz or  $\leq 479 \mu\text{g}$  PM<sub>10</sub>). Regression of the data points in Figure 3 to a straight line passing through the origin yielded:

$$I_{Q(101)} = 628 (\pm 11) M_Q \quad (r^2 = 0.996) \quad \text{for PM}_{10} \quad (9)$$

Where  $I_{Q(101)}$  and  $M_Q$  are the intensity of the quartz primary peak (in area counts) and the mass of quartz in PM<sub>10</sub> ( $\mu\text{g}$ ), respectively.

Intensities of three mass concentrations of pure quartz standards were also measured under identical conditions as those used for PM<sub>10</sub>. These results are also shown in Figure 3. The three quartz standard points also showed good linearity, although the intensity for the pure quartz standard was 13% higher than that for PM<sub>10</sub> at a given mass concentration. Data regression to a straight line passing through the origin yielded:

$$I_{Q(101)} = 791 (\pm 11) M_Q \quad (r^2 = 0.998) \quad \text{for pure quartz} \quad (10)$$

Assuming  $K_j$  and  $\rho_j$  were equivalent for the quartz and the PM<sub>10</sub> standards and  $X_Q$  in Equation 2 can be replaced by  $M_Q$ , the total mass absorption coefficient for PM<sub>10</sub> was calculated from the ratio of slopes of these two regression lines (see Equation 2). Using a mass absorption coefficient for pure quartz of 34.9 (Davis, 1978), the mass absorption coefficient of the resuspended PM<sub>10</sub> sample was calculated to be 44.0. To check the validity of the calibration curve obtained, the intensity of the quartz primary peak was measured for a binary mixture of

pure quartz + kaolinite whose calculated total mass absorption coefficient was 35.5. The mass concentration of quartz in the mixture on a Cu-tape was 60.1  $\mu\text{g}$  (total mass of the mixture was 121  $\mu\text{g}$ ). Taking into account the difference in total mass absorption coefficients (see Table 6), the quartz mass in the binary mixture was  $56.4 \pm 6.8$  ( $2\sigma$ )  $\mu\text{g}$ , showing that the  $\text{PM}_{10}$  calibration line was valid.

## 2.6 OTHER LABORATORY ANALYTICAL TECHNIQUES

### 2.6.1 Electron Microscopy

The morphology and grain size of some DRUM samples were observed using an International Scientific Instruments model DS-130 scanning electron microscope. DRUM samples (Cu-tape substrates mounted on glass slide) were coated with gold and observed at an accelerating voltage of 10 kV. The chemical composition of individual grains was determined by a KEVEX energy-dispersive spectrometer (EDS).

### 2.6.2 Mass/PIXE/XRF/PESA

All Teflon filters collected by the IMPROVE samplers were analyzed for mass and elemental content using several analytical procedures. The analytical techniques followed established CNL procedures in accordance with laboratory Standard Operating Procedure documents. The mass analysis was gravimetric; the filters were weighed before and after sampling using a Cahn 28 microbalance with a 1  $\mu\text{g}$  sensitivity. After the post-weighing, the filters were analyzed for carbon soot using a laser integrating sphere technique that measures light absorption. The light absorption has been calibrated to the filter density of carbon soot particles. Next, the filters were analyzed by x-ray fluorescence (XRF); this procedure gives highly sensitive and accurate measurements of elements with atomic numbers of iron and heavier. Finally, the filters were analyzed using Proton Induced X-ray Emission (PIXE) for elements with atomic numbers from sodium through iron, and simultaneously analyzed for hydrogen using Proton Elastic Scattering Analysis (PESA). All data were merged to provide a database of  $\text{PM}_{2.5}$  and  $\text{PM}_{10}$  elemental composition that includes hydrogen, carbon soot, and elements sodium and heavier.

The accumulation of a large database of measurements of PM<sub>10</sub> and PM<sub>2.5</sub> mass and elemental profiles through the operation of the IMPROVE particulate matter sampling and analysis network led to the development of a series of composite variables that are defined by assumptions regarding the likely atomic mass ratio of the dominant elements of an aerosol constituent (Cahill et al., 1977; Eldred et al., 1997). These assumptions have been tested against independent analyses of related measurements for the database of IMPROVE samples (Cahill et al., 1981) and for agricultural source samples (James et al., 2000). For example, the gravimetric mass has been shown to be consistently well correlated with the composite variable “RCMA” which is the reconstructed mass obtained by summing factors of the common crustal elements (Al, Si, Ca, Ti, Fe), sulfur, light absorbing elemental carbon, hydrogen and non-soil potassium to emulate an average aerosol (Cahill et al., 1989):

$$RCMA = 0.5BABS + 2.5Na + SOIL + 13.75(H - 0.25S) + 4.125S + 1.4(K - 0.6Fe) \quad (11)$$

where,  $SOIL = 2.2Al + 2.49Si + 1.63Ca + 1.94Ti + 2.42Fe$ ; BABS is an estimate of the mass concentration of light absorbing carbon (Bond et al., 1999; Campbell et al., 1995), and the elemental mass concentrations are represented by their atomic symbols. Other composite variables are: SOOT = “light absorbing carbon from optical measurement” = BABS – 0.11 \* SOIL and OMH = “organic mass by hydrogen” = 13.75\* (H-0.25 \* S).

DRUM samples cannot be used to measure mass at this time because there is no way to measure the substrate mass prior to sampling. The great advantage of the DRUM samples is that they provide size-resolved particulate matter for analysis. The DRUM samples were analyzed for crystalline silica mass using powder X-Ray Diffraction (XRD).

## 2.7 QUALITY ASSURANCE/QUALITY CONTROL

### Field Sampling

Sampler flow rates were adjusted and recorded prior to sampling and checked and recorded after each sampling period using calibration magnehelics. Elapsed times on the PM samplers were

recorded similarly before and after sampling. The DRUM rollers were moved manually to define individual sampling periods on different portions of the Cu-tape substrates. All sampler stacks were removed overnight. Generator exhaust controls were used to ensure that exhaust was ducted downwind of the sampler inlets. All QA/QC procedures routinely used by CNL field sampling personnel were employed for meteorology and PM sample collection, handling, and data entry and analysis.

### XRD Methods & Detection Limits

The quartz XRD detection limit was calculated as the average peak area for analysis of blank Cu-tape at four perpendicular orientations plus three standard deviations. The peak area was calculated by integrating over the 2-theta range 26.6 – 27.2 degrees. This measurement gave 3349 area counts as the minimum peak area that could be distinguished from the background counts. Based on the PM<sub>10</sub> calibration curve (Equation 9), the minimum detectable mass of quartz in an aerosol sample collected using the DRUMs was therefore 5.3 µg.

One difficulty in the direct XRD analysis of the DRUM samples is the fact that the PM<sub>10</sub> standard calibration curve was prepared from liquid suspensions applied to the Cu-tape whereas the field sample aerosol deposition was by impaction. These two techniques could result in different response factors in the XRD instrument due to preferred grain orientations. The most obvious way to evaluate the effect of different sample and standard preparations is to prepare XRD standards using an aerosol suspension and deposition technique such as used by Davis and Johnson (1982) or the CNL resuspension chamber (Carvacho et al., 1996). Unfortunately, the DRUM impactor substrate material cannot be accurately weighed before and after sampling; thus, the mass of standard applied to the DRUM substrate from a resuspension experiment cannot be determined gravimetrically. An alternative technique for verifying the applicability of the PM<sub>10</sub> calibration curve is to compare direct XRD analysis of the PM<sub>10</sub> resuspended on a Teflon filter with the analysis of the same sample after transferring to Cu-tape via liquid suspension. This comparison was attempted for one sample, but the Teflon filter X-ray pattern overwhelmed any mineral peaks. This result is in contrast to literature reports that direct analysis of Teflon filters by XRD is feasible. The discrepancy is likely explained by the need for very high mass loadings of PM to alleviate the background problem.

Use of the quartz Cu-tape calibration curve for analysis of the silver filter PM<sub>10</sub> deposits (both from liquid suspensions) was verified by comparing the quartz peak areas for quartz standards of approximately 44 µg quartz prepared by both methods. The peak areas were equal within the measurement error (35033 ± 2166 on Cu-tape vs. 36332 ± 3402 on Ag membrane; see Figure 3).

### PM Laboratory Analyses & Quality Control

All PM samples were analyzed for gravimetric mass, light absorbing carbon, and elemental composition in accordance with IMPROVE protocols (Eldred et al., 1997; Eldred et al., 1990; Eldred et al., 1989). The elemental and carbon analyses are used chiefly for quality assurance purposes but also provide chemical characterization of these near-source aerosols for comparison with IMPROVE ambient monitoring data. The mass gain of dynamic field blanks (i.e., filters loaded into the samplers, subjected to flow measurement, but no air sampling) was used to calculate blank concentrations and minimum quantifiable limits (MQLs) for both PM<sub>10</sub> and PM<sub>2.5</sub> (Eldred et al., 1990). The MQLs were calculated from the standard deviation of the average of the blanks and the sampled air volumes. Uncertainties in mass concentration were calculated by propagation of the analytical errors introduced in the measurements of mass and air volume.

The hybrid integrating plate and sphere (HIPS) laser analysis technique (Bond et al., 1999; Campbell et al., 1995) was used to provide an estimate of light absorbing carbon soot (BABS). Particle induced x-ray emission (PIXE) and x-ray fluorescence (XRF) spectroscopy were used to determine the mass concentration of the elements of atomic mass between sodium and manganese and between iron and lead, respectively (Cahill, 1995). There is considerable overlap in the range of elements analyzed by these two methods such that independent analyses of the transition metals facilitate quality control between them (Cahill, 1995). Proton elastic scattering analysis (PESA), performed simultaneously with PIXE, provided a measure of the mass concentration of the bound hydrogen (as these analyses are performed under vacuum). Mass concentrations in air of each element were calculated from concentrations (ng cm<sup>-2</sup>) measured on a representative portion of the filter (at least 28%), the area of the sample on the filter, and the volume of air sampled. Minimum detectable limits (MDLs) were defined as 3.3 times the square root of the background counts. Analytical uncertainties were based on the propagation of

counting errors and uncertainties in the measurement of the elemental mass (from reanalysis) and air volume.

### 3.0 RESULTS & DISCUSSION

#### 3.1 SITE PLAN AND SAMPLING TESTS

The five PM sampling locations (“SAMLOC”, Table 7; “LOC”, Table 8) were sampled in eight separate test periods during the Pilot Study between June 13 and June 21, 2000 (Table 8). Note that the actual sampling time at each sampling location varied because of the time it took to travel between each site and also because of sampling equipment difficulties in some cases. The SAMLOC designations indicate the sampler site ID (U1, D1, D2, D3, D4) and the height of sampling was 3 meters from the ground at all locations.

*Table 7. X-Y coordinates of all sampling locations [meters].*

<b>SAMLOC</b>	<b>N-S DIST</b>	<b>E-W DIST</b>
U1	-1099.2	-1013.4
D1	7.5	-20.7
D2	61.5	-10.2
D33	234.5	110.5
D4	436	604.7
MET tower	86.5	433.5
LIDAR	424.5	77.5
D1 pile	0	0

Table 8. Pilot Study Sample Test Periods and Elapsed Sampling Times

TESTID	LOC	DATE	START TIME	END TIME	DURAT. HOURS
00-003	U1	6/13/00	0936	1954	10.38
	D1	6/13/00	0954	1820	8.45
	D2	6/13/00	1001	1830	8.48
	D3	6/13/00	1011	1845	8.57
	D4	6/13/00	1142	1915	7.55
00-004	U1	6/14/00	0711	1626	9.24
	D1	6/14/00	0723	1613	8.83
	D2	6/14/00	0658	1635	9.62
	D3	6/14/00	0740	1652	9.20
	D4	6/14/00	0614	1741	11.45
00-005	U1	6/15/00	0604	1346	7.70
	D1	6/15/00	NO POWER		
	D2	6/15/00	0720	1351	6.52
	D3	6/15/00	0646	1402	7.27
	D4	6/15/00	0636	1416	7.67
00-006	U1	6/16/00	0602	1310	7.13
	D1	6/16/00	0651	1320	6.49
	D2	6/16/00	0659	1325	6.43
	D3	6/16/00	0637	1329	6.87
	D4	6/16/00	0716	1339	6.38
00-007	U1	6/20/00	0555	1305	7.17
	D1	6/20/00	0856	1320	4.46
	D2	6/20/00	0900	1324	4.40
	D3	6/20/00	0912	1330	4.30
	D4	6/20/00	0920	1338	4.30
00-008	U1	6/20/00	1307	1815	5.12
	D1	6/20/00	1320	1730	4.11
	D2	6/20/00	1324	1736	4.27
	D3	6/20/00	1330	1742	4.20
	D4	6/20/00	1344	1750	4.12
00-009	U1	6/21/00	1054	1335	2.69
	D1	6/21/00	1101	1345	2.71
	D2	6/21/00	1106	1350	2.80
	D3	6/21/00	1112	1355	2.72
	D4	6/21/00	1123	1406	2.72
00-010	U1	6/21/00	1336	1924	5.76
	D1	6/21/00	1345	1807	4.37
	D2	6/21/00	1350	1815	4.42
	D3	6/21/00	1355	1822	4.45
	D4	6/21/00	1406	1834	4.47

Note that the origin of the coordinate system (0, 0) was the pile of road base product material located near the downwind D1 site. Samples from this pile were resuspended in the laboratory and used for characterization of the source material by X-ray diffraction.

### 3.2 METEOROLOGICAL CONDITIONS

The wind direction, wind speed, relative humidity and temperature during the Pilot Study were relatively similar from day to day (Figure 4). Wind direction was plotted on an adjusted scale of 180 to 540 degrees to avoid exaggeration of the wind direction when it varied between NW and

NE. On the adjusted scale, 180 degrees was added to the measured wind directions if the original wind direction was between 0 and 180 degrees. There was a noticeable difference in wind speed, RH and temperature on 6/20 and 6/21 between 7 and 8am in the morning (Figure 4) prior to the start of the PM tests, but the mean meteorological values over the sampling test periods were generally similar (Table 9) with the exception of higher mean wind speeds on June 16. Note that mean wind direction was from the W – N W for all test periods.

Table 9. Test Period Meteorological Data Averages and Standard Deviations\*

TESTID	START	END	DATE	Wind Direction (4m)		RH (2m) (%)	SR (4m) (Watt m <sup>-2</sup> )	Temperature (°C)				Wind Speed (ms <sup>-1</sup> )			
				0-360°	180-540°			1 m	2 m	4m	7.5 m	1 m	2 m	4m	7.5 m
00-003	9:36	19:54	6/13/00	320.66 32.21	323.72 13.67	20.43 4.83	664.95 230.18	33.71 2.95	33.49 2.95	33.20 2.95	32.65 2.98	2.81 0.91	3.41 0.88	4.60 1.22	5.35 1.36
00-004	6:14	17:41	6/14/00	319.10 33.73	322.37 15.51	24.13 5.18	667.39 228.34	34.83 4.26	34.63 4.15	34.39 4.01	33.86 3.86	2.96 0.71	3.53 0.58	4.77 0.72	5.54 0.75
00-005	6:04	14:16	6/15/00	320.31 61.01	331.97 19.33	22.34 2.19	594.11 280.87	34.88 2.72	34.67 2.54	34.46 2.32	33.99 2.05	2.25 0.74	3.06 0.71	4.16 1.05	4.90 1.02
00-006	6:02	13:39	6/16/00	311.09 11.79	311.09 11.79	22.09 2.73	566.44 284.28	30.39 1.66	30.27 1.56	30.13 1.42	29.71 1.24	3.80 0.72	4.20 0.64	5.51 0.92	6.32 1.06
00-007	5:55	13:38	6/20/00	269.33 105.16	325.33 50.39	40.50 14.81	509.08 261.06	27.43 3.92	27.24 3.82	27.00 3.69	26.53 3.48	2.01 1.25	2.58 1.33	3.44 1.90	4.01 2.22
00-008	13:07	18:15	6/20/00	315.89 93.70	345.08 11.74	18.85 2.76	683.16 188.32	35.31 1.04	34.95 1.08	34.52 1.12	33.82 1.16	2.15 0.54	3.31 0.59	4.57 0.75	5.39 0.75
00-009	10:54	14:06	6/21/00	294.42 112.31	342.92 20.29	28.26 2.96	754.67 212.23	34.05 1.82	33.64 1.81	33.20 1.79	32.44 1.74	1.65 0.63	2.59 0.73	3.41 1.10	4.04 1.26
00-010	13:36	19:24	6/21/00	303.68 48.52	309.96 28.01	18.43 4.25	588.50 230.91	36.68 0.92	36.42 0.85	36.15 0.76	35.64 0.70	2.93 0.96	3.68 0.83	4.51 0.84	5.16 0.87

\* Averages (first row) and standard deviations (second row) based on all 1-minute data collected over the test period duration.

### 3.3 LIDAR PROFILES OF PLUMES DOWNWIND OF PLANT

As expected, most of the fugitive dust plumes originated from the Main Plant located about 500 m North of the lidar (see Figure 1). The lidar horizontal scans collected at 3 degrees elevation angle indicate that the general direction of all the plumes corresponded to the NW wind direction during the data collection period (Figure 5a). Dust plumes originating from other nearby sources are also visible in the lidar horizontal scans (Figure 5a). Plumes associated with traffic on the E-W road (trucks entering through E gate) seem to be significant as well. However, there is not enough horizontal scan data to investigate propagation of plumes originating from the unpaved road and the horizontal scans were collected at too high an elevation angle to monitor ground-level sources as well as the plant emissions. Measured intensities and lengths of all the plumes originating at the Main Plant that appeared on lidar horizontal scans collected over a 4 day period (13-16 June) were combined into a vector plot (Figure 5b). It is noteworthy that the majority of plumes determined to be originating from the Main Plant did not propagate further

than 400 m (East direction) from the lidar. This observation may be a result of the data analysis method, however, and should be interpreted with caution. Horizontal scans at other elevation angles might give different plume lengths. Also, as documented in Figure 5a, many of the plumes had intensities that varied greatly or were discontinuous along the plume centerline (see discontinuity at x,y coordinates (0,450) in Figure 5a). Only those plumes that were continuous were included in the vector plot of Figure 5b. The relative intensities at the beginning and end of the continuous plumes measured on June 13, 2000 (Figure 5c) indicate that there was significant temporal variability in the plumes.

The lidar average vertical profiles tended to vary between morning (Figure 6a) and afternoon (Figure 6b), probably due to changes in activity at and around the Main Plant as well as variations in meteorological conditions. Note, for example, that on June 14 the dust plumes were significantly more intense in the morning than in the afternoon (Figure 6a,b). In the afternoon (Figure 6b), only the two azimuth locations closest to the Main Plant showed average lidar signals that exceeded background. In other words, the East gate (80 degrees) and D4 (102 degrees) plume centerlines were not significantly different from background in the afternoon on this date, but the lidar profiles collected at the D3 and meteorological tower azimuths were significantly higher than background. The relationship between the plume profile collected at the background azimuth and the other azimuths varied from day to day (see profiles for June 13, 15, and 16 in the Appendix). On June 16<sup>th</sup>, vertical scans were collected only at D3 and the E gate locations and the plumes from both locations appeared to be more intense compared to previous days. This could be due to a higher intensity of plant operations on that day or differences in atmospheric conditions. Unfortunately, background files (SE pit corner) were not collected on June 16<sup>th</sup>. The background scans on June 13<sup>th</sup> show plumes more intense than the plumes identified at the other locations. It is possible that this is due to high activity levels in both the aggregate and asphalt plants and corresponding high traffic on the EW road on June 13 relative to the other test days. On June 14<sup>th</sup> and 15<sup>th</sup> the background was about the same (slight change between morning and afternoon scans on June 15<sup>th</sup>).

It is also important to note that the plume heights significantly exceeded the 3 m height of the PM samplers. In order to summarize the trends in plume heights depending on the vertical scan location, the measured plume heights corresponding to a specific location and sampling day were averaged (Figure 6c). Average plume heights determined from the lidar vertical scans

(Figure 6c) ranged from approximately 25 m to over 200 m above the lowest lidar vertical scan elevation angle (2.5 degrees). In general, the average height of the plumes, as determined from the lidar vertical scans, increased with distance from the Main Plant (Figure 6c). Average plume heights were highest at the D4 location for all days (about 500 m from the lidar and 740 m from main plant). This is consistent with vertical dispersion of the plumes and with rising plumes due to surface heating on these hot summer days. The series of 2D vertical scans (Figure 7a,b,c) collected at three different azimuths (24, 80 and 102 degrees respectively) illustrate the increase in plume height with increasing azimuth (= increasing distance from Main Plant). Plume heights dropped significantly at the background azimuth location (“SE corner”), except on June 13<sup>th</sup> (this agrees well with the higher background observed on June 13<sup>th</sup>).

The very high plumes generated by the Main Plant operations suggest that ground-level point samplers will be ineffective in capturing all of the PM emissions from these operations. Therefore, the crystalline silica concentrations reported here for locations downwind of the plant should be considered representative of only the ground-level concentrations at those locations and should not be used to estimate the total emissions from the plant.

### **3.4 PM<sub>10</sub> AND PM<sub>2.5</sub> MASS CONCENTRATIONS**

As expected, PM<sub>10</sub> and PM<sub>2.5</sub> mass concentrations were higher at the downwind sites than the upwind site. PM<sub>10</sub> concentrations ranged from ~26 to 1026  $\mu\text{g m}^{-3}$  over the study period (Figure 8). PM<sub>2.5</sub> was not detectable gravimetrically for 22 of the 39 samples collected (see Table 10). The average ratio of PM<sub>2.5</sub> to PM<sub>10</sub> was about 8% ( $\pm 18\%$ ) for all the samples collected (Table 11). The mean upwind mass concentrations were 35.2 ( $\pm 7.6$ ) and 1.6 ( $\pm 4.5$ )  $\mu\text{g m}^{-3}$  for PM<sub>10</sub> and PM<sub>2.5</sub>, respectively. Downwind average concentrations were 191 ( $\pm 181$ ) and 16.9 ( $\pm 20.6$ )  $\mu\text{g m}^{-3}$  for PM<sub>10</sub> and PM<sub>2.5</sub>, respectively, with the highest measured concentrations occurring at the second downwind location, D2 (see Tables 10 & 11).

Table 10. Mass and elemental Si data for Teflon filter samples. Units are  $\mu\text{g m}^{-3}$  for mass and  $\text{ng m}^{-3}$  for Si.

TEST#	LOC	DATE	START TIME	END TIME	DURAT. HOURS	MASS PM <sub>2.5</sub>	M_ERR PM <sub>2.5</sub>	M_MDL PM <sub>2.5</sub>	Si PM <sub>2.5</sub>	Si_ERR PM <sub>2.5</sub>	Si_MDL PM <sub>2.5</sub>	MASS PM <sub>10</sub>	M_ERR PM <sub>10</sub>	M_MDL PM <sub>10</sub>	Si PM <sub>10</sub>	Si_ERR PM <sub>10</sub>	Si_MDL PM <sub>10</sub>
00-003	U13	06/13/00	0936	1954	10.38	0.000	0.000	8.489	5.61E+02	29.88	4.90	44.15	2.41	4.03	7.45E+03	379	18.66
00-003	D13	06/13/00	0954	1820	8.45	16.372	4.941	9.833	3.65E+03	186.09	10.19	207.00	6.68	4.95	2.84E+04	1441	47.36
00-003	D23	06/13/00	1001	1830	8.48	31.079	5.187	10.205	3.78E+03	192.26	10.03	202.27	6.57	5.06	5.72E+04	2899	90.45
00-003	D33	06/13/00	1011	1845	8.57	0.000	0.000	10.445	1.03E+03	53.04	5.50	75.83	3.27	4.70	1.60E+04	814	33.06
00-003	D43	06/13/00	1142	1915	7.55	0.000	0.000	11.270	9.72E+02	50.91	6.62	104.57	4.09	5.24	1.15E+04	587	28.09
00-004	U13	06/14/00	0614	1741	11.45	0.000	0.000	7.568	5.12E+02	26.74	3.94	26.51	1.99	3.65	5.40E+03	276	15.74
00-004	D13	06/14/00	0711	1626	9.24	24.098	6.113	12.141	5.60E+03	283.81	12.64	182.21	5.92	4.53	1.95E+02	12	6.84
00-004	D23	06/14/00	0723	1613	8.83	19.448	4.893	9.716	3.94E+03	201.23	11.38	140.49	4.83	4.73	2.35E+04	1189	40.16
00-004	D33	06/14/00	0658	1635	9.62	12.736	4.552	9.071	2.25E+03	115.40	7.90	120.40	4.20	4.28	3.50E+04	1776	57.54
00-004	D43	06/14/00	0740	1652	9.20	0.000	0.000	9.174	1.14E+03	58.88	5.74	43.83	2.55	4.38	9.11E+03	464	22.93
00-005	U13	06/15/00	0604	1346	7.70	0.000	0.000	11.254	4.20E+02	22.78	6.22	32.92	2.86	5.37	5.45E+03	279	18.25
00-005	D13	06/15/00	NO POWER														
00-005	D23	06/15/00	0720	1351	6.52	20.307	6.452	12.846	3.56E+03	182.59	12.81	198.36	6.77	6.45	5.24E+04	2651	83.64
00-005	D33	06/15/00	0646	1402	7.27	0.000	0.000	12.312	1.48E+03	76.24	6.88	102.55	4.22	5.76	2.38E+04	1207	45.90
00-005	D43	06/15/00	0636	1416	7.67	12.329	5.698	11.372	1.31E+03	68.50	8.68	81.15	3.60	5.31	1.80E+04	914	40.92
00-006	U13	06/16/00	0602	1310	7.13	0.000	0.000	12.063	4.37E+02	24.28	7.31	33.41	3.15	5.97	4.96E+03	254	18.39
00-006	D13	06/16/00	0651	1320	6.49	23.413	6.483	12.889	6.05E+03	307.88	14.72	242.37	7.94	6.40	7.18E+04	3634	107.02
00-006	D23	06/16/00	0659	1325	6.43	61.118	7.247	14.022	1.20E+04	612.90	26.98	462.54	14.29	6.80	1.43E+05	7295	229.54
00-006	D33	06/16/00	0637	1329	6.87	18.034	6.522	13.000	3.84E+03	197.45	14.73	226.71	7.44	6.05	7.58E+04	3845	118.65
00-006	D43	06/16/00	0716	1339	6.38	0.000	0.000	13.534	2.24E+03	116.09	11.87	95.57	4.28	6.36	2.57E+04	1307	51.26
00-007	U13	06/20/00	0555	1305	7.17	12.803	6.058	12.091	5.77E+02	31.56	7.90	42.14	3.18	5.83	5.92E+03	302	19.95
00-007	D13	06/20/00	0856	1320	4.46	0.000	0.000	18.606	2.56E+03	132.45	13.79	241.81	8.60	9.25	6.71E+04	3396	101.63
00-007	D23	06/20/00	0900	1324	4.40	35.629	9.956	19.798	8.27E+03	421.48	21.92	210.02	7.98	9.81	6.34E+04	3215	106.25
00-007	D33	06/20/00	0912	1330	4.30	0.000	0.000	20.770	3.45E+03	178.96	18.00	156.22	6.69	9.55	3.57E+04	1814	71.30
00-007	D43	06/20/00	0920	1338	4.30	0.000	0.000	20.081	1.39E+03	75.00	13.69	64.67	5.10	9.43	1.07E+04	548	36.09
00-008	U13	06/20/00	1307	1815	5.12	0.000	0.000	16.799	3.68E+02	21.44	8.75	27.07	4.09	8.02	4.68E+03	241	21.07
00-008	D13	06/20/00	1320	1730	4.11	0.000	0.000	20.353	4.10E+03	208.99	14.79	170.68	7.15	9.99	4.42E+04	2243	78.01
00-008	D23	06/20/00	1324	1736	4.27	0.000	0.000	20.231	3.86E+03	198.09	15.62	192.29	7.71	10.24	5.83E+04	2953	100.13
00-008	D33	06/20/00	1330	1742	4.20	0.000	0.000	21.264	2.06E+03	108.62	15.20	146.10	6.81	10.41	3.78E+04	1917	73.35
00-008	D43	06/20/00	1344	1750	4.12	0.000	0.000	20.626	1.07E+03	57.82	11.41	33.00	5.02	9.84	5.69E+03	295	26.69
00-009	U13	06/21/00	1054	1335	2.69	0.000	0.000	32.142	8.45E+02	47.74	16.77	45.17	8.14	16.04	8.52E+03	438	38.01
00-009	D13	06/21/00	1101	1345	2.71	53.946	15.505	30.841	8.21E+03	418.87	23.58	240.90	10.67	15.71	5.98E+04	3030	108.01
00-009	D23	06/21/00	1106	1350	2.80	48.806	14.878	29.612	8.71E+03	447.30	30.20	1026.29	31.74	15.39	4.81E+04	2442	94.08
00-009	D33	06/21/00	1112	1355	2.72	0.000	0.000	30.483	1.51E+03	82.67	20.96	121.50	8.54	15.45	3.05E+04	1549	73.55
00-009	D43	06/21/00	1123	1406	2.72	61.672	15.844	31.472	9.64E+02	53.11	16.25	56.50	7.81	15.26	1.09E+04	561	44.85
00-010	U13	06/21/00	1336	1924	5.76	0.000	0.000	15.130	3.75E+02	21.78	9.17	29.89	3.95	7.68	4.06E+03	210	21.94
00-010	D13	06/21/00	1345	1807	4.37	50.519	10.326	20.428	6.91E+03	352.33	20.12	324.71	10.87	9.64	7.58E+04	3835	116.05
00-010	D23	06/21/00	1350	1815	4.42	34.787	9.588	19.062	4.93E+03	252.14	15.42	288.44	10.03	10.16	9.49E+04	4814	152.09
00-010	D33	06/21/00	1355	1822	4.45	0.000	0.000	19.237	1.27E+03	67.31	10.34	108.48	5.74	9.45	2.67E+04	1356	60.73
00-010	D43	06/21/00	1406	1834	4.47	0.000	0.000	19.301	7.92E+02	42.78	9.25	51.51	4.89	9.28	9.15E+03	470	32.83

Table 11. Mass and elemental Si concentration statistics for Teflon filter samples according to sampling location. Units are  $\mu\text{g m}^{-3}$  for mass and  $\text{ng m}^{-3}$  for Si.

	DURAT HOURS	MASS PM <sub>2.5</sub>	MASS PM <sub>10</sub>	Si PM <sub>2.5</sub>	Si PM <sub>10</sub> <sup>a</sup>	PM <sub>2.5</sub> /PM <sub>10</sub> %	Si <sub>2.5</sub> /Si <sub>10</sub> <sup>a</sup> %
<b>upwind</b>							
min	2.7	0.0	26.5	368.0	4061.8	0.0	7.5
max	11.5	12.8	45.2	845.1	8521.7	30.4	9.9
ave	7.2	1.6	35.2	511.7	5806.5	3.8	8.8
stdev	2.8	4.5	7.6	156.4	1483.5	10.7	1.0
<b>all downwinds</b>							
min	2.7	0.0	33.0	792.2	5693.5	0.0	3.8
max	9.6	61.7	1026.3	12048.6	143495.4	109.2	18.9
ave	5.8	16.9	190.9	3643.7	42354.9	9.6	9.1
stdev	2.2	20.6	180.9	2805.6	30810.4	19.7	4.0
<b>D1</b>							
min	2.7	0.0	170.7	2555.9	28442.3	0.0	3.8
max	9.2	53.9	324.7	8212.1	75780.1	22.4	13.7
ave	5.7	24.0	230.0	5297.0	57859.0	9.8	9.5
stdev	2.4	21.6	51.2	1976.0	18193.5	8.2	3.5
<b>D2</b>							
min	2.8	0.0	140.5	3557.5	23468.3	0.0	5.2
max	8.8	61.1	1026.3	12048.6	143495.4	17.0	18.1
ave	5.8	31.4	340.1	6137.6	67670.5	10.8	10.2
stdev	2.2	18.8	294.3	3157.2	36406.1	5.7	5.1
<b>D3</b>							
min	2.7	0.0	75.8	1026.0	16040.1	0.0	4.8
max	9.6	18.0	226.7	3844.1	75848.3	10.6	9.7
ave	6.0	3.8	132.2	2111.6	35160.8	2.3	6.1
stdev	2.4	7.3	45.6	1032.7	17935.9	4.3	1.6
<b>D4</b>							
min	2.7	0.0	33.0	792.2	5693.5	0.0	7.3
max	9.2	61.7	104.6	2237.3	25735.1	109.2	18.9
ave	5.8	9.3	66.4	1235.3	12605.3	15.5	10.8
stdev	2.2	21.6	25.3	448.5	6334.4	38.2	3.9

<sup>a</sup>without 6/14 D1

### 3.5 MINERALOGY OF PM<sub>10</sub> AND DRUM SAMPLES

**Resuspended PM<sub>10</sub>.** The XRD patterns of PM<sub>10</sub> collected by resuspending soil from the upwind U1 and downwind D1 sites showed no significant difference in mineralogy between the resuspended PM<sub>10</sub> samples from the upwind and nearest downwind site (Figure 9, upper panels). The resuspended PM<sub>10</sub> was analyzed using a glass slide mount without the Cu-tape substrate and PM<sub>10</sub> was applied to the glass as an aqueous slurry paste. As seen in the figure, the diffraction pattern of PM<sub>10</sub> from the downwind D1 site showed distinct peaks of quartz, feldspar (albite), kaolinite, mica, gibbsite, and smectite. Peaks in the pattern of PM<sub>10</sub> from upwind U1 site soil were less distinct than those from downwind D1 site, probably due to the much lower resuspended PM<sub>10</sub> mass obtained from the upwind U1 sample for X-ray diffraction analysis (the mass fraction of PM<sub>10</sub> in the upwind soil material was ~ 10x lower than for downwind D1 soil; see Section 2.4.4). However, despite the lower intensity of peaks in the upwind sample, the primary and secondary peaks of quartz and feldspar and the primary peaks of kaolinite, mica, and smectite are recognized in the diffraction pattern of PM<sub>10</sub> from upwind U1 site soil.

**Teflon Filter and DRUM Samples.** The X-ray diffraction pattern of the Teflon filter and the Stage-1 DRUM samples collected at the upwind U1 and downwind D1 sites on June 16 show similar mineralogy to the resuspended PM<sub>10</sub>, although the diffraction pattern peak intensities are lower (Figure 9, lower panels). The diffraction pattern of the Cu-tape substrate blank is also shown in the figures. This blank pattern included broad peaks around at  $2\theta = 5^\circ$ ,  $18^\circ$ , and  $24^\circ$ . The pattern of the sample collected on 6/16/00 included distinct quartz (primary and secondary), feldspar (primary only), and an unknown peak at  $36^\circ$ , as well as lower intensity primary peaks of kaolinite and mica. The diffraction by smectite at low  $2\theta$  was not distinct in the 6/16/00 downwind D1 Stage-1 sample (Figure 9b). The downwind D1 Stage-1 sample collected on 6/20/00 (data not shown) showed a similar XRD pattern to that collected on 6/16/00, indicating that the mineralogy of the PM samples did not vary between sampling dates. This result is expected for a constant stationary source and essentially invariant wind direction over the Pilot Study period. Comparison of all diffraction patterns in Figure 9 suggests that the mineralogy of the DRUM Stage-1 samples is quite similar to that of the resuspended and Teflon filter PM<sub>10</sub>,

although it remains unclear whether or not smectite, probably occurring as small grains adhering to larger grains, was a major constituent of Stage-1 samples.

The XRD data in Figure 9 also compare the relative intensities of the two types of field samples collected for crystalline silica analysis – the DRUM and PM<sub>10</sub> Teflon filter samples. The DRUM peak intensities are lower than those of the Teflon filter probably because the DRUM sampler flow rate (~ 1 Lpm) was 15x lower than the IMPROVE sampler flow rate (~17 Lpm). The lower flow rate resulted in lower sample mass collection over the test period.

### **3.6 MORPHOLOGY AND GRAIN SIZE OF DRUM SAMPLES**

SEM images (Figure 10) indicate that Stage-1 DRUM samples contained many particles with diameters significantly larger than 10  $\mu\text{m}$ . This reflects the fact that the DRUMs have no size-specific inlet to restrict the upper bound on particle size. The Stage-1 sample collected at the downwind D1 site on 6/16/00 contained many grains larger than ~50  $\mu\text{m}$  (some were larger than 100  $\mu\text{m}$ ) as well as grains smaller than ~10  $\mu\text{m}$ . Many of the small grain appear to be attached to the larger grains. The number of grains between ~10 to ~50  $\mu\text{m}$  was small (Figure 10a). The Stage-1 (> 8.54  $\mu\text{m}$ ) sample collected at the downwind D1 site on 6/20/00 also contained many large grains (Figure 10b). However, the 6/20/00 sample generally contained more grains whose size varied in a continuous distribution up to ~100  $\mu\text{m}$ , compared to the 6/16/00 Stage-1 sample whose distribution was more bimodal. Unlike these two Stage-1 samples, large grains were rare in Stage-2 (4.26 – 8.54  $\mu\text{m}$ ) and Stage-3 (2.12 – 4.26  $\mu\text{m}$ ) samples collected at downwind D1 site on 6/20/00 (Figures 10c and 10d), indicating that particle bounce was minimal when the adhesive Cu-tape substrate was employed. The Stage-1 sample collected at site D2 on 6/20/00 included some large grains (up to 50  $\mu\text{m}$ ), but the number of large grains was small (Figure 10e). The Stage-1 sample collected at site D3 on 6/20/00, however, included many grains larger than ~50  $\mu\text{m}$  (Figure 10f). The SEM images document that the DRUM samplers near the Main Plant collected numerous very large particles on Stage-1. The Stage-2 (4.26 – 8.54  $\mu\text{m}$ ) and Stage-3 (2.12 – 4.26  $\mu\text{m}$ ) grain sizes observed by SEM are in agreement with the experimental DRUM size cuts (see Table 3).

Overall, the shape of grains in all samples observed was highly variable (many were angular, some were elongated or round). Many of the large grains were aggregates of smaller grains. No

ehedral quartz grains were found in any of the samples observed. Some grains in the Stage-1 sample collected at site downwind D1 on 6/16/00 were analyzed by energy-dispersive X-ray spectroscopy (EDS) (n=45, grains were both larger than  $\sim 50 \mu\text{m}$  and smaller than  $\sim 10 \mu\text{m}$ ). However, grains having a pure silica composition were not found in this sample that had the highest quartz concentration measured by XRD. Because a previous investigation of a cotton gin source located pure silica grains in the Stage-1 samples with relative ease, it was determined that use of the SEM for quantifying silicate mineral abundances was not a reliable technique for the sand and gravel source particles.

### 3.7 QUARTZ RELATIVE INTENSITY IN DRUM SAMPLES

Quartz and Particle Size Fraction. XRD diffraction patterns for the five DRUM stages collected at the downwind D1 site on 6/13 show obvious quartz peaks in the Stage-1 ( $> 8.54 \mu\text{m}$ ) and Stage-2 ( $4.26 - 8.54 \mu\text{m}$ ) samples, but the peak is difficult to quantify in the Stage-3 ( $2.12 - 4.26 \mu\text{m}$ ) and hard to identify in the Stage-4 ( $1.15 - 2.12 \mu\text{m}$ ) and “Stage-5” ( $0.07 - 1.15 \mu\text{m}$ ; combined Stages 5 to 8) samples (Figure 11a). Figure 11b shows peak area intensities for the quartz (101) plane (primary peak) of DRUM Stages-1 to -4 samples collected at the downwind D1 site on June 13, 16, and 20 (Stage-4 sample of 6/13/2000 was not quantified). Stage-1 samples collected on 6/16/00 and 6/20/00 showed much higher intensity (39300 and 32200 counts, respectively) than that collected on 6/13/00 (7520 counts). Those two samples also showed a much larger intensity dependence on sample orientation than the 6/13/00 sample (i.e., larger error bars, Figure 11b). Despite the difference in the Stage-1 values between sampling periods, the quartz peaks for the Stage-2 to -4 samples collected on all three days had quite similar and low values. For example, those of Stage-2 samples ranged from 990 to 3400 counts and Stage-3 and -4 samples were below the detection limit (value: 3349 counts). The trends with size fraction seen for quartz peak intensities were also observed for the quartz concentration data for different DRUM stages collected on June 13, 16, and 20 (Figure 11c).

The Stage-1 ( $> 8.54 \mu\text{m}$ ) samples consistently contained the most quartz and the quartz content decreased as grain size decreased (i.e., the number of stage increased). This observation has been made by previous researchers (e.g., see Table 2) and is as expected for airborne quartz –

it should occur in the larger grain sizes because it is formed by mechanical breakdown of larger mineral fragments. It should also be noted, however, that the very large grain sizes observed with SEM for Stage- 1 samples may affect interpretation of the XRD data. Because of the presence of large grains in Stage-1, the calibration curve that was developed using the quartz standard and resuspended PM<sub>10</sub> may not be directly applicable to the Stage-1 samples because grain size is known to affect diffraction peak intensity. Thus, the relative relationships between DRUM quartz concentrations presented in Figure 11c should be interpreted with caution because the Stage-1 concentrations may be either too high or too low because of grain size artifacts regarding XRD analysis. However, as discussed below, there was no consistent trend between the Stage-1 DRUM and Teflon PM<sub>10</sub> quartz concentration results for samples measured at different locations (See Section 3.8). Therefore, no systematic bias in the XRD analysis of the DRUM Stage -1 samples can be confirmed at this time.

Site-to-Site Variations. Figure 12 compares the quartz mass concentrations based on Stage-1 DRUM samples collected at all sampling sites on June 13, 16 and 20, 2000. On June 13, the mass concentrations at the upwind and downwind sites were not significantly different, within measurement error (Figure 12a). In contrast, samples collected at all downwind sites on 6/16/00 and 6/20/00 had higher peak intensities than the samples collected at the upwind site, which was close to the method detection limit (Figure 12b,c). Among the downwind samples on 6/16/00, the downwind D1 site sample intensity was about 4 times higher than samples from the other three downwind sites, whose intensities were the same within error. The upwind-downwind sample intensity pattern for 6/20/00 was similar to that for 6/16/00, except for a higher intensity at the D3 site relative to D2 and D4 (Figure 12c). The intensity of the quartz peak at the D3 site was 48% of that of downwind D1 and was significantly higher than the D2 and D4 samples. Interestingly, samples from the D3 site collected on these 6/16 and 6/20 showed a large intensity dependence on the orientation similar to that observed for the downwind D1 site samples. The reason for this variability in sample from two of the four downwind locations is unclear, but could be related to the fact that downwind D1 and D3 sites were closer to areas on the plant subject to higher levels of material moving activity by front-loader equipment (D2 was somewhat out of the way of this activity due to being located across the creek bed). However, the 6/13 data indicate that there was no overall systematic relationship between sampling

location and intensity variability during the Pilot Study (see Figure 12a, compare error bars on downwind D1 and D3).

### 3.8 TEFLON FILTER QUARTZ AND ELEMENTAL COMPOSITION

**Quartz.** The upwind and downwind PM<sub>10</sub> filter quartz concentrations were significantly different, but the mass fraction of quartz in PM<sub>10</sub> was indistinguishable between the upwind and downwind sites (Table 12). As mentioned above, PM<sub>2.5</sub> was below gravimetric detection limits in many samples collected (22 of 39) and whereas reliable quartz concentrations could be measured in some samples (i.e., 6/16/00, U1 and D1 were quantified), meaningful trends could not be elucidated between sampling locations with such sporadic data.

*Table 12. Average quartz mass detected by XRD, quartz concentration and quartz mass fraction in PM<sub>10</sub> collected on Teflon filters.*

	mass Q ( $\mu\text{g}$ )	Qtz ( $\mu\text{g}/\text{m}^3$ )	Qtz/PM <sub>10</sub> (%)	number of analyses
<b>U1</b>	<b>13.9</b>	<b>6.0</b>	<b>15.6</b>	<b>n = 3</b>
$\sigma$	<b>3.4</b>	<b>1.5</b>	<b>4.7</b>	
<b>D1 to D4</b>	<b>42.4</b>	<b>33.7</b>	<b>16.6</b>	<b>n = 13</b>
$\sigma$	<b>22.4</b>	<b>20.3</b>	<b>4.3</b>	

The Teflon PM<sub>10</sub> filter quartz concentrations varied as a function of sampling location (Figure 13), and the pattern between sites was generally similar to that observed for the DRUM Stage-1 samples. On 6/16/00, quartz concentrations downwind exceeded those measured at upwind U1 for D1, D2 and D3, but the D4 PM<sub>10</sub> quartz concentration was similar to that measured at the upwind site (Figure 13a). On 6/20/00, the DRUM sampler ran as one continuous sampling period whereas two Teflon filters were collected (AM and PM samples), therefore the patterns are more difficult to compare. However, it is interesting to note that on 6/20 the D1 sampler had the highest quartz concentrations both in the AM and PM filter samples (Figure 13b) and the

Stage-1 DRUM sample (Figure 12c). Also, the 6/20/00 data support the 6/16/00 observation that downwind concentrations at locations downwind D1, D2 and D3 were significantly higher than the concentration measured at the upwind site for both DRUM and Teflon samples. Note also that PM<sub>10</sub> filter mass concentrations did not track directly with quartz concentrations between sampling locations, especially over the shorter sampling periods on 6/20/00 (Figure 13). There was an overall linear relationship between both PM<sub>10</sub> mass concentration and PM<sub>10</sub> Si concentration with quartz concentration for the 15 PM<sub>10</sub> Teflon filters that were analyzed by XRD (Figure 14). These relationships suggest the possibility of apportioning elemental concentration data to individual mineral assemblages based on empirical mineral – elemental composition relationships. Such a technique would greatly improve the efficiency of determining crystalline silica concentrations in large numbers of PM samples, but would require a thorough research effort to assess its applicability to a wide range of sample compositions.

It is interesting to note that there was no consistent trend in the relationship between the Teflon and DRUM quartz concentrations between sampling stations. Teflon sample quartz concentrations ( $\mu\text{g m}^{-3}$ ) were lower, higher and approximately equal to the values measured in Stage-1 DRUM samples on 6/16/00. This observation suggests that there was no systematic bias due to the large grain sizes observed in the Stage-1 DRUM samples. Further investigation would be necessary to examine this issue in more detail.

**Elemental Composition.** Comparison of the upwind and downwind elemental composition of the PM<sub>10</sub> and PM<sub>2.5</sub> collected on Teflon filters was expected to provide a marker species for distinguishing source and background PM. Note that the D1 soil was collected from the pile of Plant product material and because X-ray diffraction analysis of resuspended bulk source material (=D1 site soil) showed identical mineralogy to the downwind D1 site PM<sub>10</sub> sample, elemental analysis of the Teflon PM<sub>10</sub> samples collected at D1 should be representative of the “source” elemental profile for fingerprinting comparisons. The PIXE and XRF elemental data were plotted as ratios of elements or sums of elements because large differences in elemental concentrations occurred between upwind and downwind samples. The ratios give the best chance for identifying an elemental signature that is characteristic of the source or of the upwind background PM composition. Because the downwind D4 site was most remote from the Main

Plant source area, it was expected that the upwind U1 and downwind D4 samples would be most similar. In other words, of all the downwind samples, D4 should have the highest “ambient PM” component and this ambient PM composition should be represented by the upwind U1 composition. This was in fact observed for some elemental ratios as discussed below.

The different elemental ratios examined were selected to identify known soil mineral groups and were plotted as averages for the upwind (U1) and for each individual downwind site (D1 to D4) (Figure 15). The average ratio for all filters collected at each location was plotted with one standard deviation error bar based on all the samples collected at a given location over the Pilot Study period (see Tables 8 & 10). The following observations were made based on the elemental data:

1. The elemental ratio differences were greater for PM<sub>2.5</sub> than for PM<sub>10</sub> (compare Figure 15a to 15b).
2. PM<sub>2.5</sub> from upwind U1 had significantly higher S/Fe than the four downwind samples (Figure 15b), but this trend was less well-defined for PM<sub>10</sub> (Figure 15a).
3. S/H was higher at upwind U1 and D4 than at other locations for both PM<sub>2.5</sub> and PM<sub>10</sub>.
4. The PM<sub>2.5</sub> (Zn+Cu)/Fe was higher at upwind U1 and D4 than at other locations.
5. Compared to all other locations, D4 had significantly lower Si/Al ratio for PM<sub>10</sub> but not for PM<sub>2.5</sub>.

Thus, there were four elemental ratios where the upwind and downwind samples showed significant differences: S/Fe, (Zn+Cu)/Fe, K/H and S/H. The ratios based on reconstructed components (see Equation 11, Section 2.6.2) such as BABS/RCMA, soot/soil, soot/RCMA, OMH/RCMA and S/soil were not significantly different between upwind and downwind locations. Figure 15 also clearly shows that the elemental ratio profiles of samples from downwind D1 and downwind D2 were very similar to each other, downwind D3 was intermediate (especially for PM<sub>2.5</sub>), and samples from upwind U1 and downwind D4 were also quite similar to one another (Figure 15, pattern of first four ratios).

### **3.9 DISTINGUISHING BACKGROUND AND SOURCE CRYSTALLINE SILICA**

A major objective of the Pilot Study was to develop a technique for quantifying the amount of background (“natural”) crystalline silica in the downwind samples. Making this distinction between background and source CS is important because of the abundance of quartz in the natural environment. For the stationary source sampled during the Pilot Study, the following factors leave little doubt that the sand and gravel plant was the source of the quartz measured in the downwind samples:

1. The wind direction was very constant during all sampling tests and the upwind sampler was therefore a reliable measure of background PM composition.
2. The downwind quartz and PM concentrations were very consistent at a given sampling location from day-to-day and were significantly higher than the upwind concentrations.
3. The lidar detected intense plumes that originated at the Main Plant and dispersed with distance away from the plant. The lidar scans indicate the plumes extend continuously for a distance of at least 400 m from the Main Plant.
4. As discussed above, the downwind D4 sampler was farthest (~ 500m) from the Main Plant and PM collected from this location had elemental signatures that most closely agreed with the signatures measured for the upwind location. However, the downwind D4 quartz concentrations determined by XRD were significantly above background concentrations on both 6/16 and 6/20, indicating that D4 was still significantly impacted by the CS source.

### **4.0 CONCLUSIONS – Sampling Limitations & Future Work**

**Sampling Limitations.** The Pilot Study results highlight several crystalline silica sampling and analysis issues. First, as outlined below, the two sample collection methods used in the Pilot Study – the 8-stage DRUM impactor and IMPROVE samplers with Teflon filters – both have limitations for accurately quantifying airborne CS concentrations. Second, scanning electron

microscopy (SEM) did not prove to be a useful technique for identifying quartz in the Pilot Study samples due to the mixed-mineral nature of individual grains from the sand and gravel plant.

The proposed DRUM sampling technique was found to have numerous problems. These included: (1) the lack of suitable PM<sub>10</sub> inlet resulted in very large grains in Stage-1 samples that could affect use of the PM<sub>10</sub> XRD calibration curve; (2) the low flow rates (~ 1 Lpm) resulted in low mass loadings and poorer quality XRD crystalline silica measurement, especially for particles below ~ 2 μm; (3) the DRUM Cu-tape substrate, while preventing particle bounce, had a variable XRD background intensity that depended on how wrinkled the tape surface was prior to analysis; and (4) the DRUM sampler cannot be used to quantify PM mass.

The problem with the IMPROVE sampling technique was that direct XRD analysis of the PM on the stretched Teflon filter was not feasible due to the high background from the Teflon. Therefore, analysis of the Teflon filter PM<sub>10</sub> by XRD was performed after transfer of the deposit to a silver membrane filter. This observation is in contrast to previous researchers who analyzed lightly loaded Teflon filters directly by XRD (Davis and Johnson, 1982). Differences in the nature of the Teflon filters employed must explain this discrepancy. Furthermore, for studies at sites suitable for SEM automated qualitative analysis for quartz, the Teflon filter substrate is inadequate and unstable for scanning electron microscopy imaging because it is non-conductive and vaporizes under the electron beam.

Despite the sampling limitations, analysis of the Teflon filter PM<sub>10</sub> by XRD after transfer of the deposit to a silver membrane filter gave consistently good X-ray diffraction peak intensities with lower background than the Cu-tape. For the Pilot Study site, downwind quartz concentrations consistently exceeded those measured in upwind samples for both the DRUM and Teflon filter samples. Elemental ratios based on PIXE data for the Teflon filter samples showed distinct differences between the near-source downwind sampling locations D1, D2 and D3 and the farthest downwind location, D4. The D4 elemental signature for PM<sub>2.5</sub> was most similar to the upwind U1 signature, indicating that D4 had the lowest contribution of source material of all the downwind samples. This is expected and suggests that at distances greater than 500 m from sources similar to that studied here, it will be increasingly difficult to distinguish source and background crystalline silica. Coincidentally, the plumes measured with the lidar as originating from the Main Plant were on average ~ 400 m in length.

**Future Sampling Recommendations.** Future efforts to quantify the CS concentrations downwind of sources in California should incorporate the following recommendations from the Air Resources Board:

1. Compare NIOSH Method 7500 (using PVC filters) to the Teflon filter method used in the Pilot Study. Distinguish which method achieves the best results when comparing near-source concentrations to background concentrations.
2. Investigate near-source emissions from other facilities such as glass recycling, asphalt, construction sites, etc.

## **5.0 ACKNOWLEDGMENTS**

This work benefited from the diligent work of researchers and resources at Crocker Nuclear Laboratory, Land Air and Water Resources and the Department of Geology at UC Davis. In particular, special thanks to Teresa James, Chris Jannusch and Barry Goodrich (U. Texas) for sitting out the heat in Tracy and keeping the samplers running; to Krystyna Trzepla-Nabaglo for lidar data analysis; Mike Brown and Omar Carvacho for soil sampling and resuspension chamber training; Tom Cahill for DRUM sampler use and Bob Flocchini for additional financial support. The PI also thanks Linda Mazur, currently with OEEHA, for her extensive site investigations without which the project would never have gotten off the ground. The ARB Contract Manager for this work was Nehzat Motallebi.

## **6.0 REFERENCES CITED**

Air Control Techniques, P.C., 1997. PM<sub>2.5</sub> and PM<sub>10</sub> Ambient Air Monitoring at the Martin Marietta Benson, North Carolina Stone Crushing Plant, Air Control Techniques, P.C., Cary, North Carolina.

- Air Control Techniques, P.C., 1998. PM<sub>2.5</sub> Ambient Air Monitoring at the CAMAS Colorado, Inc. Morrison, Colorado Stone Crushing Plant, Air Control Techniques, P.C., Cary, North Carolina.
- Bond, T.C., Anderson, T.L. and Campbell, D., 1999. Calibration and Intercomparison of Filter-based Measurements of Visible Light Absorption by Aerosols. *Aerosol Sci. Technol.*, 30: 582-600.
- Cahill, T.A., 1995. Compositional analysis of atmospheric aerosols. In: S.A.E. Johansson, J.L. Campbell and K.G. Malmqvist (Editors), *Particle-Induced X-Ray Emission Spectrometry*. Chemical Analysis Series Vol. 133. John Wiley & Sons, Inc., New York.
- Cahill, T.A. et al., 1981. Comparisons between size-segregated resuspended soil samples and ambient aerosols in the western United States, *Atmospheric Aerosol: Source/Air Quality Relationships*. ACS Symposium Series # 167. American Chemical Society, Washington, D.C., pp. 269-285.
- Cahill, T.A., Eldred, R.A., Flocchini, R.G. and Barone, J., 1977. Statistical techniques for handling PIXE data. *Nuclear Instruments and Methods*, 142: 259-261.
- Cahill, T.A., Eldred, R.A., Motallebi, N. and Malm, W.C., 1989. Indirect measurement of hydrocarbon aerosols across the US by nonsulfate hydrogen-remaining gravimetric mass correlations. *Aerosol Sci. Technol.*, 10: 421-429.
- Campbell, D., Copeland, S. and Cahill, T., 1995. Measurement of Aerosol Absorption Coefficient from Teflon Filters Using Integrating Plate and Integrating Sphere Techniques. *Aerosol Sci. Technol.*, 22: 287-292.
- Carvacho, F.O., Ashbaugh, L.L. and Flocchini, R.G., 1996. Characteristics of the UC Davis Dust Resuspension Test Chamber, The American Association for Aerosol Research, Fifteenth Annual Conference. October 14 - 18, 1996, Orlando, Florida.
- CEIDARS, 1999. California Emission Inventory Development and Reporting System. California Air Resources Board.
- Chung, F.H., 1974a. Quantitative interpretation of X-ray diffraction patterns of mixtures. I. Matrix-flushing method for quantitative multicomponent analysis. *J. Appl. Cryst.*, 7: 519-525.
- Chung, F.H., 1974b. Quantitative interpretation of X-ray diffraction patterns of mixtures. II. Adiabatic principle of X-ray diffraction analysis of mixtures. *J. Appl. Cryst.*, 7: 526-531.

- Chung, F.H., 1975. Quantitative interpretation of X-ray diffraction patterns of mixtures. III. Simultaneous determination of a set of reference intensities. *J. Appl. Cryst.*, 8: 17-19.
- Crosby, M.T. and Hamer, P.S., 1971. The determination of quartz on personal sampler filters by X-ray diffraction. *Ann. Occup. Hyg.*, 14: 65-70.
- Davis, B.L., 1978. Additional suggestions for X-ray quantitative analysis of high-volume filter samples. *Atmos. Environ.*, 12: 2403-2406.
- Davis, B.L., 1981a. Quantitative analysis of crystalline and amorphous airborne particulates in the Provo-Orem vicinity, Utah. *Atmos. Environ.*, 15: 613-618.
- Davis, B.L., 1981b. A study of the errors in X-ray quantitative analysis procedures for aerosols collected on filter media. *Atmos. Environ.*, 15: 291-296.
- Davis, B.L. and Jixiang, G., 2000. Airborne particulate study in five cities of China. *Atmos. Environ.*, 34: 2703-2711.
- Davis, B.L. and Johnson, L.R., 1982a. On the use of various filter substrates for quantitative particulate analysis by X-ray diffraction. *Atmos. Environ.*, 16(2): 273-282.
- Davis, B.L. and Johnson, L.R., 1982b. Sample preparation and methodology for X-ray quantitative analysis of thin aerosol layers deposited on glass fiber and membrane filters. *Adv. X-ray Anal.*, 25: 295-300.
- Davis, B.L., Johnson, L.R., Stevens, R.K., Courtney, W.J. and Safriet, D.W., 1984. The quartz content and elemental composition of aerosols from selected sites of the EPA Inhalable Particulate Network. *Atmos. Environ.*, 18(4): 771-782.
- Drees, L.R., Wilding, L.P., Smeck, N.E. and Senkayi, A.L., 1989. Silica in Soils: Quartz and disordered silica polymorphs. In: J.B. Dixon and S.B. Weed (Editors), *Minerals in Soil Environments*. Soil Science Society of America, Madison, WI, pp. 913-974.
- Eldred, R.A., Cahill, T.A. and Flocchini, R.G., 1997. Composition of PM<sub>2.5</sub> and PM<sub>10</sub> aerosols in the IMPROVE network. *J. Air & Waste Manage. Assoc.*, 47: 194-201.
- Eldred, R.A., Cahill, T.A., Pitchford, M. and Malm, W.C., 1988. IMPROVE- A new remote area particulate monitoring system for visibility studies, Air Pollution Control Association 81st Annual Meeting, Dallas, TX, pp. Paper 88-54.3.
- Eldred, R.A. et al., 1990. Measurement of fine particles and their chemical components in the IMPROVE/NPS network. In: C.V. Mathai (Editor), *Visibility and Fine Particles*. Air & Waste Management Association, pp. 187-196.

- Eldred, R.A., Cahill, T.A., Wilkinson, L.K., Feeney, P.J. and Malm, W.C., 1989. Particulate characterization at remote sites across the U.S.: First year results of the NPS/IMPROVE network, Air & Waste Management Association 82nd Annual Meeting. Air & Waste Management Association, Anaheim, CA, pp. 89-151.3.
- Esteve, V., Ruis, J., Ochando, L.E. and Amigo, J.M., 1997. Quantitative X-ray diffraction phase analysis of coarse airborne particulate collected by cascade impactor sampling. *Atmos. Environ.*, 31(23): 3963-3967.
- Fukasawa, T., Iwatsuki, M. and Tillekeratne, S.P., 1983. X-ray diffraction analysis of airborne particulates collected by an Andersen sampler. Compound distribution vs. particle size. *Environ. Sci. Technol.*, 17: 596-602.
- Holmén, B.A., Eichinger, W.E. and Flocchini, R.G., 1998. Application of elastic lidar to PM<sub>10</sub> emissions from agricultural nonpoint sources. *Environ. Sci. Technol.*, 32: 3068-3076.
- IARC, 1987. Silica and some silicates, International Agency for Research on Cancer, Lyon, France.
- James, T.A., Fan, T.W.-M., Higashi, R.M. and Flocchini, R.G., 2000. Size and elemental characterization of dust from agricultural sources, Second international conference on air pollution from agricultural operations specialty conference, St. Joseph, MI.
- John, W. and Reischl, G., 1980. A cyclone for size-selective sampling of ambient air. *APCA Journal*, 30: 872-876.
- Lorberau, C.D. and Abell, M.T., 1995. Methods used by the United States National Institute for Occupational Safety and Health to monitor crystalline silica. *Scand. J. Work Environ. Health*, 21(suppl 2): 35-38.
- Morgan, L.E. and DiCarlo, L., 1994. Quantitative determination of respirable quartz in bulk samples of organoclay by combined air classification/ X-ray diffraction. *Analytica Chimica Acta*, 286: 81-86.
- Nieuwenhuijsen, M.J., Noderer, K.S., Schenker, M.B., Vallyathan, V. and Olenchock, S., 1999. Personal exposure to dust, endotoxin and crystalline silica in California agriculture. *Ann. occup. Hyg.*, 43(1): 35-42.
- Perkins, R.L., Ennis, J.T. and Greene, L.C., 1998. PM<sub>10</sub> Compositional Analyses by Polarized Light Microscopy and X-ray Diffraction, Job Number 388. 91C-7048-10A, Research Triangle Institute, Research Triangle Park, NC.

- Raabe, O.G., Braaten, D.A., Axelbaum, R.L., Teague, S.V. and Cahill, T.A., 1988. Calibration studies of the DRUM impactor. *J. Aerosol Sci.*, 19(2): 183-195.
- Richards, J., Brozell, T., Palm, B. and Holder, T., 1998.  $PM_{2.5}$  Upwind-Downwind Ambient Air Monitoring at the Luck Stone Corporation Leesburg, Virginia Stone Crushing Plant. ACTPC Job Number 424, Air Control Techniques, P.C., Cary, North Carolina.
- Schwartz, J., Dockery, D.W. and Neas, L.M., 1996. Is daily mortality associated specifically with fine particles? *J. Air & Waste Manage. Assoc.*, 46: 927-939.
- Sturges, W.T., Harrison, R.M. and Barrie, L.A., 1989. Semi-quantitative X-ray diffraction analysis of size fractionated atmospheric particles. *Atmos. Environ.*, 23(5): 1083-1098.

## RECOMMENDATIONS

### Field Studies

Before crystalline silica is listed as a Toxic Air Contaminant by the California Air Resources Board, significantly more work needs to be done to understand the potential impacts of crystalline silica sources on human health. Critical to this effort is quantifying the concentrations of CS downwind of large non-point sources such as sand and gravel plants, quarries, construction sites, etc. The literature review conducted as part of the Pilot Study clearly shows that further field sampling near CS sources is necessary in order to quantify actual emissions from these sources. The two published near-source studies that quantified crystalline silica (Davis, 1981a and Air Control Techniques, 1997) suffer from very few sampling locations downwind of the source and lack of replicate samples.

Further, it should be recognized that a ground-level sampling program would not necessarily be able of quantifying all of the emissions from large-area sources such as the plant studied here because a significant fraction of the fugitive dust is emitted above the height of the samplers (see Pilot Study Lidar data). There is potential, therefore, for long-range transport of the dust beyond the 500 m distance studied here. *Future studies should be designed to sample at multiple vertical heights at multiple downwind locations so more accurate CS concentrations and emission factors can be quantified.* UCD researchers routinely sample ground-based PM sources at three sampling heights (at 1, 3 and 9 meters) using 10 m towers. Addition of another sampler at ~5 m would allow quantification of PM (and corresponding CS) emission factors from the sand and gravel plant sources. The drawbacks associated with sampling on towers include increased sampler footprint at the site, the need for additional samplers at each downwind location as well as the time it takes to raise and lower the towers to change samples or measure flows.

While the lidar added significantly to the Pilot Study project in terms of characterizing the fugitive dust plumes from the site, the onerous logistical requirements for siting the lidar instrument probably outweigh the benefits in terms of quantifying crystalline silica. Therefore, it

is recommended that future studies be performed with PM samplers and the meteorological tower only.

During the field sampling, *the field team should make every effort to quantify the level of activity at the site on an hourly basis.* Data such as number of trucks entering the site and identifying the locations of activity within the site hour-by-hour would enable comparisons to be made between the PM results at each downwind location and site activity. Relationships such as these could be used to improve overall plant emissions estimates.

## Sampling Methods

Comparison of the Pilot Study DRUM impactor and the PM Teflon filter results indicates that the Teflon filter sampling technique has the following advantages:

1. Allows accurate total mass quantification (PM<sub>10</sub> and PM<sub>2.5</sub>),
2. Allows field personnel to use routine PM sampling equipment and techniques,
3. Samples can be analyzed by non-destructive PIXE, PESA and XRF techniques to give trace element fingerprint of upwind and downwind samples,
4. Sample mass is easily transferred from Teflon filter to silver membrane filter for X-ray diffraction analysis for crystalline silica. The silver membrane filters have lower X-ray background than the copper tape impactor substrate used in the Pilot Study.
5. Quartz is easily detectable in PM<sub>10</sub> samples collected over periods less than ~ 7 hours (longer sampling times may be required for reproducible PM<sub>2.5</sub> quantification by X-ray diffraction (see below)),

Because of these advantages and the fact that the sample flow rate is > 10 x higher for the Teflon filters, *future studies should employ the Teflon filter sampling technique.* No significant improvement in CS detectability was gained by size-fractionating the aerosols using the DRUM impactors in the Pilot Study because quartz was easily detected in the bulk PM<sub>10</sub> samples. Further, it is expected that PM<sub>10</sub> samples will generally have higher quartz mass than the PM<sub>2.5</sub> fraction due to the nature of quartz genesis.

Note that the NIOSH Method 7500 calls for use of PVC filters that can be ashed or dissolved in solvent prior to sample transfer to silver membrane filters. The disadvantage of the polycarbonate filters is that determination of the PIXE fingerprint would not be possible using routine techniques such as those used at UC Davis. *For research studies such as the current one where one objective is to distinguish background from source quartz, the source fingerprint is important.* So, development of PIXE/XRF analysis fingerprinting methods for other types of filters might be worthwhile, if PVC filters are used for sampling.

## Sample Analysis

X-ray diffraction is really the only reliable technique for determining crystalline silica in PM samples. Drawbacks of XRD include long analysis times, sensitivity to sample preparation methodology, and the requirement of determining sample mass absorption effects for accurate quantification. For the Pilot Study, resuspended source material served as the XRD standard material, thus eliminating the need for separate determination of the mixture's mass absorption coefficient. Therefore, *in future studies collection of source material followed by resuspension for use in XRD calibration is recommended.*

The main drawback of XRD analysis is the sample analysis time because this affects the overall project cost (see below). The Pilot Study employed 75-minute analyses at each of four sample orientations and therefore involved extensive use of a single XRD instrument. Fortunately, there were few other users of this particular instrument, but in other situations access may not be available and therefore the timeliness of sample analysis and data reporting will be affected.

## Budget

The budget allocated for the Pilot Study was inadequate. Personnel and instrument time for sample analysis required at least 50% more time than the budget permitted. The PI's time for sampling and report preparation was also significantly more than budgeted. Future studies should be aware of the time commitment required to analyze the bulk resuspended material, pure standards, and samples and to synthesize all the data.

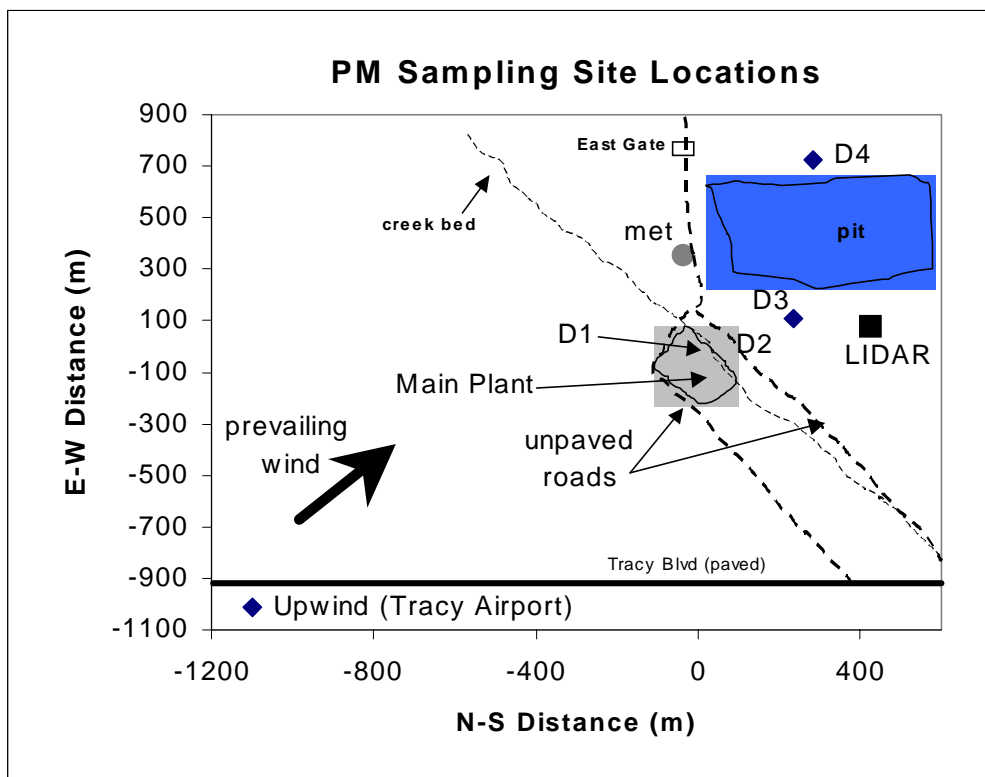
## Phase 2

Regarding Phase 2 of the Technical Proposal, *it is recommended that the project be scaled back to focus solely on crystalline silica sources rather than adding fine mineral fibers to the analytical scope.* The resources are available to sample and analyze a maximum of 2 additional sites one time each or one additional site in both the wet and dry seasons. The Pilot Study should also be re-sampled during the wet season in order to understand annual variability in emissions. It is expected that emissions will be highest in the hot, dry summer months for sources similar to the Pilot Study site and therefore the results reported here should be considered worst-case for this site.

## Silicon – Quartz Relationship

Future investigations should also more closely examine the relationship between the bulk silicon concentration and the quartz concentration. If an empirical relationship can be obtained between Si and Q (or quartz + cristobalite for sites where cristobalite occurs) for a range of crystalline silica source types, then routine PM sampling/PIXE analyses combined with ‘spot-check’ XRD analyses for quartz could greatly expand estimates of airborne crystalline silica concentrations. Caution must be used however in applying such relationships to sources with different mineral assemblages, but the payoff for such work could be significant.

Figure 1. Relative locations of the sampling sites during Pilot Study at the sand and gravel plant. The origin of the coordinate system (0,0) was the pile of road base product material that was sampled for soils analysis and PM<sub>10</sub> resuspension. The shaded area around D1 sampler encompasses the Main Plant.



Arrows show lidar azimuths for 2D vertical scans:

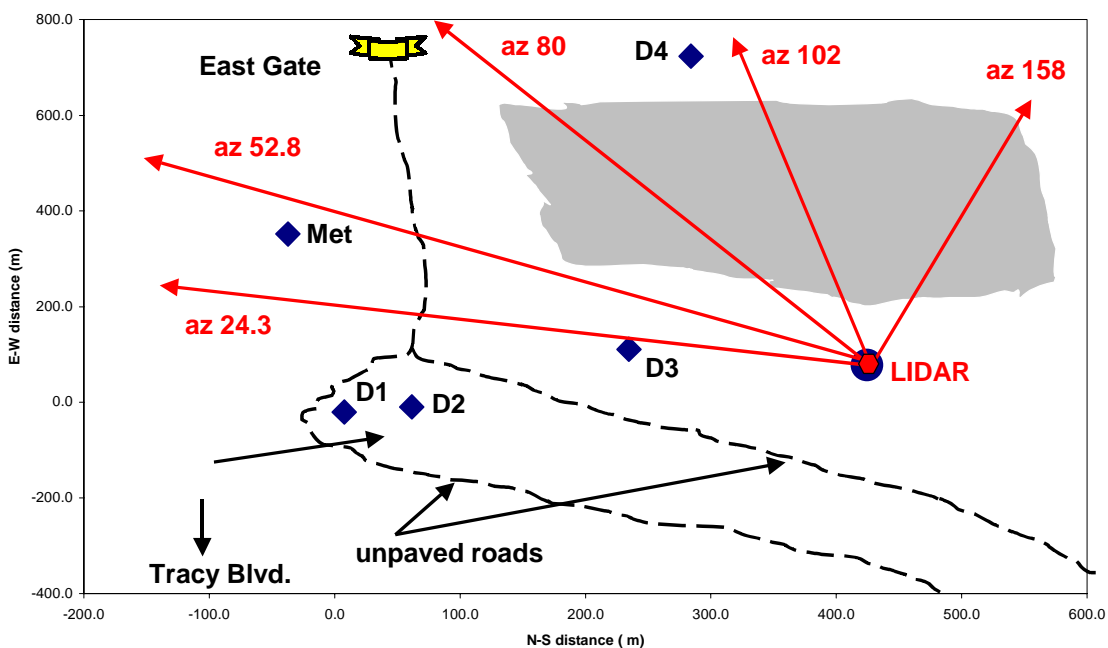


**Figure 2: X-ray diffraction intensity ratio  $I(Q)/I(TiO_2)$  vs.  $PM_{10}/TiO_2$  mass-ratio plot in internal reference analysis for the determination of quartz content in  $PM_{10}$  from downwind D1 site soil (see Sections 2.5.1 and 2.5.4 in text) . Filled circles: quartz primary/ $TiO_2$  primary peak ratio, Open circles: quartz secondary/ $TiO_2$  primary peak ratio  $\times 10$ . Regression lines given by Equation (7) and Equation (8) (multiplied by 10) are also shown.**

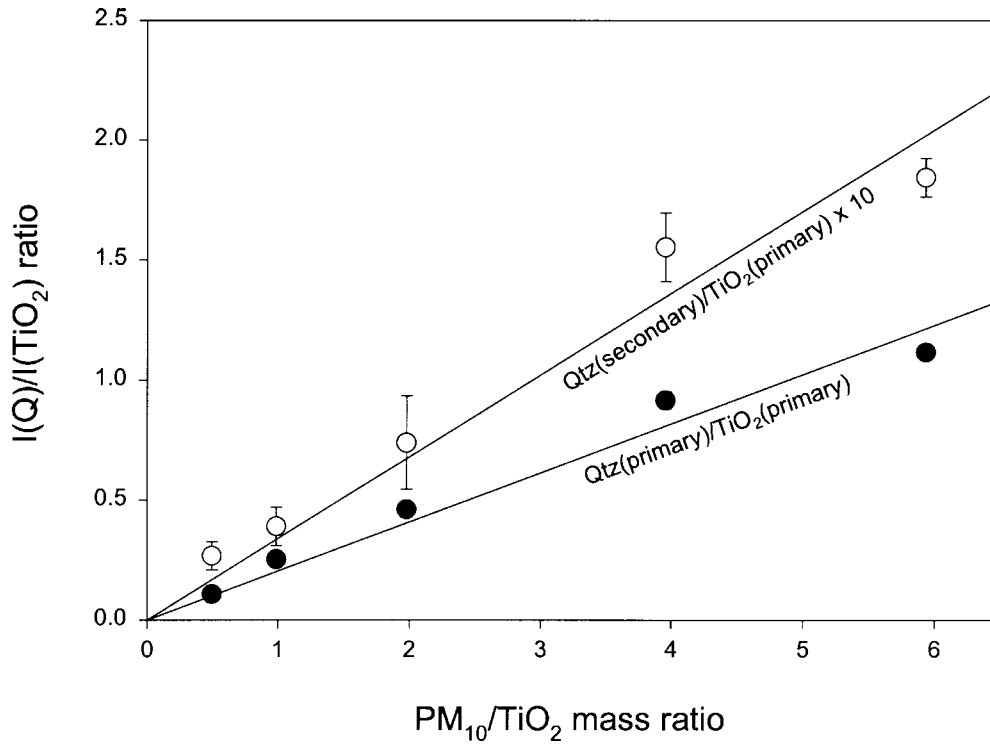


**Figure 3: Calibration curve for quartz quantification by XRD. Filled circles: PM<sub>10</sub> on Cu-tape; Open circles: pure quartz standard on Cu-tape. Straight lines are regression lines given by Equations (9) and (10). Quartz mass for PM<sub>10</sub> was calculated by multiplying the mass of PM<sub>10</sub> by 0.163. All points were measured in duplicate or triplicate and each was measured at four perpendicular orientations. A single sample of pure quartz prepared on a silver membrane filter is shown to fall on the same line as pure quartz on Cu-tape, thereby confirming that substrate composition had no significant effect on the calibration curve.**

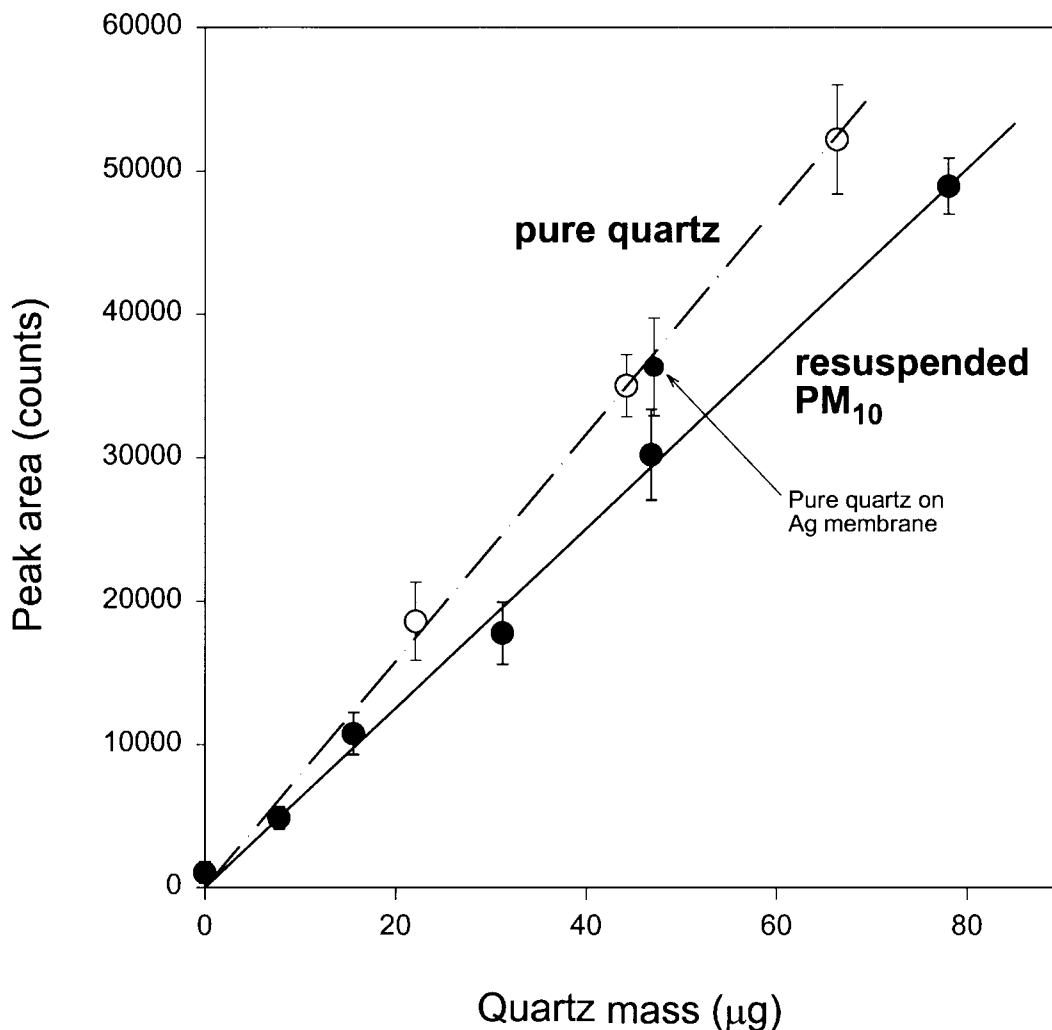


Figure 4. Meteorological data for Pilot Study. All data collected is plotted.

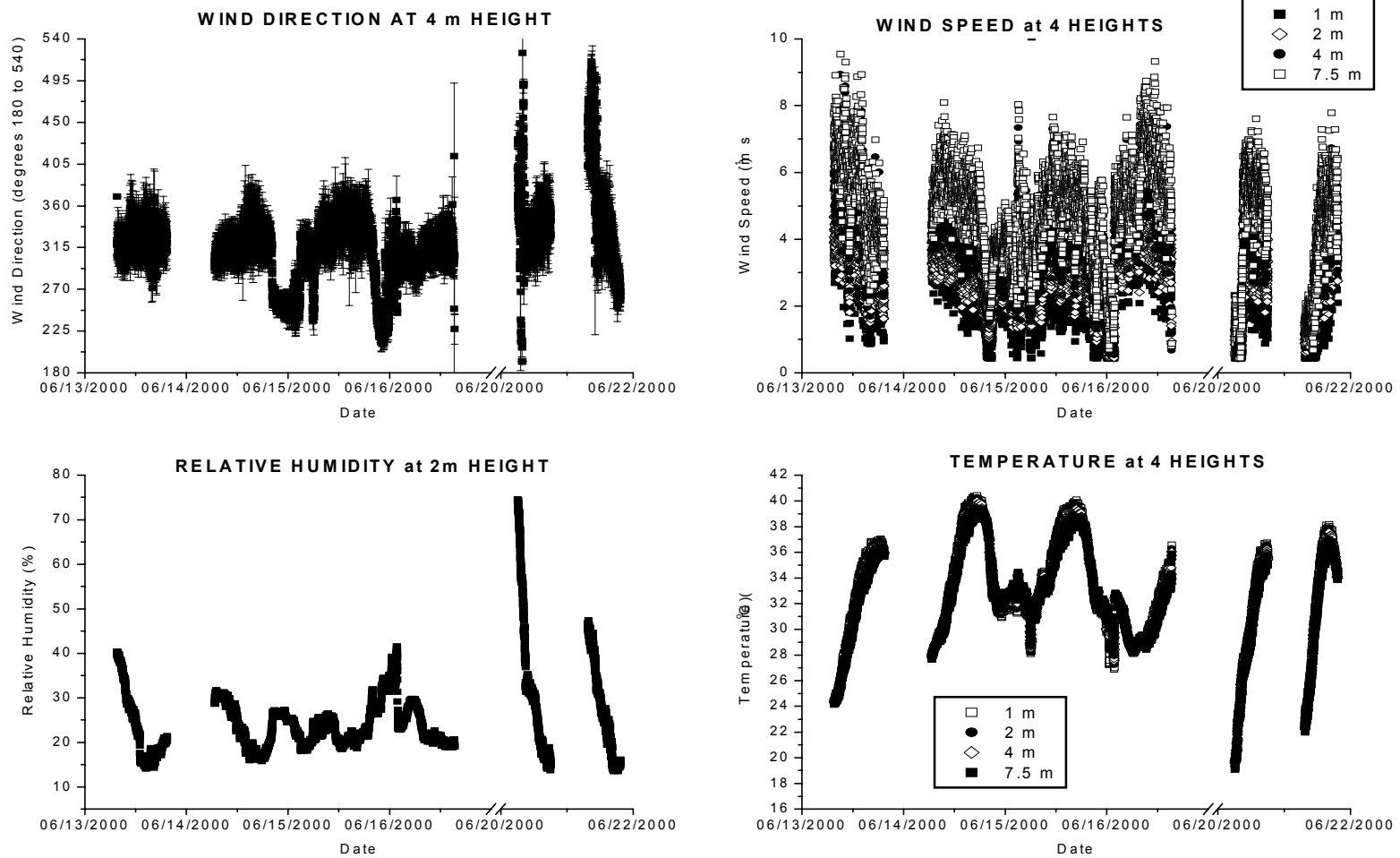
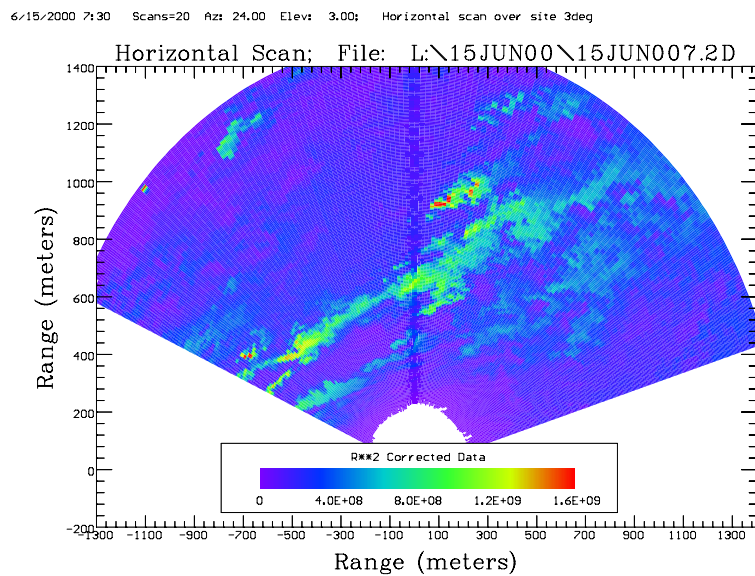
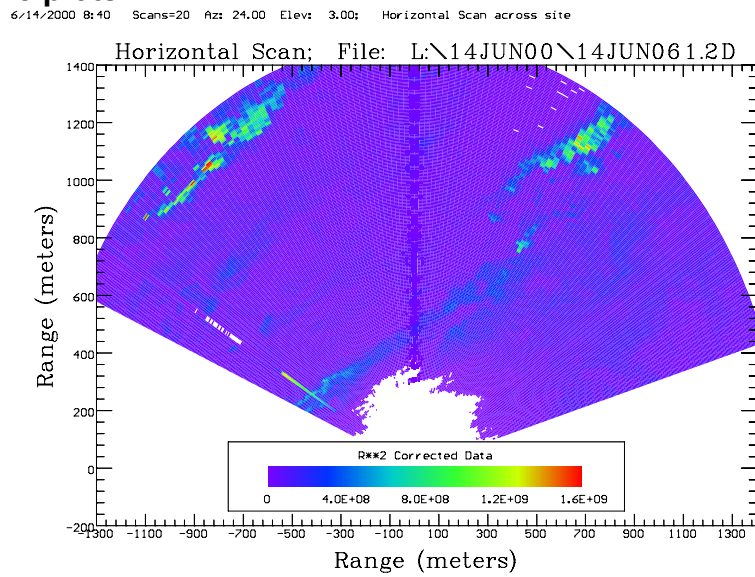
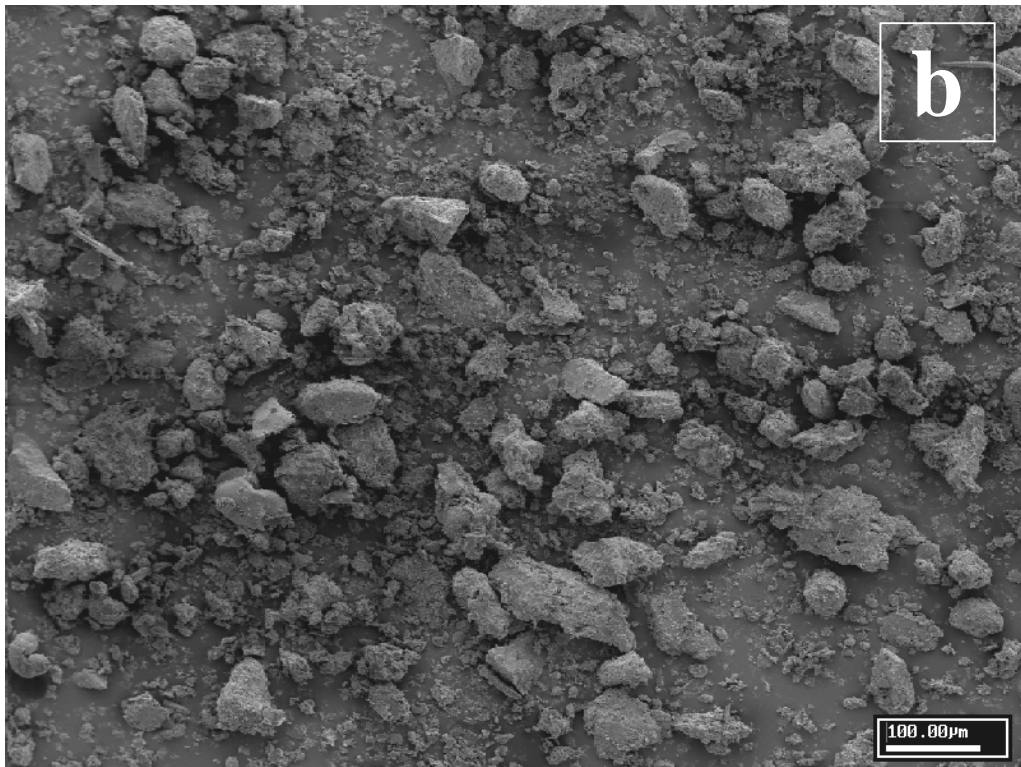
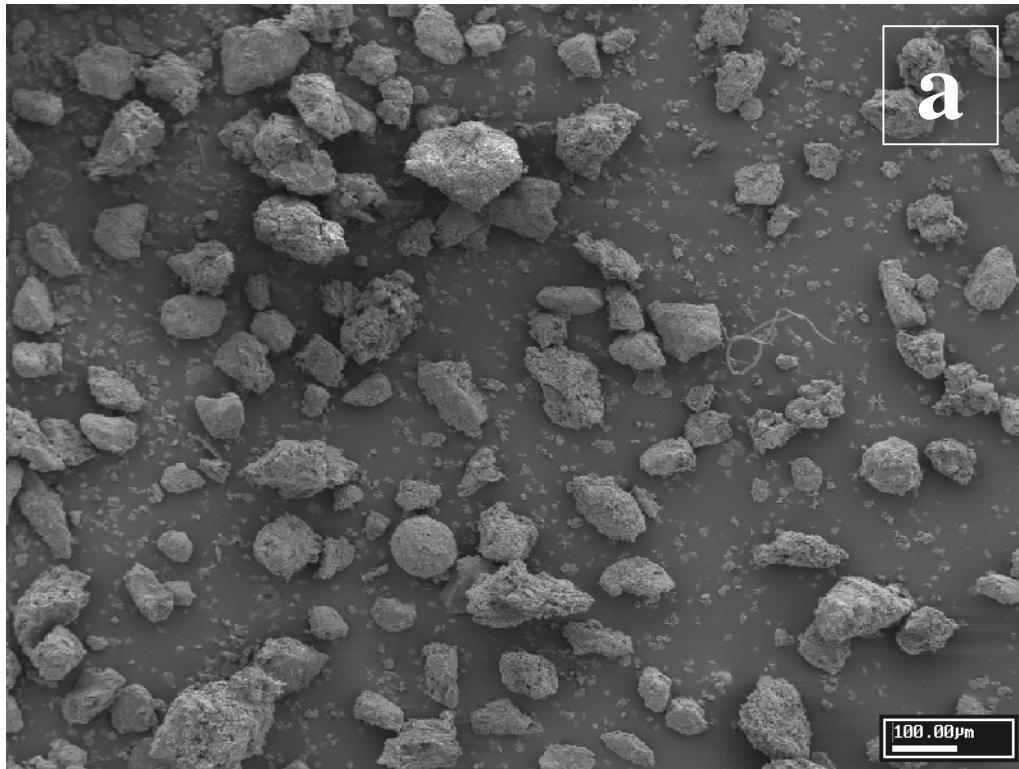


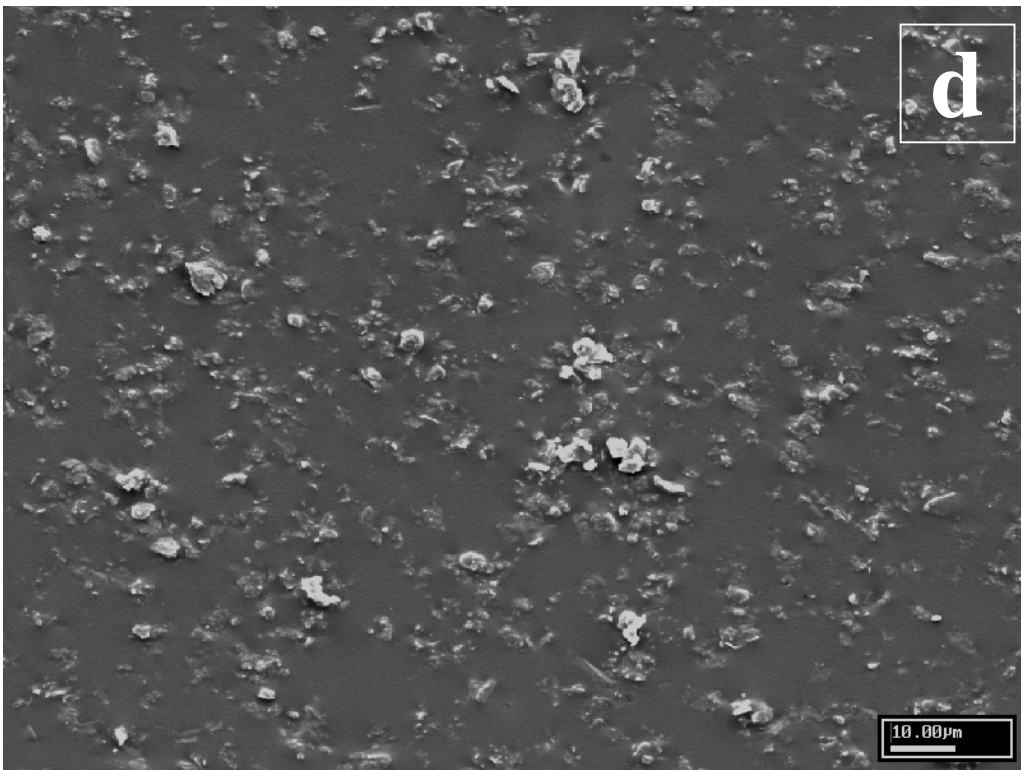
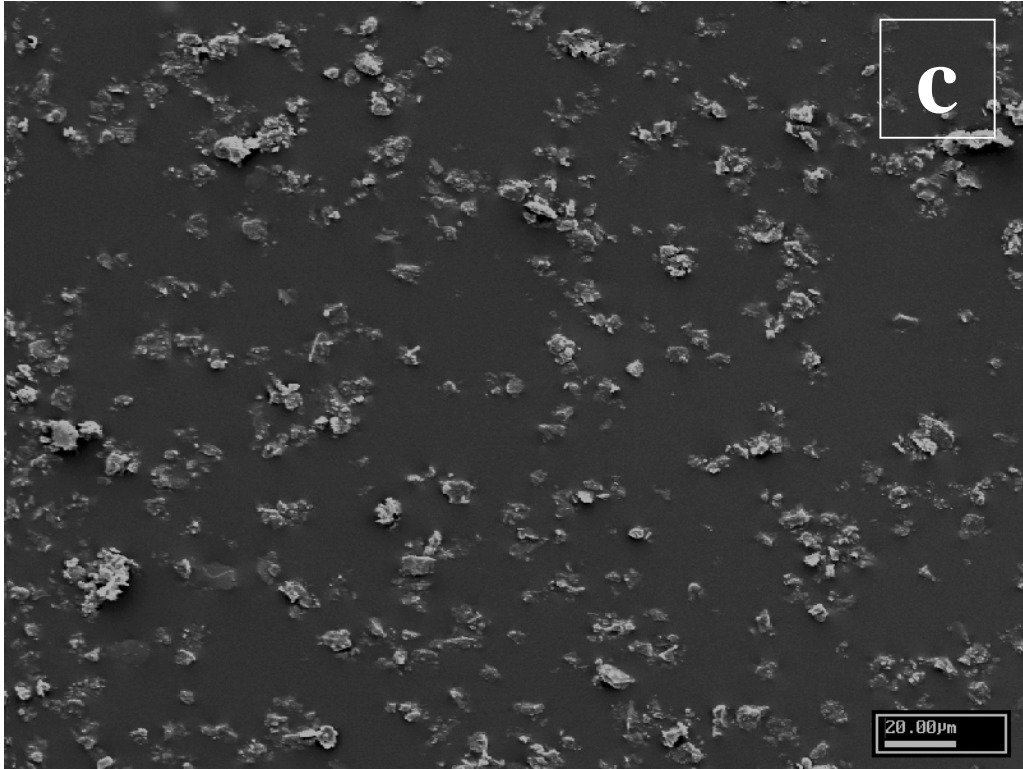
Figure 5a. Lidar horizontal scans (3d elevation angle) on June 14 and June 15, 2000. The lidar was located at (0,0) in the range coordinates of the plots. The lidar scanned from 24 to 158 degrees azimuth downwind of the Main Plant (see Figure 1). The dust plumes originating from the plant start near coordinates (-500,200) on the plots.



**Figure 10 (next 3 pages). Scanning electron microphotographs of DRUM samples:**

- a: Stage-1 (>8.54  $\mu\text{m}$ ) sample at D1 site (6/16/00),**
- b: Stage-1 (>8.54  $\mu\text{m}$ )sample at D1 site (6/20/00),**
- c: Stage-2 (4.26 – 8.54  $\mu\text{m}$ )sample at D1 site (6/20/00),**
- d: Stage-3 (2.12 – 4.26  $\mu\text{m}$ )sample at D1 site (6/20/00),**
- e: Stage-1 (>8.54  $\mu\text{m}$ )sample at D2 site (6/20/00),**
- f: Stage-1 (>8.54  $\mu\text{m}$ )sample at D3 site (6/20/00)**





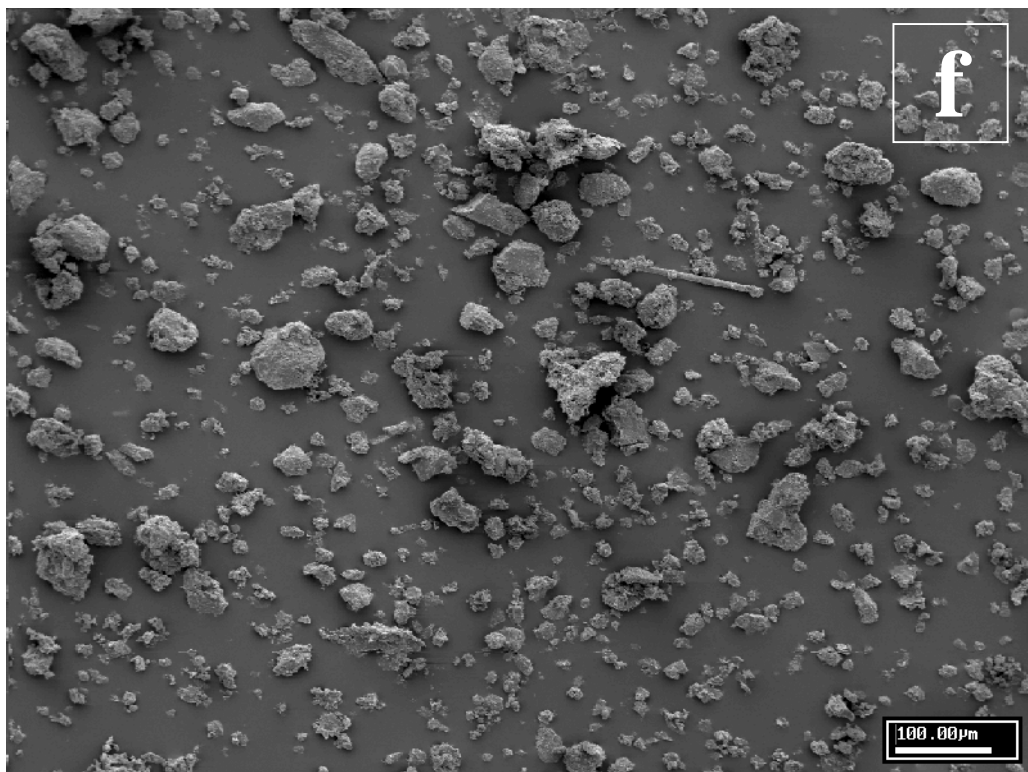
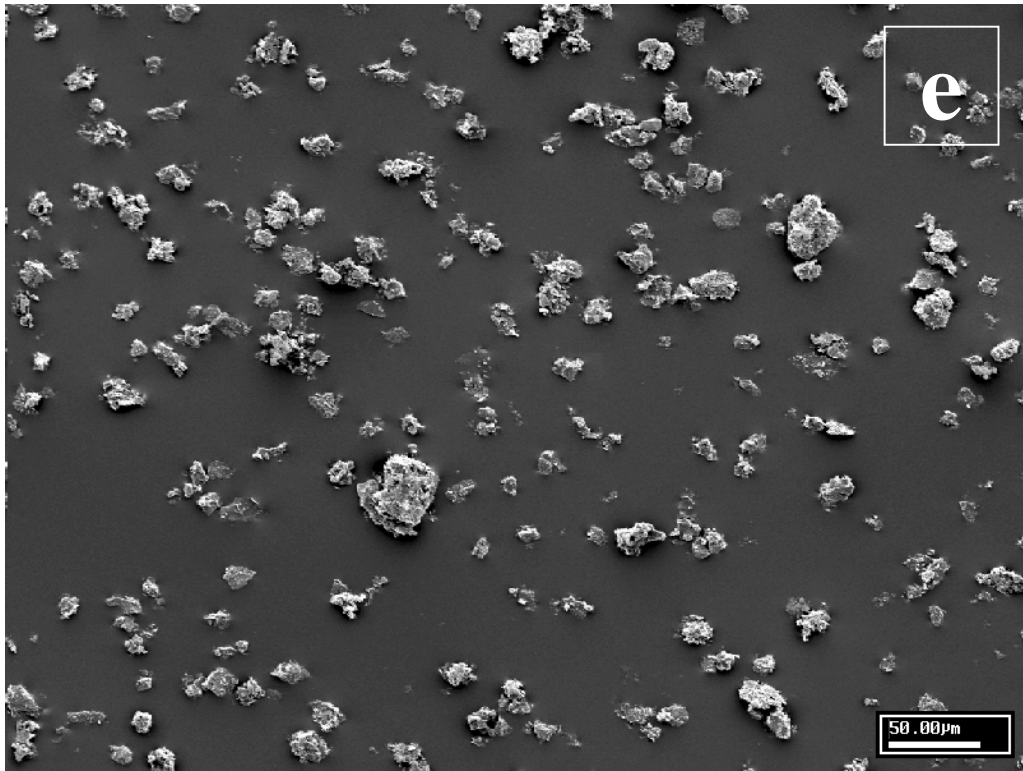
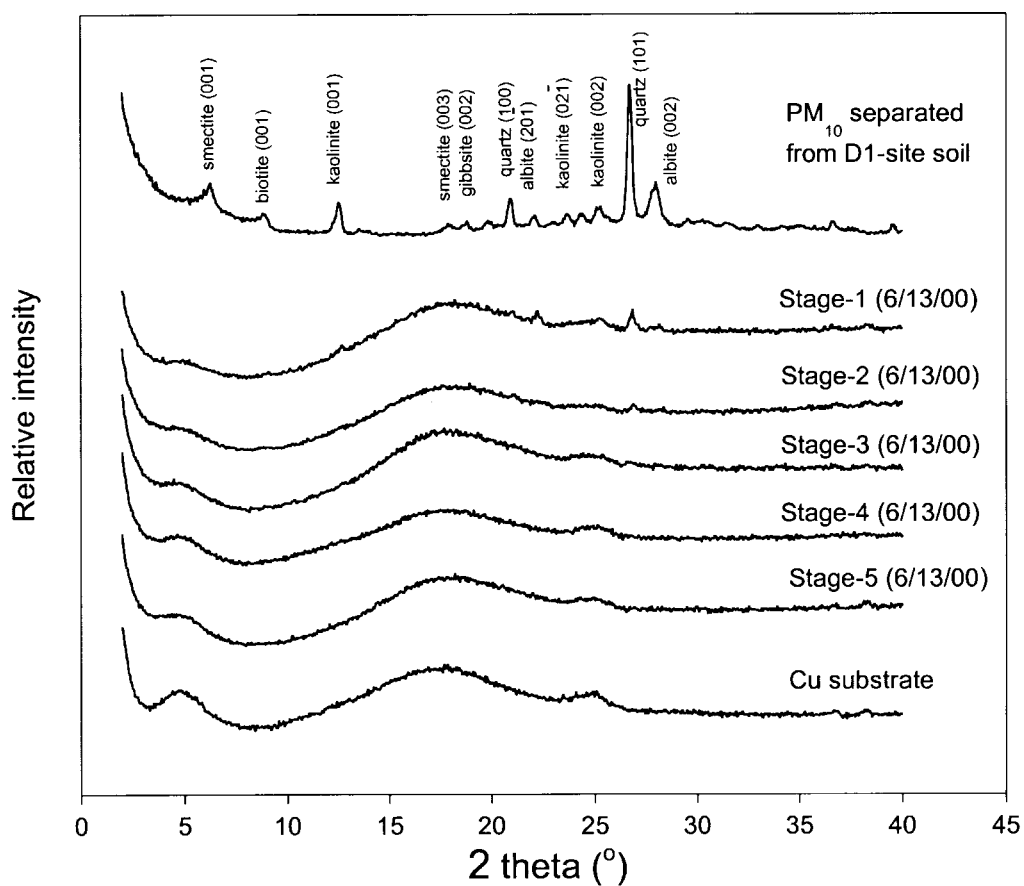


Figure 11a. X-ray diffraction patterns for D1-site samples. Upper pattern is resuspended PM<sub>10</sub>, middle patterns are different DRUM size fractions for sampling on 6/13/00 and lower pattern is Cu-tape substrate.

DRUM Stage	Size Range (μm)
1	> 8.54
2	4.26 – 8.54
3	2.12 – 4.26
4	1.15 – 2.12
5 to 8	0.07 – 1.15



**Figure 11b. Intensity of quartz primary peak on different DRUM stages collected at D1 site on three sampling days. All points are an average of four measurements at different perpendicular orientations. Error bars for stage-3 sample on 6/13/00 and stage-4 samples on 6/16/00 and 6/20/00 are within symbols.**

DRUM Stage	Size Range ( $\mu\text{m}$ )
1	> 8.54
2	4.26 – 8.54
3	2.12 – 4.26
4	1.15 – 2.12
5 to 8	0.07 – 1.15

$I_{Q(101)}$  of samples at different stages

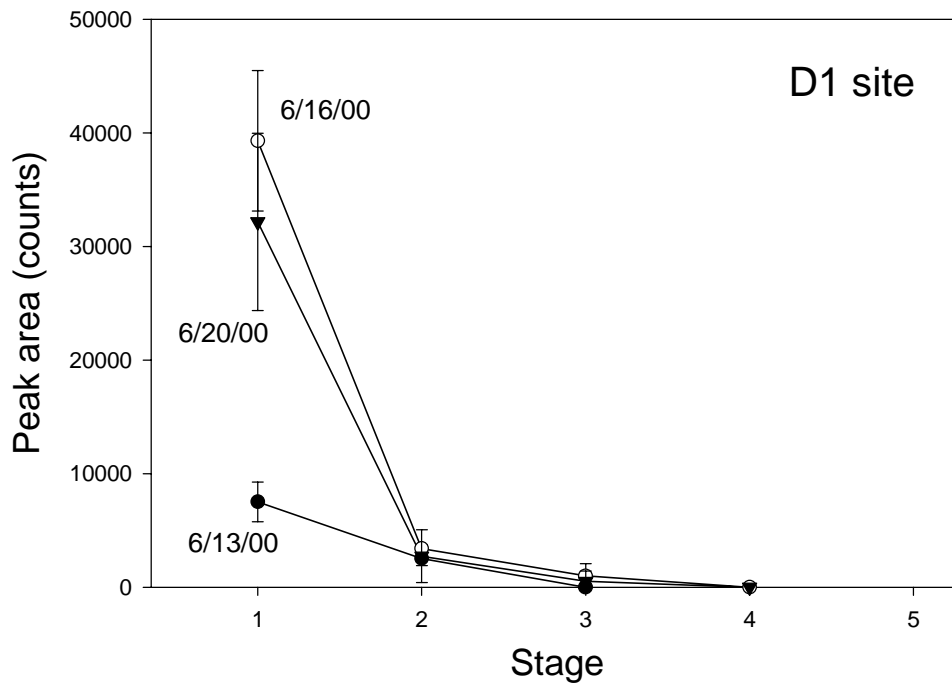
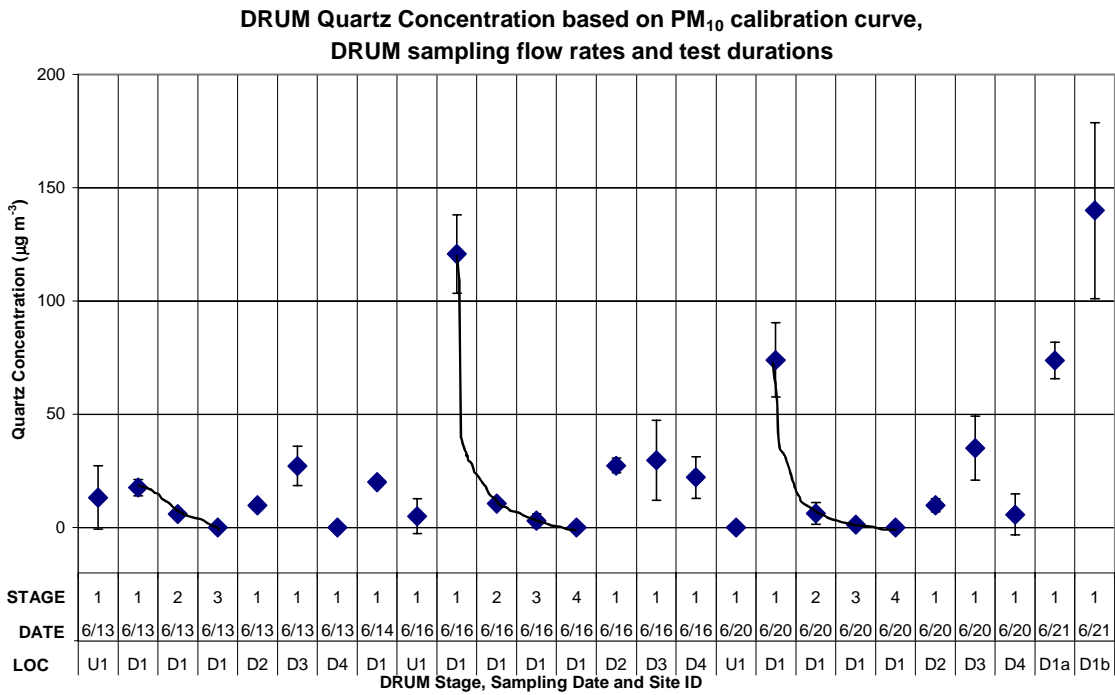


**Figure 11c. DRUM relative quartz concentrations ( $\mu\text{g m}^{-3}$ ) for all Stages analyzed by XRD. Hand-drawn lines connect samples collected on different DRUM stages during a single test period.**



DRUM Stage	Size Range ( $\mu\text{m}$ )
1	> 8.54
2	4.26 – 8.54
3	2.12 – 4.26
4	1.15 – 2.12
5 to 8	0.07 – 1.15

**Figure 12a. Mass concentrations of quartz in Stage-1(> 8.54  $\mu\text{m}$ ) DRUM samples collected at all sampling sites on June 13, 2000. All points are an average of four measurements at different orientations that were perpendicular to each other. Mass concentrations were calculated based on XRD analysis and measured sampling flow rates and test durations.**

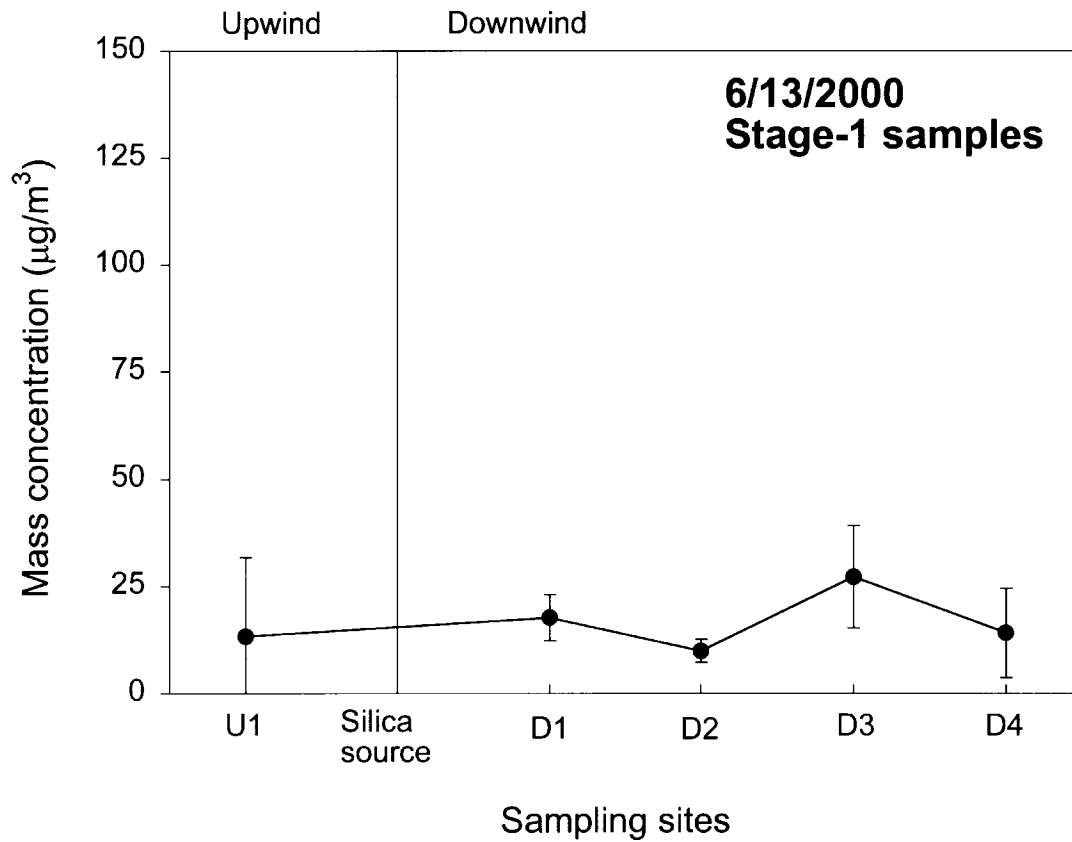


Figure 12b. Mass concentrations of quartz in Stage-1 (> 8.54  $\mu\text{m}$ ) DRUM samples collected at all sampling sites on June 16, 2000. All points are an average of four measurements at different orientations that were perpendicular to each other. Mass concentrations were calculated based on XRD analysis and measured sampling flow rates and test durations.

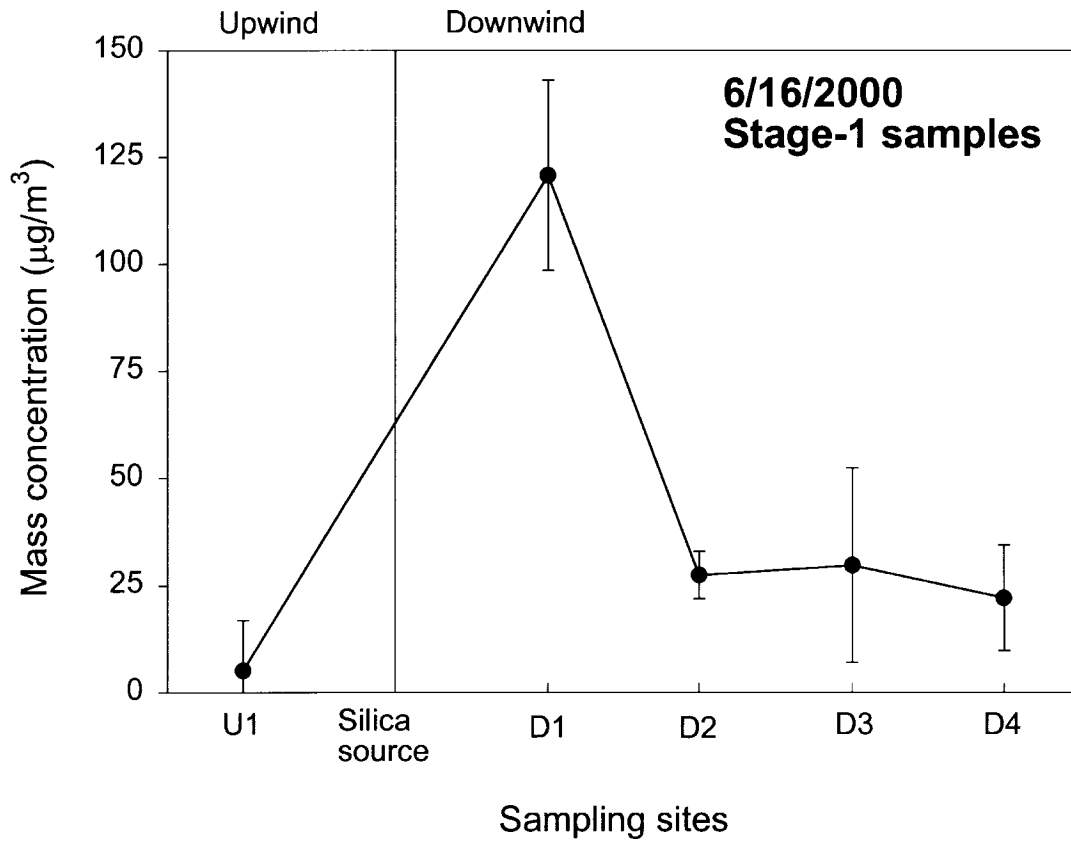


Figure 12c. Mass concentrations of quartz in Stage-1(> 8.54  $\mu\text{m}$ ) DRUM samples collected at all sampling sites on June 20, 2000. All points are an average of four measurements at different orientations that were perpendicular to each other. Mass concentrations were calculated based on XRD analysis and measured sampling flow rates and test durations. Error bar for the sample collected at U1 site is within symbol.

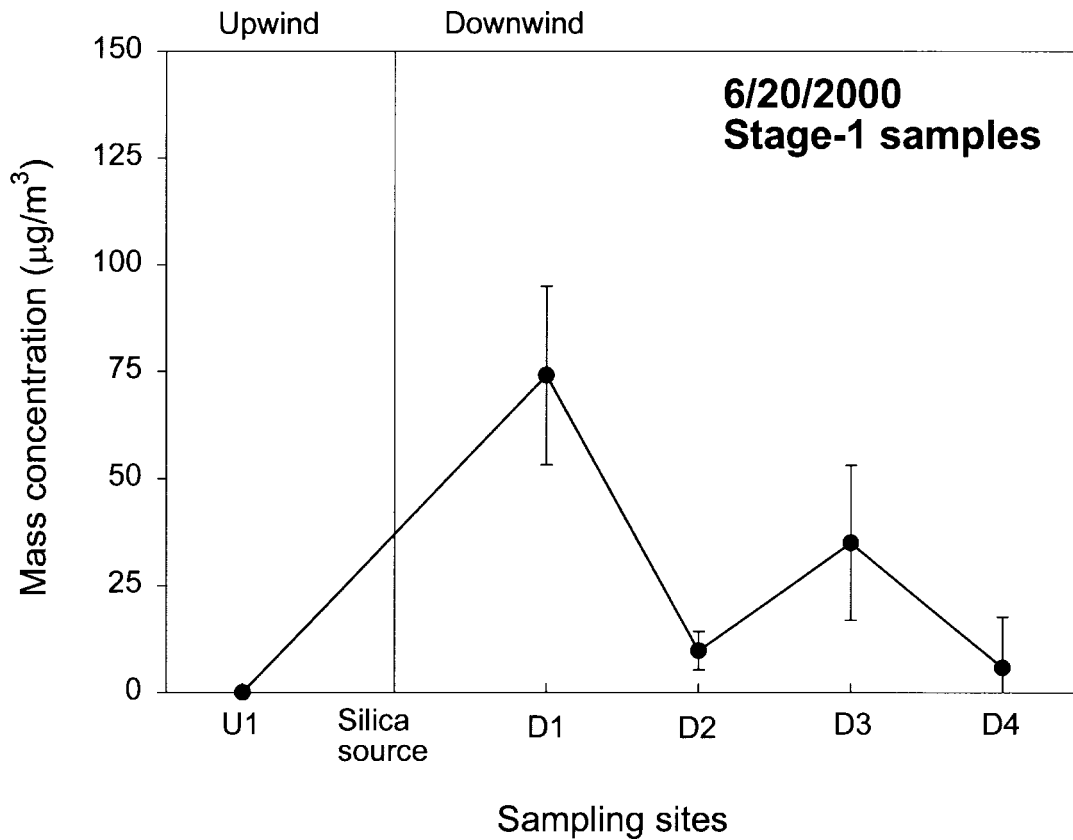


Figure 13a. Quartz mass concentrations and PM<sub>10</sub> mass concentrations for Teflon filter samples collected at all sampling locations on 6/16/00. The upwind U1 quartz concentration is an estimate of the maximum concentration due to sample handling problems.

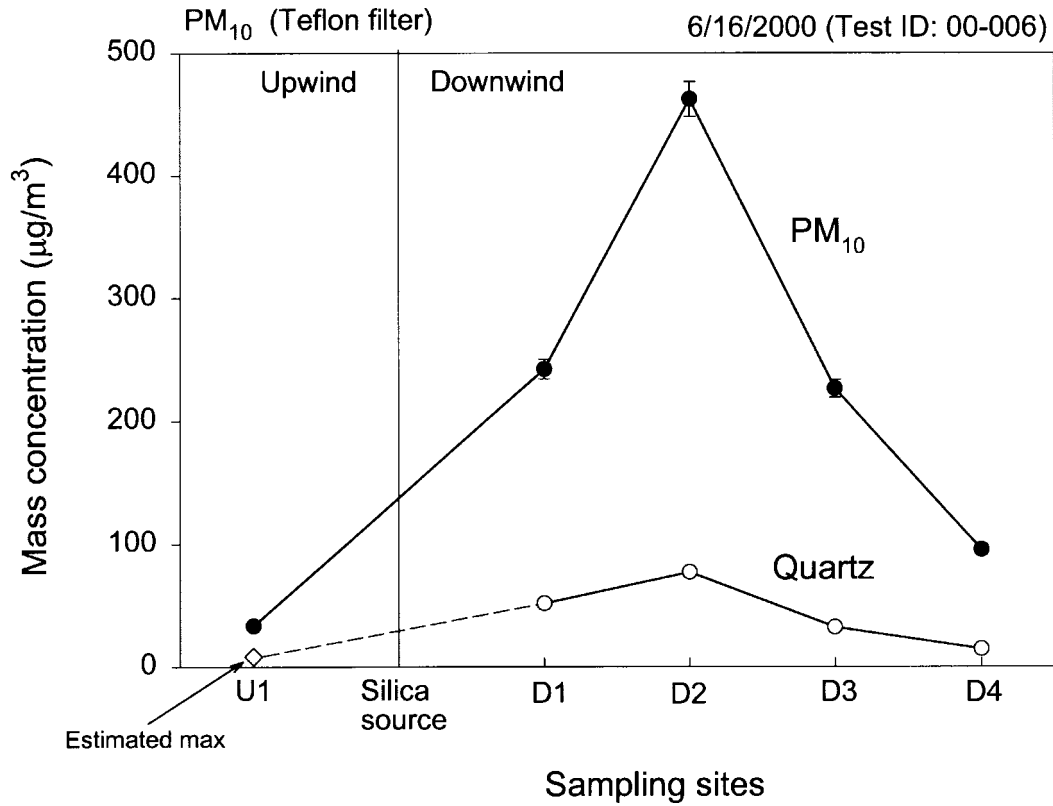


Figure 13b. Quartz mass concentrations and PM<sub>10</sub> mass concentrations for Teflon filter samples collected at all sampling sites for the two sampling periods on 6/20/00.

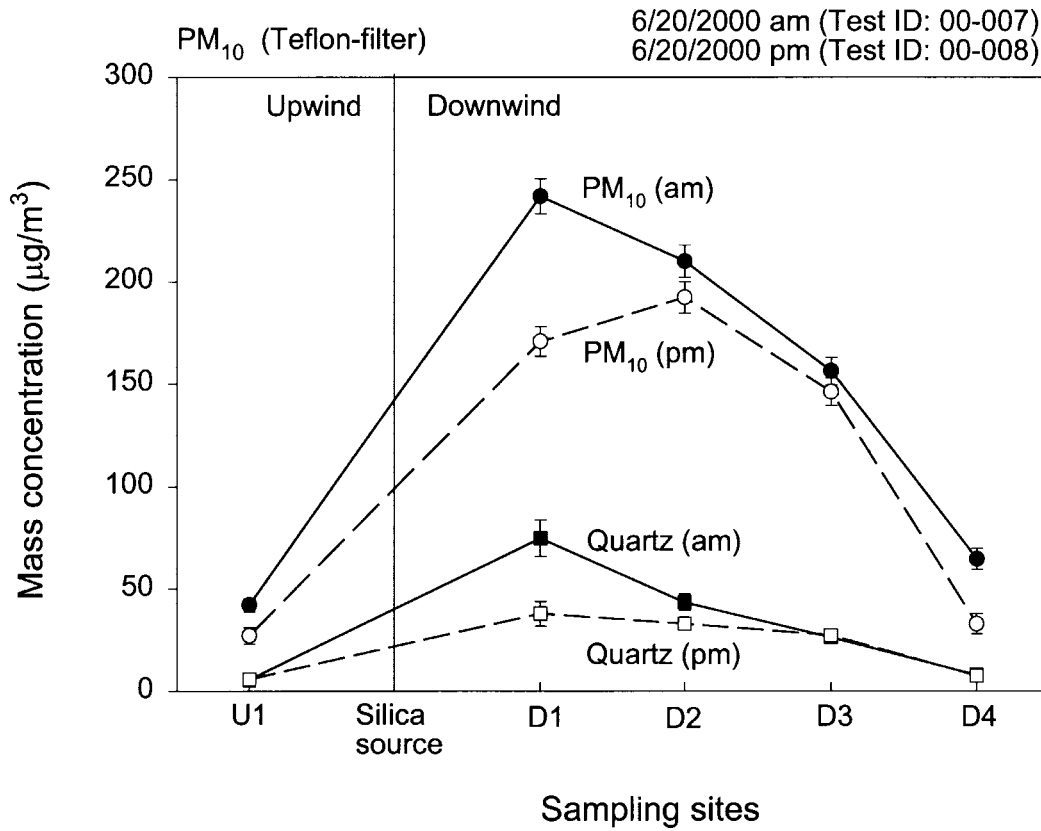


Figure 14. PM<sub>10</sub> Teflon filter mass and quartz concentration relationships. (a) PM<sub>10</sub> mass concentration and quartz mass concentration; (b) Si elemental concentration and quartz mass concentration.

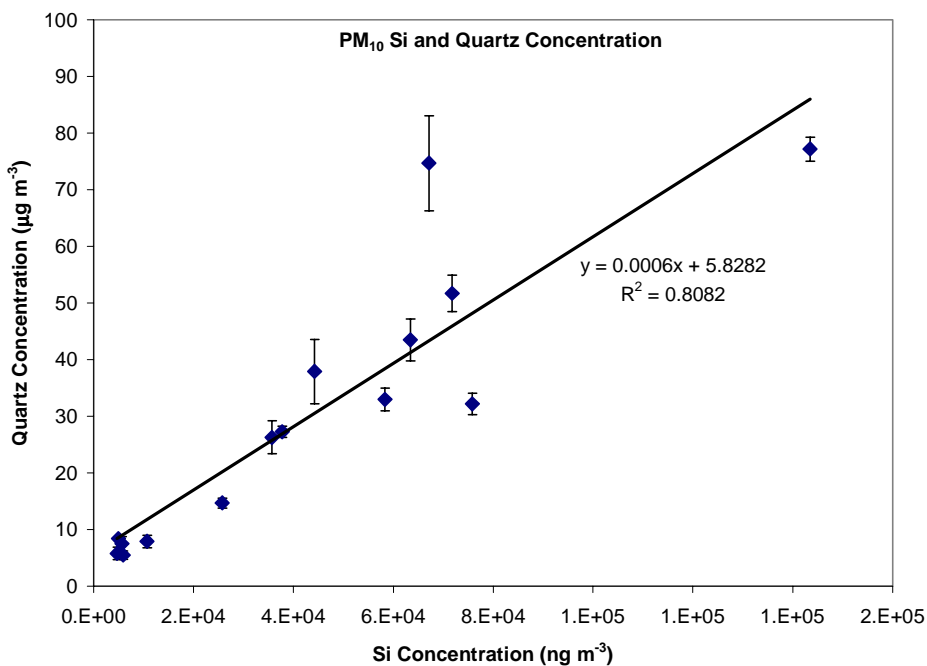
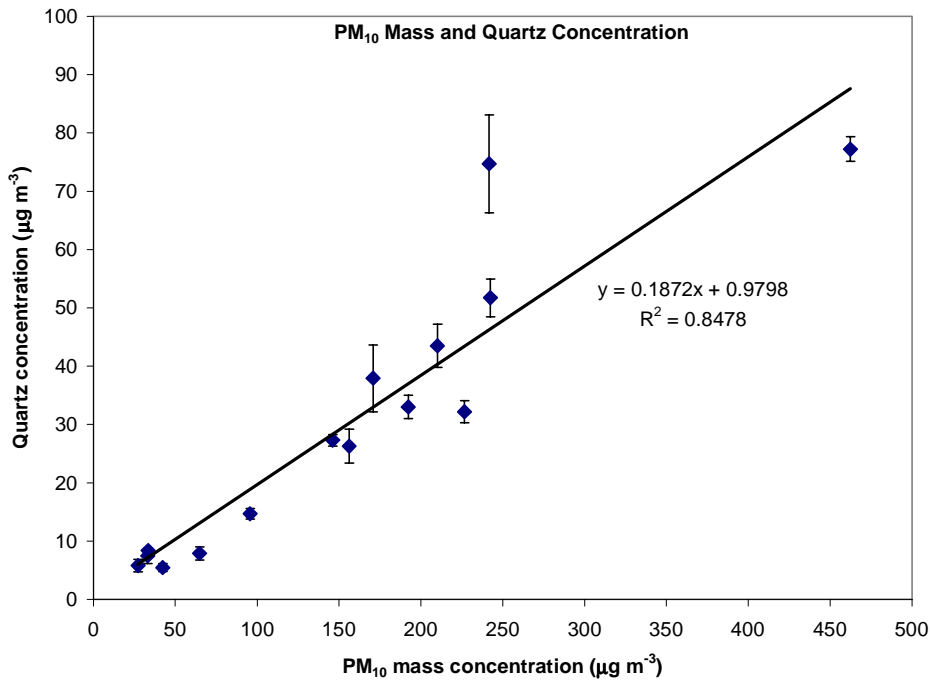


Figure 15a. PM<sub>10</sub> Elemental Signatures for Pilot Study Teflon filter analyses.

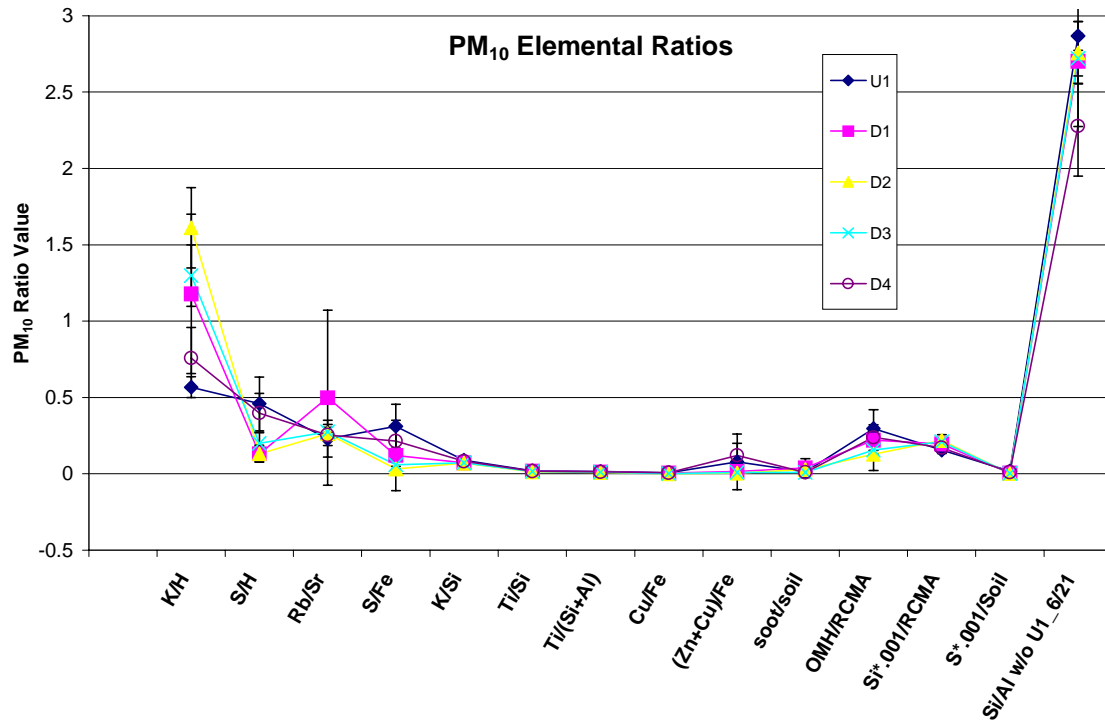
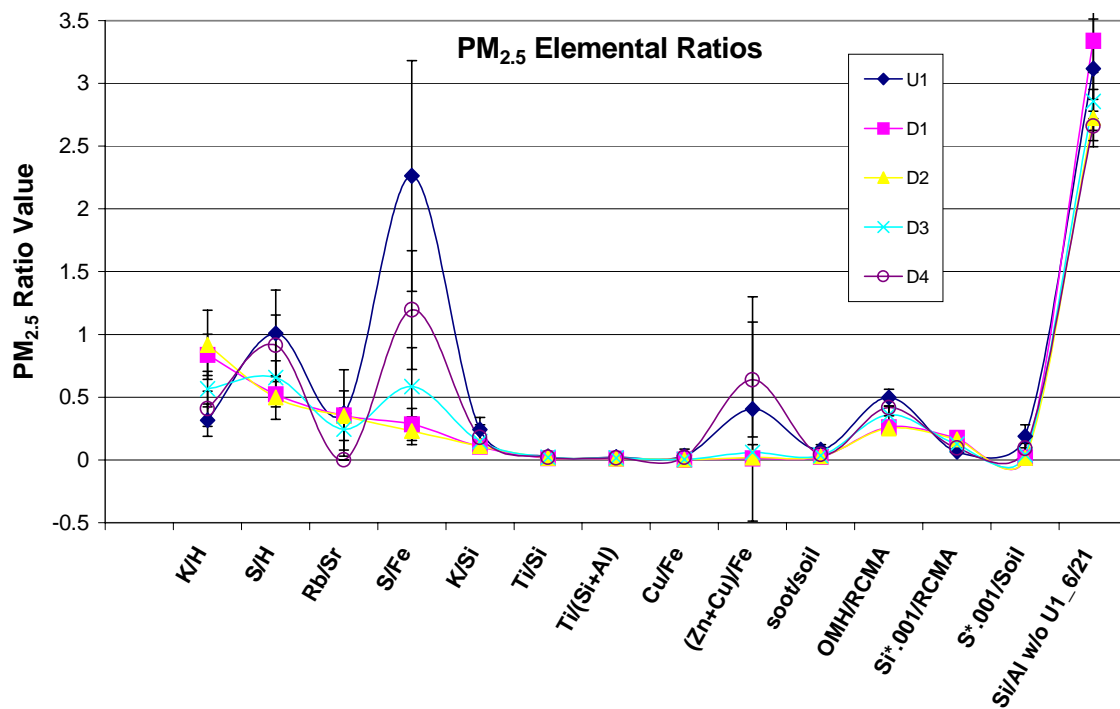


Figure 15b. PM<sub>2.5</sub> Elemental Signatures for Pilot Study Teflon filter analyses.



## APPENDIX A. LIDAR DATA ANALYSIS

Table A.1. Fugitive dust plume vectors for plumes originating at Main Plant.

Date	Time of scan	X coordinates		Y coordinates		Intensity		Vector Length meters
		X beg	X end	Y beg	Y end	Z beg	Z end	
June 13th	8:28:09	64.70	288.00	460.38	217.32	2.77E+08	1.44E+08	330.32
	10:16:09	17.60	187.00	504.19	420.23	7.08E+08	3.75E+08	189.15
	10:48:52	0.00	60.60	504.50	431.16	8.17E+08	5.58E+08	95.13
	12:31:18	0.00	72.70	464.90	373.90	3.98E+08	2.40E+08	116.46
	13:22:45	0.00	274.00	539.20	264.53	5.67E+08	1.21E+08	387.92
	13:48:59	0.00	335.00	479.80	261.90	6.58E+08	4.68E+08	399.81
	14:16:21	0.00	69.60	509.50	394.61	1.56E+08	1.49E+08	134.32
	14:48:26	0.00	281.00	499.60	271.47	3.04E+08	8.69E+07	362.04
	15:06:52	0.00	216.00	499.60	331.86	8.17E+08	1.41E+08	273.10
	15:18:17	0.00	230.00	425.40	284.44	2.88E+08	2.71E+08	270.04
	15:30:00	0.00	177.00	460.00	348.21	1.98E+08	1.20E+08	209.70
	15:36:42	0.00	67.50	534.20	479.98	3.61E+08	9.42E+07	86.54
	16:06:50	17.10	67.00	489.40	379.94	2.95E+08	2.34E+07	120.30
	16:20:31	0.00	111.00	469.90	364.26	6.46E+08	2.54E+08	153.50
	16:38:56	0.00	101.00	395.70	331.17	3.08E+08	9.88E+07	120.06
	16:43:40	0.00	110.00	460.00	359.47	1.65E+08	1.21E+08	148.94
	16:57:22	0.00	129.00	366.00	374.14	6.15E+07	8.43E+07	129.08
	17:45:39	0.00	377.00	356.00	235.81	4.31E+08	1.34E+08	396.06
	June 14th	7:40:18	0.00	362.00	544.10	314.78	9.50E+08	6.06E+08
7:45:01		0.00	84.90	539.20	437.02	8.76E+08	2.21E+08	132.88
8:10:08		0.00	128.00	435.30	332.54	1.79E+08	1.12E+08	163.87
8:21:49		8.37	145.00	479.73	399.75	1.83E+08	1.45E+08	158.74
8:35:31		0.00	193.00	524.30	395.65	2.45E+08	1.51E+08	231.92
8:40:14		0.00	406.00	484.70	215.96	4.18E+08	1.24E+08	487.02
8:53:55		0.00	252.00	524.30	373.15	2.07E+08	1.47E+08	293.59
8:58:38		0.00	332.00	469.90	224.07	6.19E+08	1.17E+08	413.26
9:12:19		0.00	320.00	499.60	249.71	3.96E+08	7.78E+07	405.71
9:17:01		0.00	361.00	494.60	234.36	4.74E+08	7.13E+07	444.93
9:35:27		0.00	76.40	514.40	433.51	2.63E+08	5.03E+07	111.29
9:42:08		0.00	239.00	514.40	381.71	2.26E+08	7.71E+07	272.94
9:53:50		70.40	287.00	444.46	258.15	2.57E+07	2.62E+07	285.48
10:00:31		0.00	171.00	484.70	367.60	4.03E+08	1.52E+08	207.59
10:12:13		0.00	85.00	410.60	340.77	1.58E+08	1.50E+08	109.98
10:18:54		16.10	94.10	459.72	328.08	2.96E+08	7.09E+07	153.03
10:25:53		0.00	213.00	484.70	303.82	8.93E+07	4.04E+07	279.24
10:30:36		0.00	240.00	464.90	276.22	1.85E+08	1.73E+07	305.38
10:37:18		0.00	405.00	479.80	172.00	3.66E+08	7.80E+07	485.18
10:49:00		0.00	143.00	420.50	353.16	3.47E+08	1.38E+07	157.78
10:55:41		0.00	302.00	549.10	292.10	2.89E+08	4.86E+07	396.92
11:02:40		0.00	210.00	469.90	364.16	1.73E+08	5.31E+07	235.34
11:32:27		121.00	227.00	397.34	336.26	1.14E+08	4.68E+07	290.99
11:44:09		0.00	205.00	539.20	355.59	1.00E+09	5.56E+07	329.72
11:50:50		0.00	376.00	509.50	122.28	8.14E+08	5.30E+07	521.99
12:02:32		0.00	749.00	484.70	65.52	1.17E+08	3.74E+07	734.26
12:16:13		0.00	115.00	430.40	352.75	7.39E+07	2.74E+07	118.28
12:34:36		6.73	128.00	385.74	273.43	7.37E+07	3.01E+07	347.03
12:39:19		0.00	105.00	494.60	422.37	1.08E+08	3.54E+07	232.86
12:51:48		0.00	98.40	375.90	321.70	7.98E+07	3.80E+07	314.18
12:51:48		0.00	93.50	469.90	404.85	2.22E+08	3.03E+07	101.83
12:56:31		0.00	109.00	430.40	380.37	8.28E+07	2.17E+07	198.84
13:10:12		0.00	186.00	375.90	297.83	1.29E+08	3.89E+07	207.34
13:14:54	0.00	364.00	469.90	404.35	1.15E+08	3.43E+07	274.90	
13:21:35	0.00	110.00	410.50	302.11	1.29E+08	1.83E+07	220.28	
13:28:35	0.00	124.00	395.70	307.27	9.03E+07	2.57E+07	145.35	
13:39:59	0.00	144.00	450.10	395.14	9.98E+07	2.56E+07	210.62	
13:51:42	0.00	259.00	474.80	258.80	4.29E+08	1.09E+08	355.87	
14:23:46	0.00	195.00	499.60	400.14	4.14E+08	5.34E+07	193.49	
14:52:45	0.00	165.00	465.00	298.51	1.77E+08	4.55E+07	286.10	
15:10:45	7.68	82.30	440.13	356.62	8.19E+07	1.76E+08	128.22	
15:19:45	0.00	177.00	484.70	320.11	2.88E+08	7.98E+07	224.42	
15:37:45	0.00	211.00	524.30	380.72	2.46E+08	5.28E+07	220.77	
15:46:45	0.00	168.00	489.70	396.19	1.05E+08	2.01E+08	196.90	
15:55:45	0.00	159.00	420.50	244.72	4.69E+08	2.89E+07	228.03	
June 15th	7:30:51	0.00	355.00	514.40	122.38	8.00E+08	1.84E+08	502.95
	7:39:51	0.00	118.00	435.30	362.26	5.64E+08	1.72E+08	120.43
	7:48:52	0.00	226.00	460.00	242.37	6.49E+08	1.37E+08	185.69
	8:06:53	0.00	102.00	395.70	315.18	5.19E+08	2.10E+08	92.78
	8:15:54	0.00	151.00	514.40	322.83	8.91E+08	2.03E+08	106.53

	8:24:54	0.00	77.10	440.20	362.79	6.49E+08	1.54E+08	123.08
	8:33:55	0.00	139.00	425.40	327.79	3.94E+08	1.80E+08	74.22
	8:42:55	0.00	133.00	435.30	314.17	4.23E+08	1.15E+08	382.89
	8:51:55	0.00	300.00	460.00	234.51	5.75E+08	1.78E+08	242.77
	9:00:56	0.00	365.00	554.00	246.16	2.92E+08	9.69E+07	198.57
	9:18:56	0.00	113.00	509.50	368.94	2.31E+08	1.20E+08	543.09
	9:36:55	0.00	91.50	469.90	430.58	2.47E+07	5.50E+07	141.97
	10:45:45	0.00	21.70	484.70	414.93	1.39E+08	3.91E+07	224.45
	11:19:58	0.00	99.30	499.60	305.76	4.13E+08	6.13E+07	142.77
	11:37:56	0.00	105.00	509.50	391.78	7.76E+07	3.16E+07	199.94
	11:46:55	0.00	117.00	474.80	304.81	6.06E+07	3.18E+07	206.36
	12:04:53	0.00	147.00	469.90	329.88	1.26E+08	7.49E+07	202.92
	12:19:32	0.00	356.00	514.40	205.30	1.47E+08	3.91E+07	53.13
	12:26:13	0.00	38.80	479.80	443.51	1.47E+08	6.57E+07	225.05
	12:33:12	0.00	132.00	464.90	282.41	3.15E+08	1.54E+08	91.69
	12:37:55	0.00	49.40	479.80	402.58	4.94E+08	1.04E+08	102.17
	12:51:35	0.00	52.30	460.00	372.24	2.83E+08	5.79E+07	194.82
	13:26:41	0.00	0.00	415.50	286.46	3.85E+08	9.63E+07	145.61
	13:26:41	0.00	0.00	509.50	415.73	3.97E+08	4.32E+08	139.40
	13:48:51	0.00	62.30	445.20	320.50	8.40E+07	4.91E+07	149.46
	13:59:56	0.00	104.00	494.60	386.95	1.74E+08	1.04E+07	140.83
	14:16:33	0.00	105.00	460.00	366.14	2.28E+08	6.14E+07	143.21
	14:38:43	0.00	94.00	415.50	307.45	4.10E+07	3.05E+07	140.78
	15:04:58	0.00	46.80	460.00	333.13	8.70E+07	5.88E+07	135.24
<b>June 16th</b>	6:57:40	6.56	850.00	375.84	165.16	4.64E+08	3.58E+08	554.73
	7:14:20	0.00	251.00	400.60	299.37	5.18E+08	2.68E+08	270.83
	8:37:38	0.00	149.00	435.30	350.53	5.11E+08	1.10E+08	171.25
	9:02:40	0.00	189.00	410.60	302.07	3.36E+08	1.95E+08	217.73
	9:15:13	0.00	529.00	410.60	27.70	5.05E+08	1.00E+08	590.42
	10:17:56	0.00	352.00	499.60	264.92	1.96E+08	1.46E+08	319.57
	10:30:28	0.00	273.00	430.40	205.40	2.37E+08	1.08E+08	353.44
	10:43:00	0.00	148.00	375.90	318.30	3.68E+08	1.17E+08	159.21
	11:33:09	0.00	381.00	395.70	211.04	1.44E+08	1.52E+08	199.84
	11:45:41	0.00	162.00	479.80	317.38	7.12E+08	1.60E+08	229.20
	11:58:13	0.00	250.00	464.90	267.68	2.46E+08	1.54E+08	318.12
	12:35:50	0.00	273.00	469.90	170.37	6.68E+08	8.86E+07	405.04
	12:48:21	0.00	336.00	440.20	226.81	2.56E+08	1.07E+08	398.25

AVE 244.82  
STDEV 131.09

Table A.2. Fugitive dust plume vectors for plumes identified as originating from EW road traffic.

Date	Time of scan	X coordinates		Y coordinates		Intensity		Length
		Xbeg	Xend	Ybeg	Yend	Zbeg	Zend	
<b>June 13th</b>								
	9:43:07	150.00	246.00	772.05	715.57	3.72E+08	4.81E+08	111.66
	11:21:34	422.00	785.00	366.67	240.07	9.42E+08	5.29E+08	287.56
	15:25:17	94.60	172.00	409.72	265.52	1.32E+08	3.25E+08	163.87
<b>June 14th</b>	7:03:15	101.00	625.00	438.56	65.66	6.53E+08	3.36E+08	613.16
	11:14:04	100.00	440.00	433.79	275.24	9.60E+07	2.22E+07	375.45
	11:25:46	72.20	442.00	409.19	126.79	8.22E+07	5.34E+07	469.94
	12:09:14	103.00	513.00	448.21	166.62	7.04E+07	1.21E+08	499.17
	12:20:56	76.50	291.00	393.34	253.11	3.74E+07	6.50E+07	304.43
	12:27:37	178.00	386.00	310.71	475.15	4.90E+07	4.25E+07	352.04
	12:39:19	75.80	523.00	478.73	130.44	1.08E+08	2.42E+07	500.15
	12:46:00	65.40	358.00	465.33	311.50	2.29E+08	1.94E+07	365.29
	13:10:12	290.00	655.00	311.12	57.34	5.97E+07	3.16E+07	393.44
	13:14:54	375.00	651.00	337.58	150.22	8.46E+07	1.05E+08	283.85
	15:01:45	63.40	121.00	400.61	271.14	5.43E+08	6.55E+07	248.60
	15:28:45	72.00	157.00	454.34	352.45	1.32E+08	9.45E+07	132.47
	15:55:45	120.00	317.00	449.06	96.89	1.51E+08	5.12E+07	408.39
<b>June 15th</b>	7:30:51	224.00	495.00	332.20	69.53	3.46E+08	2.40E+08	357.08
	8:06:53	158.00	205.00	389.88	315.26	5.94E+08	3.22E+08	115.18
	8:33:55	152.00	316.00	496.70	418.72	2.13E+08	2.10E+08	181.30
	9:09:56	205.00	324.00	355.59	226.96	2.58E+08	1.93E+08	175.12
	9:27:56	251.00	477.00	299.37	84.17	2.36E+07	7.20E+07	453.70
	9:36:55	328.00	398.00	377.05	249.01	1.24E+08	1.15E+08	146.28
	9:57:34	71.30	206.00	404.36	284.13	3.95E+08	1.28E+08	180.88
	10:15:58	84.90	302.00	437.02	262.88	2.69E+08	1.50E+08	278.59
	11:28:56	184.00	233.00	394.52	320.13	9.13E+07	8.42E+07	88.87
	11:28:56	325.00	460.00	282.30	64.70	1.21E+08	4.83E+07	490.18
	11:46:55	265.00	348.00	326.79	226.30	1.97E+07	4.65E+07	130.87
	13:32:13	171.00	295.00	334.93	285.16	3.43E+08	3.41E+08	134.20
	13:32:13	302.00	432.00	347.17	229.90	3.64E+07	4.95E+07	175.52
	13:37:46	458.00	702.00	384.71	283.50	8.32E+07	2.36E+07	611.53
	13:48:51	271.00	339.00	301.42	150.86	6.23E+08	1.46E+08	399.69
	14:11:01	305.00	387.00	389.83	291.70	1.08E+08	9.66E+07	128.22
	14:33:10	224.00	294.00	332.20	264.77	8.48E+07	6.03E+07	97.18
<b>June 16th</b>	11:01:05	100.00	261.00	433.79	310.71	1.31E+08	9.79E+07	202.31
	11:38:42	95.60	325.00	449.95	325.27	3.66E+08	1.94E+08	261.29

AVE            289.07  
STDEV        152.51

Figure A.1. June 14 Average plume centerline vertical profiles, (a) morning, (b) afternoon.

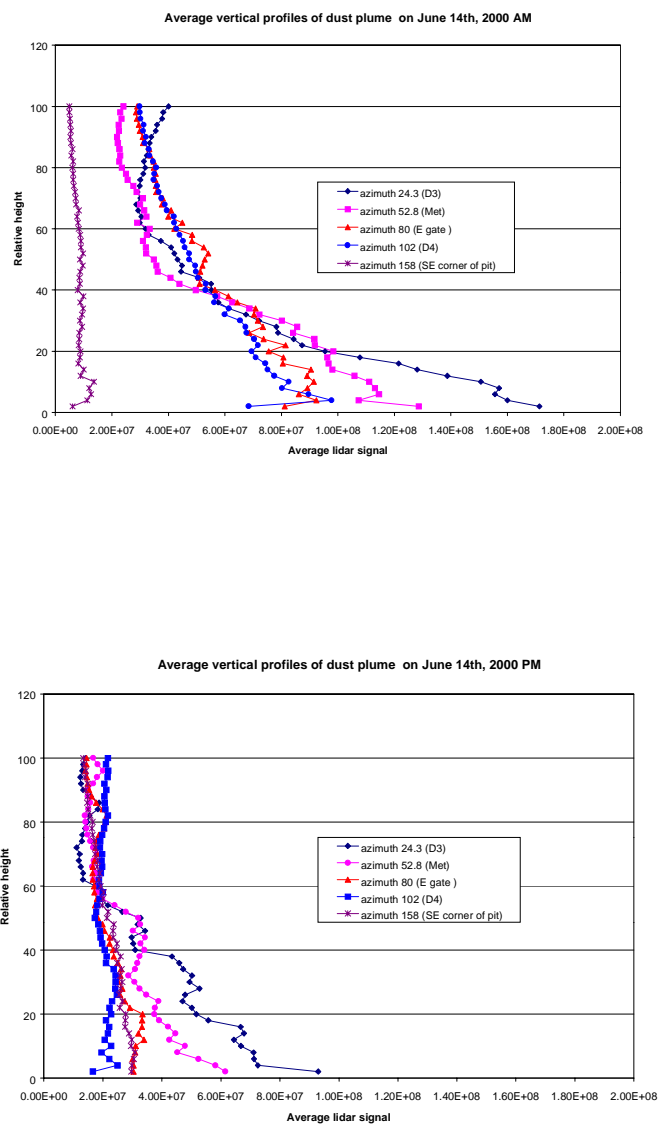


Figure A.2. June 13 Average plume centerline vertical profiles, (a) morning, (b) afternoon..

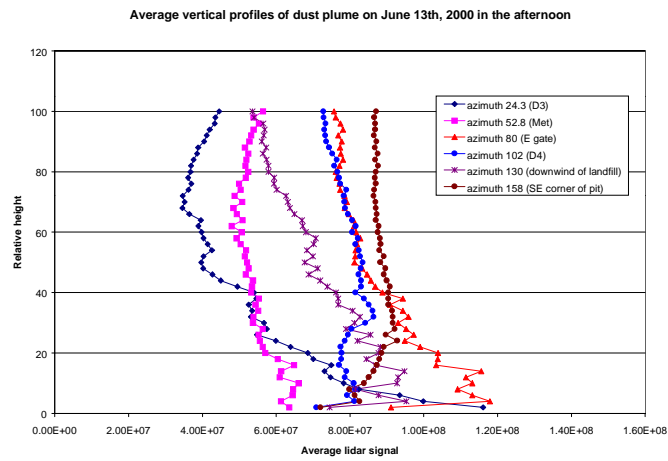
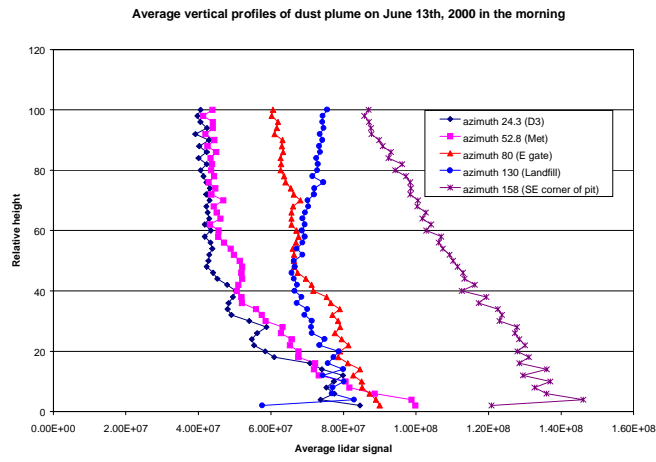


Figure A.3. June 15. Average plume centerline vertical profiles, (a) morning, (b) afternoon.

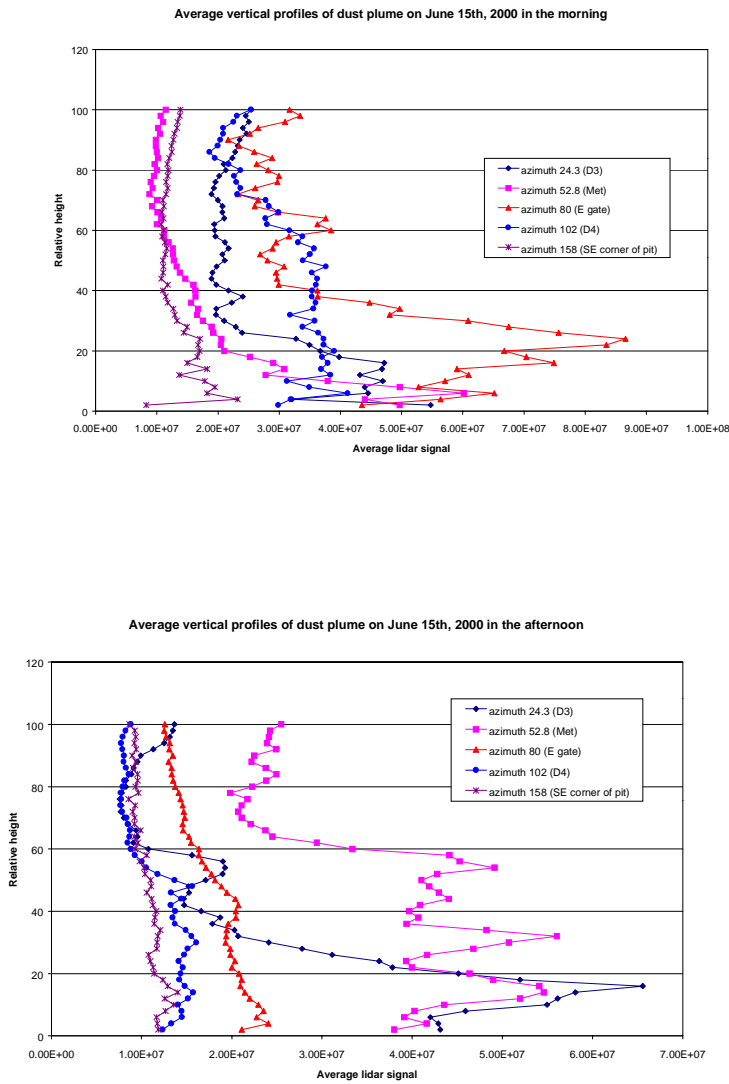
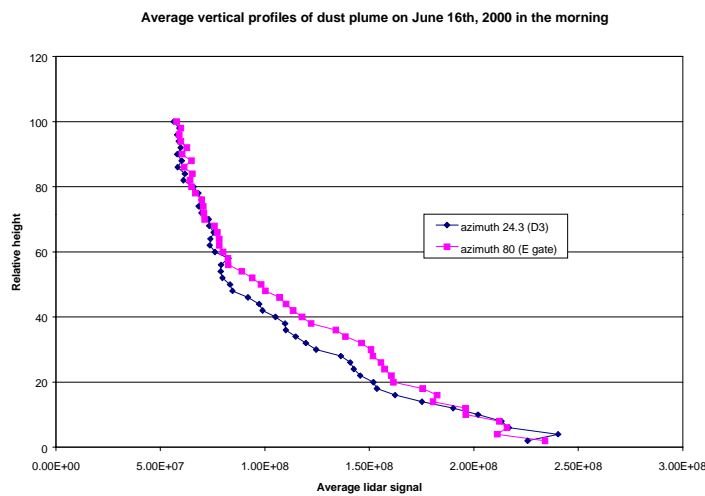


Figure A.4. June 16 Average plume centerline vertical profiles in the morning (no afternoon scans collected).



### Appendix B. Raw XRD Data

Table B.1 DRUM quartz peak area and height as determined by Rigaku Miniflex XRD analysis. Standard deviations based on analysis of 4 sample orientations.

Date	Loc	Stage	DRUM ID#	area (counts)	avg (counts)	std (abs) (counts)	std (rel) (%)	height (counts)	avg (counts)	std (abs) (counts)	std (rel) (%)
06/13/2000	U1	1	KU1A1-00	10058				522			
06/13/2000	U1	1	KU1A1-09	0				0			
06/13/2000	U1	1	KU1A1-18	0				0			
06/13/2000	U1	1	KU1A1-27	3994				410			
06/13/2000	U1	1			<b>3513</b>	<b>4752</b>	<b>135.3</b>		<b>233</b>	<b>273</b>	<b>117.1</b>
06/13/2000	D1	1	KD1A1-00	4709				692			
06/13/2000	D1	1	KD1A1-09	7598				381			
06/13/2000	D1	1	KD1A1-18	9360				536			
06/13/2000	D1	1	KD1A1-27	8397				584			
06/13/2000	D1	1			<b>7516</b>	<b>2005</b>	<b>26.7</b>		<b>548</b>	<b>129</b>	<b>23.6</b>
06/13/2000	D1	2	KD1A2-00	3190				305			
06/13/2000	D1	2	KD1A2-09	3011				271			
06/13/2000	D1	2	KD1A2-18	1678				238			
06/13/2000	D1	2	KD1A2-27	2236				309			
06/13/2000	D1	2			<b>2529</b>	<b>702</b>	<b>27.8</b>		<b>281</b>	<b>33</b>	<b>11.8</b>
06/13/2000	D1	3	KD1A3-00	0				0			
06/13/2000	D1	3	KD1A3-09	0				0			
06/13/2000	D1	3	KD1A3-18	0				0			
06/13/2000	D1	3	KD1A3-27	0				0			
06/13/2000	D1	3			<b>0</b>	<b>0</b>	<b>#DIV/0!</b>		<b>0</b>	<b>0</b>	<b>#DIV/0!</b>
06/13/2000	D2	1	KD2A1-00	3881				510			
06/13/2000	D2	1	KD2A1-09	4508				324			
06/13/2000	D2	1	KD2A1-18	3939				453			
06/13/2000	D2	1	KD2A1-27	4247				443			
06/13/2000	D2	1			<b>4144</b>	<b>291</b>	<b>7.0</b>		<b>433</b>	<b>78</b>	<b>18.1</b>
06/13/2000	D3	1	KD3A1-00	4924				578			
06/13/2000	D3	1	KD3A1-09	5166				630			
06/13/2000	D3	1	KD3A1-18	10510				792			
06/13/2000	D3	1	KD3A1-27	5580				545			
06/13/2000	D3	1			<b>6545</b>	<b>2657</b>	<b>40.6</b>		<b>636</b>	<b>110</b>	<b>17.2</b>
06/13/2000	D4	1	KD4A1-00	10328				827			
06/13/2000	D4	1	KD4A1-09	1225				218			
06/13/2000	D4	1	KD4A1-18	4157				522			
06/13/2000	D4	1	KD4A1-27	5716				598			
06/13/2000	D4	1			<b>5357</b>	<b>3801</b>	<b>71.0</b>		<b>541</b>	<b>251</b>	<b>46.5</b>
06/14/2000	D1	1	KD17B1-00	9066				675			
06/14/2000	D1	1	KD17B1-09	10994				824			
06/14/2000	D1	1	KD17B1-18	8402				698			
06/14/2000	D1	1	KD17B1-27	9902				647			
06/14/2000	D1	1			<b>9591</b>	<b>1119</b>	<b>11.7</b>		<b>711</b>	<b>78</b>	<b>11.0</b>
06/16/2000	U1	1	KU1D1-00	0				0			
06/16/2000	U1	1	KU1D1-09	3617				353			
06/16/2000	U1	1	KU1D1-18	0				0			
06/16/2000	U1	1	KU1D1-27	0				0			
06/16/2000	U1	1			<b>904</b>	<b>1809</b>	<b>200.0</b>		<b>88</b>	<b>177</b>	<b>200.0</b>
06/16/2000	D1	1	KD1D1-00	39324				2377			
06/16/2000	D1	1	KD1D1-09	42524				2966			
06/16/2000	D1	1	KD1D1-18A	28215				1769			
06/16/2000	D1	1	KD1D1-18B	30565	29390	1175	4.0	1889	1829	60	3.3
06/16/2000	D1	1	KD1D1-27	45928				2607			
06/16/2000	D1	1			<b>39292</b>	<b>7131</b>	<b>18.1</b>		<b>2445</b>	<b>413</b>	<b>16.9</b>
06/16/2000	D1	2	KD1D2-00	3582				432			
06/16/2000	D1	2	KD1D2-09	3016				350			
06/16/2000	D1	2	KD1D2-18	3129				365			
06/16/2000	D1	2	KD1D2-27	3889				346			
06/16/2000	D1	2			<b>3404</b>	<b>405</b>	<b>11.9</b>		<b>373</b>	<b>40</b>	<b>10.7</b>
06/16/2000	D1	3	KD1D3-00	2639				298			
06/16/2000	D1	3	KD1D3-09	0				0			
06/16/2000	D1	3	KD1D3-18	1306				227			
06/16/2000	D1	3	KD1D3-27	0				0			
06/16/2000	D1	3			<b>986</b>	<b>1262</b>	<b>128.0</b>		<b>131</b>	<b>154</b>	<b>117.6</b>
06/16/2000	D1	4	KD1D4-00	0				0			
06/16/2000	D1	4	KD1D4-09	0				0			
06/16/2000	D1	4	KD1D4-18	0				0			
06/16/2000	D1	4	KD1D4-27	0				0			
06/16/2000	D1	4			<b>0</b>	<b>0</b>	<b>#DIV/0!</b>		<b>0</b>	<b>0</b>	<b>#DIV/0!</b>

Table B.1 *continued* DRUM quartz peak area and height as determined by Rigaku Miniflex XRD analysis.

Date	Loc	Stage	DRUM ID#	area (counts)	avg (counts)	std (abs) (counts)	std (rel) (%)	height (counts)	avg (counts)	std (abs) (counts)	std (rel) (%)
06/16/2000	D2	1	KD2D1-00	8646				620			
06/16/2000	D2	1	KD2D1-09	7832				564			
06/16/2000	D2	1	KD2D1-18	10457				739			
06/16/2000	D2	1	KD2D1-27	7500				816			
06/16/2000	D2	1		<b>8609</b>		<b>1323</b>	<b>15.4</b>		<b>685</b>	<b>114</b>	<b>16.6</b>
06/16/2000	D3	1	KD3D1-00	8451				695			
06/16/2000	D3	1	KD3D1-09	21543				1842			
06/16/2000	D3	1	KD3D1-18	6021				578			
06/16/2000	D3	1	KD3D1-27	4763				382			
06/16/2000	D3	1		<b>10195</b>		<b>7719</b>	<b>75.7</b>		<b>874</b>	<b>658</b>	<b>75.3</b>
06/16/2000	D4	1	KD4D1-00	11262				845			
06/16/2000	D4	1	KD4D1-09	4564				431			
06/16/2000	D4	1	KD4D1-18	5769				507			
06/16/2000	D4	1	KD4D1-27	3787				346			
06/16/2000	D4	1		<b>6346</b>		<b>3378</b>	<b>53.2</b>		<b>532</b>	<b>219</b>	<b>41.1</b>
06/20/2000	U1	1	KU1E1-00	0				0			
06/20/2000	U1	1	KU1E1-09	0				0			
06/20/2000	U1	1	KU1E1-18	0				0			
06/20/2000	U1	1	KU1E1-27	0				0			
06/20/2000	U1	1		<b>0</b>		<b>0</b>	<b>#DIV/0!</b>		<b>0</b>	<b>0</b>	<b>#DIV/0!</b>
06/20/2000	D1	1	KD1E1-00	28608				2055			
06/20/2000	D1	1	KD1E1-09	45396				3088			
06/20/2000	D1	1	KD1E1-18	25330				1668			
06/20/2000	D1	1	KD1E1-27	29287				1902			
06/20/2000	D1	1		<b>32155</b>		<b>8995</b>	<b>28.0</b>		<b>2178</b>	<b>627</b>	<b>28.8</b>
06/20/2000	D1	2	KD1E2-00	6422				522			
06/20/2000	D1	2	KD1E2-09	0				0			
06/20/2000	D1	2	KD1E2-18	2401				287			
06/20/2000	D1	2	KD1E2-27	2107				281			
06/20/2000	D1	2		<b>2733</b>		<b>2682</b>	<b>98.2</b>		<b>273</b>	<b>214</b>	<b>78.4</b>
06/20/2000	D1	3	KD1E3-00	2107				281			
06/20/2000	D1	3	KD1E3-09	0				0			
06/20/2000	D1	3	KD1E3-18	0				0			
06/20/2000	D1	3	KD1E3-27	0				0			
06/20/2000	D1	3		<b>527</b>		<b>1054</b>	<b>200.0</b>		<b>70</b>	<b>141</b>	<b>200.0</b>
06/20/2000	D1	4	KD1E4-00	0				0			
06/20/2000	D1	4	KD1E4-09	0				0			
06/20/2000	D1	4	KD1E4-18	0				0			
06/20/2000	D1	4	KD1E4-27	0				0			
06/20/2000	D1	4		<b>0</b>		<b>0</b>	<b>#DIV/0!</b>		<b>0</b>	<b>0</b>	<b>#DIV/0!</b>
06/20/2000	D2	1	KD2E1-00	2045				317			
06/20/2000	D2	1	KD2E1-09	3975				379			
06/20/2000	D2	1	KD2E1-18	5293				480			
06/20/2000	D2	1	KD2E1-27	5460				512			
06/20/2000	D2	1		<b>4193</b>		<b>1579</b>	<b>37.6</b>		<b>422</b>	<b>90</b>	<b>21.3</b>
06/20/2000	D3	1	KD3E1-00	26726				2037			
06/20/2000	D3	1	KD3E1-09	9478				600			
06/20/2000	D3	1	KD3E1-18	14574				983			
06/20/2000	D3	1	KD3E1-27	10751				668			
06/20/2000	D3	1		<b>15382</b>		<b>7866</b>	<b>51.1</b>		<b>1072</b>	<b>665</b>	<b>62.0</b>
06/20/2000	D4	1	KD4E1-00	0				0			
06/20/2000	D4	1	KD4E1-09	0				0			
06/20/2000	D4	1	KD4E1-18	0				0			
06/20/2000	D4	1	KD4E1-27	9846				930			
06/20/2000	D4	1		<b>2462</b>		<b>4923</b>	<b>200.0</b>		<b>233</b>	<b>465</b>	<b>200.0</b>
06/21/2000	D1a	1	KD1F1-00	10619				723			
06/21/2000	D1a	1	KD1F1-09	8195				581			
06/21/2000	D1a	1	KD1F1-18	11527				903			
06/21/2000	D1a	1	KD1F1-27	10332				696			
06/21/2000	D1a	1		<b>10168</b>		<b>1411</b>	<b>13.9</b>		<b>726</b>	<b>133</b>	<b>18.4</b>
06/21/2000	D1p	1	KD1G1-00A	29082				1860			
06/21/2000	D1p	1	KD1G1-00B	28092	28587	495	1.7	2041	1951	90.5	4.6
06/21/2000	D1p	1	KD1G1-09	25295				1633			
06/21/2000	D1p	1	KD1G1-18A	42201				3168			
06/21/2000	D1p	1	KD1G1-18B	52680	47441	5240	11.0	3899	3534	366	10.3
06/21/2000	D1p	1	KD1G1-27	23574				1650			
06/21/2000	D1p	1		<b>31224</b>		<b>11009</b>	<b>35.3</b>		<b>2192</b>	<b>906</b>	<b>41.4</b>

Table B.2. Regression Results for Resuspended PM<sub>10</sub> and Quartz Standards

<b>Regression for calibration curve with resuspended PM<sub>10</sub></b>						
<b>X (Q) = 0.163</b>				<b>y=ax</b>	<b>Regression Output:</b>	
suspension	PM10	qtz	l	Constant		0
				Std Err of Y Est		1098.668
0	0	0	1063	R Squared		0.996258
50	47.9	7.80	4875	No. of Observations		6
100	95.7	15.60	10782	Degrees of Freedom		5
200	191.4	31.20	17793			
300	287.1	46.80	30223	X Coefficient(s)	627.5219	
500	478.5	78.00	48947	Std Err of Coef.	11.2421	
					rel. error	0.0179
<b>Data regression for pure quartz standards</b>						
				<b>y=ax</b>	<b>Regression Output:</b>	
		qtz	l	Constant		0
				Std Err of Y Est		925.6751
		0	1063	R Squared		0.998207
		22.1	18608	No. of Observations		4
		44.2	35033	Degrees of Freedom		3
		66.3	52036			
				X Coefficient(s)	791.1506	
				Std Err of Coef.	11.19444	
					rel. error	0.0141

Table B.3. XRD quartz peak areas and heights for resuspended PM<sub>10</sub> standard on Cu-tape.

	ID	area (counts)	avg (counts)	std (abs) (counts)	std (rel) (%)	height (counts)	avg (counts)	std (abs) (counts)	std (rel) (%)	
<b>Blank</b>	Cu-f-00	0								
	Cu-f-09	1479								
	Cu-f-18	1725								
	Cu-f-27	1049	1063	762	71.7	437	437	#DIV/0!	#DIV/0!	
			<b>1063</b>	<b>762</b>	<b>71.7</b>		<b>437</b>	<b>#DIV/0!</b>	<b>#DIV/0!</b>	
<b>PM<sub>10</sub> Standards</b>	P050A-000	5677				691				
	P050A-090	3830				422				
	P050A-180	3943				477				
	P050A-270	4141	4398	862	19.6	479	517	119	23.0	
	P050B-000	5508				501				
	P050B-090	4881				444				
	P050B-180	4370				380				
	P050B-270	4386	4786	536	11.2	570	474	81	17.1	
	P050C-000	6493				526				
	P050C-090	4989				471				
	P050C-180	4947				485				
	P050C-270	5332	5440	723	13.3	437	480	37	7.7	
			<b>4875</b>	<b>791</b>	<b>16.2</b>		<b>490</b>	<b>80</b>	<b>16.3</b>	
		P100A-000	10692				909			
		P100A-090	6914				735			
		P100A-180	9306				834			
		P100A-270	11376	9572	1970	20.6	934	853	89	10.5
		P100B-000	12147				1055			
		P100B-090	11064				951			
		P100B-180	10734				829			
		P100B-270	12455	11600	830	7.2	943	945	92	9.8
		P100C-000	10743				824			
		P100C-090	11368				964			
		P100C-180	10611				860			
		P100C-270	11975	11174	628	5.6	911	890	61	6.9
			<b>10782</b>	<b>1478</b>	<b>13.7</b>		<b>896</b>	<b>84</b>	<b>9.4</b>	
		P200A-000	15068				1059			
		P200A-090	16351				1323			
		P200A-180	19947				1467			
		P200A-270	16092	16865	2128	12.6	1135	1246	184	14.8
		P200B-000	17358				1400			
		P200B-090	19277				1286			
		P200B-180	14904				1284			
	P200B-270	19479	17755	2127	12.0	1413	1346	70	5.2	
	P200C-000	18654				1296				
	P200C-090	15664				1181				
	P200C-180	19239				1451				
	P200C-270	21485	18761	2398	12.8	1482	1353	140	10.4	
		<b>17793</b>	<b>2166</b>	<b>12.2</b>		<b>1315</b>	<b>136</b>	<b>10.4</b>		
	P300B-000	32068				2302				
	P300B-090	25325				1580				
	P300B-180	29054				2152				
	P300B-270	29194	28910	2764	9.6	1903	1984	316	15.9	
	P300C-000	36448				2747				
	P300C-090	30924				2127				
	P300C-180	29199				2003				
	P300C-270	29571	31536	3358	10.6	1995	2218	358	16.1	
		<b>30223</b>	<b>3174</b>	<b>10.5</b>		<b>2101</b>	<b>336</b>	<b>16.0</b>		
	P500D-000	50101				3206				
	P500D-090	46859				3221				
	P500D-180	47398				3220				
	P500D-270	48171	48132	1419	2.9	2573	3055	321	10.5	
	P500E-000	46740				3548				
	P500E-090	50185				3294				
	P500E-180	52238				3632				
	P500E-270	49885	49762	2270	4.6	3615	3522	156	4.4	
		<b>48947</b>	<b>1957</b>	<b>4.0</b>		<b>3289</b>	<b>342</b>	<b>10.4</b>		

Table B.4. Quartz peak areas and heights for quartz standards.

	ID	area (counts)	avg (counts)	std (abs) (counts)	std (rel) (%)	height (counts)	avg (counts)	std (abs) (counts)	std (rel) (%)
Quartz standards	Q221A00	22623				1666			
	Q221A09	14593				1244			
	Q221A18	21081				1626			
	Q221A27	15392	18422	4023	21.8	1270	1452	225	15.5
	Q221C00	19990				1540			
	Q221C09	17425				1455			
	Q221C18	18872				1359			
	Q221C27	18889	18794	1052	5.6	1477	1458	75	5.1
			<b>18608</b>	<b>2730</b>	<b>14.7</b>		<b>1455</b>	<b>156</b>	<b>10.7</b>
		Q442A00	38705				2615		
	Q442A09	34228				2749			
	Q442A18	31742				2569			
	Q442A27	35174	34962	2885	8.3	2453	2597	122	4.7
	Q442B00	36139				2570			
	Q442B09	32745				2424			
	Q442B18	35354				2440			
	Q442B27	36175	35103	1617	4.6		2446	80	3.3
		<b>35033</b>	<b>2166</b>	<b>6.2</b>		<b>2546</b>	<b>117</b>	<b>4.6</b>	
	Q663A00	50599				3523			
	Q663A09	50720				3465			
	Q663A18	55626				3669			
	Q663A27	49351	51574	2771	5.4	3372	3507	124	3.5
	Q663B00	47843				3254			
	Q663B09	51637				3422			
	Q663B18	59664				3915			
	Q663B27	50845	52497	5050	9.6	3173	3441	333	9.7
		<b>52036</b>	<b>3803</b>	<b>7.3</b>		<b>3474</b>	<b>235</b>	<b>6.8</b>	
	QK-A00	43014				2828			
	QK-A09	44195				3008			
	QK-A18	46721				2866			
	QK-A27	41812	43936	2096	4.8	2745	2862	110	3.8
		<b>43936</b>	<b>2096</b>	<b>4.8</b>		<b>2862</b>	<b>110</b>	<b>3.8</b>	
(on Ag filter)	Q01AG00	37374				2360			
	Q01AG09	35771				2273			
	Q01AG18	30762				1899			
	Q01AG27	36682	35147	2996	8.5	2272	2201	206	9.3
	Q02AG00	32926				1969			
	G02AG09	38614				2460			
	G02AG18	41955				2577			
	G02AG27	36575	37518	3780	10.1	2246	2313	267	11.6
		<b>36332</b>	<b>3402</b>	<b>9.4</b>		<b>2257</b>	<b>229</b>	<b>10.1</b>	

Table B.5. TiO<sub>2</sub> – Quartz mixture XRD Internal Reference Method Results

Regression based on the Internal Reference Method			y=ax	Regression Output:		Primary Q peak	
			Constant			0	
PM10/TiO2	I(Qp)/I(T)	I(Qs)/I(T)	Std Err of Y Est			0.081601	
5.9344	1.1171	0.1844	R Squared			0.964184	
3.9562	0.9158	0.1553	No. of Observations			5	
1.9781	0.4618	0.0740	Degrees of Freedom			4	
0.9891	0.2532	0.0391					
0.4945	0.1087	0.0268	X Coefficient(s)	0.204803		<b>X(Q)= 0.164</b>	
			Std Err of Coef.	0.010904	std (rel)	0.111	
				0.0532	std (abs)	0.018	
			Regression Output:		Secondary Q peak		
			Constant			0	
			Std Err of Y Est			0.015072	
			R Squared			0.954181	
			No. of Observations			5	
			Degrees of Freedom			4	
			X Coefficient(s)	0.034045		<b>X(Q)= 0.161</b>	
			Std Err of Coef.	0.002014	std (rel)	0.146	
				0.0592	std (abs)	0.023	
						<b>X(Q)= 0.163</b>	
						0.021	

## Appendix C. Pilot Study Site Photographs

View along 24 degrees azimuth looking toward eastern side of Main Plant from lidar.



D1 sampler location



D2 sampler



D3 sampler with Main Plant in background



Two views from D4 sampler looking upwind to Main Plant



IMPROVE and DRUM samplers mounted on stand. DRUM is in center.



View toward lidar trailer (white, near center of photo) from location east of the Main Plant.



View of Main Plant from lidar.



Fugitive dust plume generated by truck leaving Main Plant on unpaved road that leads to East Gate.



Upwind samplers at Tracy Airport. Pilot Study site is visible in background at center of image.

